ELECTROCHEMISTRY OF BORON DEPOSITION FROM FLUOROBORATE CONTAINING MIXED CHLORIDE-FLUORIDE MELTS

By

Rahul Pal
Enrolment No.: CHEM02200704017

Indira Gandhi Centre for Atomic Research
Kalpakkam 603 102, Tamil Nadu, India

A thesis submitted to the
Board of Studies in Chemical Sciences
In partial fulfillment of requirements
For the Degree of

DOCTOR OF PHILOSOPHY

of

Homi Bhabha National Institute
Deemed University, Mumbai, India

AUGUST 2012

ELECTROCHEMISTRY OF BORON DEPOSITION FROM FLUOROBORATE CONTAINING MIXED CHLORIDE-FLUORIDE MELTS

A thesis submitted to the
Board of Studies in Chemical Sciences
In partial fulfillment of requirements
For the Degree of

DOCTOR OF PHILOSOPHY

of

Homi Bhabha National Institute

By

RAHUL PAL
Enrolment No.: CHEM02200704017

Indira Gandhi Centre for Atomic Research
Kalpakkam 603 102, Tamil Nadu, India

Research Supervisor

Dr. S. Anthonysamy
Head, Materials Processing Chemistry Section
Materials Chemistry Division, Chemistry Group
Indira Gandhi Centre for Atomic Research
Kalpakkam 603 102, Tamil Nadu, India

AUGUST 2012

Homi Bhabha National Institute

Recommendations of the Viva Voce Board

As members of the Viva Voce Board, we certify that we have read the dissertation prepared by **Rahul Pal** entitled **"Electrochemistry of Boron Deposition from Fluoroborate Containing Mixed Chloride-Fluoride Melts"** and recommend that it may be accepted as fulfilling the dissertation requirement for the Degree of Doctor of Philosophy.

______________________________ **Date:** 17/4

Chairman-**Dr. P. R. Vasudeva Rao**

S. Anthonysamy ______________________________ **Date:** 17/4/13

Convener-**Dr. S. Anthonysamy**

______________________________ **Date:** 17 04 2013

External examiner- **Prof. S. Sriman Narayanan**

______________________________ **Date:** 17.04.2013

Member 1-**Dr. V. Ganesan**

______________________________ **Date:** [illegible]

Member 2- **Dr. K. Nagarajan**

Final approval and acceptance of this dissertation is contingent upon the candidate's submission of the final copies of the dissertation to HBNI.

Date: 17.04.13

Place: Indira Gandhi Centre for Atomic Research, Kalpakkam

CERTIFICATE

I hereby certify that I have read this dissertation prepared under my direction and recommend that it may be accepted as fulfilling the dissertation requirement.

S. Anthonysamy

S. Anthonysamy

(Research Supervisor)

Date: 23/8/2012

Place: Indira Gandhi Centre for Atomic Research, Kalpakkam

STATEMENT BY AUTHOR

This dissertation has been submitted towards partial fulfillment of requirements for an advanced degree at Homi Bhabha National Institute (HBNI) and is deposited in the library to be made available to borrowers under the rules of HBNI.

Brief quotations from this dissertation are allowable without special permission, provided that accurate acknowledgement of source is made. Requests for permission for extended quotation from or reproduction of this manuscript in whole or in part may be granted by the Competent Authority of HBNI when in his or her judgment the proposed use of the material is in the interests of scholarship. In all other instances, however, permission must be obtained from the author.

Rahul Pal
23.08.12
Rahul Pal

Kalpakkam
August 2012

DECLARATION

I, hereby declare that the investigation presented in the thesis entitled **"Electrochemistry of Boron Deposition from Fluoroborate Containing Mixed Chloride-Fluoride Melts"** submitted to **Homi Bhabha National Institute (HBNI)**, Mumbai, India, for the award of degree of **Doctor of Philosophy** in **Chemical Sciences** is the record of work carried out by me during the period from September 2007 to August 2012 under the guidance of **Dr. S. Anthonysamy**, Head, Materials Processing Chemistry Section, Materials Chemistry Division, Chemistry Group, Indira Gandhi Centre for Atomic Research, Kalpakkam. The work is original and has not been submitted earlier as a whole or in part thereof for a degree / diploma at this or any other Institution / University.

Rahul Pal
23.08.12
Rahul Pal

Kalpakkam

August 2012

Dedicated to my father Late Shri Ramendu Pal

and

mother Smt. Shima Rani Pal

ACKNOWLEDGEMENTS

I would like to express my deep and sincere gratitude to Dr. S. Anthonysamy for his invaluable guidance. I am also grateful to him for critically reviewing this thesis.

I wish to express my sincere thanks to Dr. K. Ananthasivan for sharing his knowledge and scientific understanding with me. His critical comments helped me to improve my understanding on the subject as well as my experimental skills.

It gives me immense pleasure to thank the members of the doctoral committee Dr. P. R. Vasudeva Rao (Chairman), Dr. V. Ganesan (Member) and Dr. K. Nagarajan (Member) for their suggestions during the progress.

My warm regards to Dr. M. Saibaba for providing a pleasant accommodation in Kalpakkam. I also acknowledge the chemistry faculty of HBNI at IGCAR campus.

This thesis would not have been possible without the help, support and valuable suggestions from Mr. Suddhasattwa Ghosh, Mr. N. Sanil, Mr. Rajan Babu, Dr. K. S. Mohandas, Dr. C. R. Mariappan and Dr. Manish Chandra.

I highly acknowledge the support extended by Mr. Subrato Roy of M/s. Purelec Carbon India Pvt. Ltd., Pondicherry for the fabrication of graphite components which were invaluable for the experimental work.

My sincere thanks to Dr. R. Sudha and Mr. Swapan Kumar Mahato for recording the SEM images. I am also grateful to Mr. R. K. Prabhu for carrying out the ICP-MS analysis. I am thankful to Mr. A. Thiruvengadasami for ion selective electrode analysis and Dr. G. Paneerselvam for XRD measurements.

I also gratefully acknowledge the help rendered by Dr. Ashish Jain, Dr. V. Chandramouli, Dr. N. Pankajavalli, Mr. R. Ranganathan, Mr. A. Veerapandian, Mr. S. Balakrishnan, Ms. Rimpi Dawar, Mrs. N. Ambika, Mrs. D. Annie, Mr. V. Paramasivam, Mr. T. Ramamoorthy, Mr. E. Gajendiran, Mr. Stanislas, Mr. V. Yuvaraj and other members of Materials Processing Chemistry Section.

I wish to express my sincere thanks to Mr. Trinadha Raja Pilladi for his diversified help and fruitful scientific discussions during the course of my work.

I acknowledge Dr. S. A. Kuznetsov, Dr. Blanka Kubikova, Dr. S. Kirrilov, Dr. E. Christensen and Dr. S. Volkov for sending their published papers which were almost impossible to get.

I express my heartfelt thanks to my friends Mr. Joy Shankar Nambam, Mr. Deepak Kumar Gupta, Mr. Pinaki Paul, Mr. Subrata Bera, Mr. Ashish Kumar Singha Deb, Mr. Pradip Pal, Mr. Surajit Brojabasi, Mrs. Priyanka Brojabasi, Mr. Prasanta Jana, Mrs. Lipika Rani Bairi, Mr. Dasarath Maji, Mr. Sundar Rajan, Mr. Diganta Gogoi, Mr. D. Sri Maha Vishnu, Mr. Biju Joseph, Mr. Bishnu Prasad Kar, Mr. Ashit Krishna Pattanaik, Mr. L. Herojit, Mr. Ch. Kishen Singh, Mr. Karuna Kara Mishra, Mr. Prasana Kumar Sahoo, Mr. Subrato Ghosh, Mr. Alok Rout and all others residing at the enclave for their numerous help, support and enjoyable company for making the life at Kalpakkam more cheerful.

I owe my gratitude and indebtness to my late father, mother, uncle Mr. Mrinmay Paul, sister Mrs. Ranjita Bera, brother in law Dr. Manindranath Bera and my beloved elder brother Dr. Manoj Pal. It is their inspiration, encouragement, blessings and support that helped me to achieve what I am today.

Kalpakkam, August 2012 **Rahul Pal**

CONTENTS

CHAPTER I

CHAPTER II

CHAPTER III

CHAPTER IV

CHAPTER V

SYNOPSIS

Nuclear power is being realized as a potentially useful and appropriate electricity source for both developed and developing countries. Expanding nuclear power's share of electricity portfolios could reduce the greenhouse gas emissions responsible for global warming. Moreover, nuclear power has long been addressed as a route to energy security due to decrease in dependence on oil imports. The development of new generation of nuclear reactors would change the global energy scenario. These new motivations have led to ‘nuclear renaissance’ to the possibility of a rapid expansion of nuclear power to satisfy a projected growing global energy demand and simultaneously reducing greenhouse gas emissions.

Early realization of the limited resources of natural uranium and the abundant availability of thorium in India led to setting up of nuclear power plants for electricity generation. This was based on a three-stage plan to eventually make use of the abundant national resource of thorium. To achieve this long-range goal, India had to necessarily start with setting up heavy water–moderated, natural uranium–fueled power reactors to produce the plutonium required for the subsequent stages. India has already embarked on the second stage of this programme and the construction of Prototype Fast Breeder Reactor (PFBR) is at an advanced stage.

The importance of boron in nuclear and non nuclear applications is well known. Compounds of boron also find their application as advanced materials in automotive, electronic, aerospace industries etc. ^{10}B finds its application as control rod (in the form of B_4C) as well as shielding material in nuclear reactors due to its high neutron absorption cross section. Boron carbide containing boron enriched in ^{10}B isotope (67 at.%) will be used in the control rods of the PFBR. An indigenous process developed for fabricating high-density boron carbide pellets for this application envisages the synthesis of boron carbide from enriched boron by reacting it with carbon. For this purpose high purity enriched elemental boron is being produced in India through a high temperature (1073 K) molten salt electrolysis process from a melt comprising KCl (72.96 mol%), KBF_4 (11.04 mol%) and KF (16 mol%). Thus the electrochemistry of the above melt system is of importance to the Indian fast reactor programme. Eventhough the electrochemistry of chloride-fluoride melt systems have been investigated, no study has so far been reported on the electrochemistry of the system KF-KCl-KBF_4. Hence a detailed experimental programme was pursued in order to understand the electrochemistry of this system.

Present doctoral work deals with the research associated with the development of a reference electrode for analyzing the thermodynamic parameters of chloride-fluoride (KCl-KF) melt system; elucidation of electrochemical process of the deposition of elemental boron from fluoroborate salts (KBF_4 and $NaBF_4$) in KCl-KF melts.

Objective

The objectives behind the present study are listed below:

1. Development and validation of a suitable reference electrode for application in chloride-fluoride melt is necessary to understand the thermodynamic parameters of the melt system as well as the corrosion potential of different metals in it.
2. Studies related to electrokinetic parameters such as electron transfer coefficient, electron transfer rate constant, diffusion coefficient and nucleation of the electroactive species would draw some more insight into the electrodeposition of boron from KBF_4 and $NaBF_4$ in KCl-KF melts.

3. The progress of the electrowinning of boron from the melt $KCl - KF - KBF_4$ would be influenced by the nature of the boron containing electroactive species. A plausible scheme of reaction(s) that is consistent with the experimental observations could be elucidated for better understanding of the process.

Overview of the thesis

The organization of the thesis is presented as below.

Chapter I	Introduction
Chapter II	Experimental techniques, principle and procedure
Chapter III	Results and discussion
Chapter IV	Conclusions
Chapter V	Scope of future studies

Chapter I

Introduction

The need of nuclear energy for meeting the present and future energy demand of the country are dealt with. Importance of FBRs in this regard was also addressed. The importance of molten salt based electrodeposition of elemental boron required for synthesizing boron carbide for control rod and shielding material applications in FBRs are elaborated. Different types of melt systems explored for boron deposition and the superiority of mixed chloride-fluoride based melt system are discussed. Importance and performance of standard reference electrode for studying the electrochemistry of melts are addressed. A detailed literature review on electroanalytical studies on boron containing melts and determination of electroactive species in KCl-KF-KBF_4 melts are discussed.

Work done on KCl-KF-KBF_4 melts system at the Indira Gandhi Centre for Atomic Research (IGCAR) in the past and the context of the present work and its objectives are stated.

Chapter II

Experimental techniques, principle and procedure

Chemicals, electrochemical cell fabrication, construction as well as the method of validation of the reference electrode and various experimental methods adopted in the present study are detailed in this chapter. The handling and purification of salts for the preparation of the melts is detailed. Brief description of various analytical methods and tools such as cyclic voltammetry, chronoamperometry, emf technique, X-ray diffraction, SEM, ICP-MS and ion-selective electrode analysis are presented. The detailed description of instrumentation for voltammetric measurements and the electrochemical transient techniques employed in the present study are elaborated.

Chapter III

Results and discussion

The performance of the Ag/AgCl reference electrode (developed in this study) on the basis of its reversibility, stability and non-polarizability in a melt containing chloride and fluoride studied over the temperature range 1073 to 1123 K is presented. Cyclic-voltammograms (CVs) of this melt on a platinum working electrode recorded at regular intervals over a period of time for determining stability of this reference electrode has been discussed. Cathodic and anodic polarization and micropolarization experiments and their results have been detailed. Reduction potentials of Fe^{2+}/Fe and Ni^{2+}/Ni couples in the KF–KCl melt measured for the first time are presented.

Electrochemistry of deposition of boron from KCl-KF-MBF_4 (M= K and Na) melts studied by cyclic voltammetry, chronoamperometry and convolution voltammetry over a temperature range are described. The boron reduction potentials, nucleation potential, quasireversibility or irreversibility, number of electron transferred for the redox process over the temperature range and composition are detailed. Electrokinetic parameters such as transfer coefficient, diffusion coefficient and electron transfer rate constant for the boron containing electroactive species measured at different temperatures and melt composition are discussed. Electrodeposition of boron on platinum electrode and analyses of the electrodeposit are also discussed.

A plausible scheme of reaction(s) that governed the electrodeposition of boron from melts containing KCl, KF and KBF_4 (at 1073 K) by formulating four different stoichiometric equations based on the existence of various chloride-fluoride complexes derived from the fluoroborate anion are deduced. The net variation in the ratio n_{Cl^-}/n_{F^-} (where n_{Cl^-} is amount of Cl^- in g and n_{F^-} is amount of F^- in g) thus computed based on these four equations by assuming uniform depletion of boron from the melt due to electrodeposition was compared with the experimental values obtained during many electrowinning runs. The progress of the electrodeposition of boron from KCl, KF and KBF_4 melt based on these analyses is described.

Chapter IV

Conclusions

An Ag/AgCl reference electrode developed for studying the electrochemistry of fluoroborate containing chloride-fluoride melts was shown to be reversible with respect to the chloride ion. Its stability and non-polarizability were tested and it was found to be performing satisfactorily over the temperature range 1073 to 1123 K. By using this electrode the reduction potentials of Fe^{2+}/Fe and Ni^{2+}/Ni in the melt KF–KCl were obtained over the temperature range 1073 – 1123 K.

The electrochemical reduction of B(III) + 3e → B in KCl (81.54 mol%)-KF (18.45 mol%)-KBF_4 (1.6×10^{-4} to 7.73×10^{-4} mol cm^{-3}) melt on a Pt electrode (over the temperature range 1073 to 1123 K) at a sweep rate of $\nu < 0.1$ V s^{-1} was found to be quasireversible and at $\nu > 0.1$ V s^{-1}, both diffusion of electroactive species and electron transfer were found to play a role in the reduction process. It was also established that the reduction of B(III) to B occurred by a single-step three-electron process. The transfer coefficients evaluated by cyclic voltammetry and various hypotheses of convolution voltammetry showed the process to be irreversible. The diffusion coefficients calculated for the reduction of B(III) to B using cyclic voltammetry and chronoamperometry were found to be comparable. Boron electrodeposited on Pt electrode at 1073 K was found to be amorphous in nature.

The electrochemical reduction of B(III) + 3e → B in KCl (81.54 mol%)-KF (18.45 mol%)-$NaBF_4$ (1.67×10^{-4} mol cm^{-3}) melt on a Pt electrode (over the temperature range 1073 to 1123 K) at a sweep rate of $\nu < 0.1$ V s^{-1} was found to be quasireversible and at $\nu > 0.1$ V s^{-1}, both diffusion of electroactive species and electron transfer were found to play a role in the reduction process. Reduction of B(III) to B occurred by a single-step three-electron process. Using chronoamperometry, the diffusion coefficients of the boron containing electroactive species (B(III)) were calculated for the fluoroborate melt systems and the values for KCl-KF-$NaBF_4$ were lower compared to KCl-KF-KBF_4 melt.

The progress of the electrowinning of boron from the melt $KCl-KF-KBF_4$ was investigated by assaying the aqueous solutions of the salt residues withdrawn from the melt at periodic intervals. For the first time such a systematic investigation on the electrowinning of boron was reported. Empirical reactions were formulated in order to arrive at the most probable reaction scheme during the course of the electrolysis. The reaction scheme was possibly influenced by many factors including the melt composition and the source of boron etc.

Chapter V

Scope of future studies

The phase diagram of KCl-KF-KBF_4 system could be studied in detail. TG-DTA analysis of the KCl-KF-KBF_4 condensed phase and MS (Mass Spectrometry) analysis of the gas phase would draw some information on the nature of the species in the head space of the melt. A detailed study on the nature of the boron containing complexes existing in the melt could be possible through NMR spectroscopy. Borides are a large class of compounds having very promising properties. Production of refractory borides is one of the challenges of today's material scientists. Molten salts could be considered as a very promising medium for electrochemical synthesis of different refractories.

LIST OF FIGURES

LIST OF TABLES

CHAPTER I

1.0 Introduction

1.1 Need of energy

Energy is an indispensable part of the global economy [1]. Energy has been universally recognized as one of the most important inputs for economic growth and human development. Getting somewhere, sharing information and production of commodities for daily use require energy. Throughout the industrial age and into the age of information technology, energy has served as the building block of mankind's progress [2]. Technology has provided the prime thrust of a nation's growth, urbanization, progress, prosperity, power and accomplishment. The greater the ability of a nation to generate, transfer and utilize technology, the faster is the nation's growth. Hence, science and technology are the wagon wheels of the development process in recent times.

India, being a developing country is advancing in the field of science and technology and industrial manufacturing activities to sustain the global competitiveness. The Indian economy has clocked an average growth rate of 7% in the last decade. A high growth rate is also predicted for the future, which implies a high rate of consumption of electrical energy. To maintain this pace, experts believe that the country will have to increase its energy consumption by at least 4% annually. This relentlessly increasing demand is a massive challenge for India, affecting not only the domestic economy, but also India's foreign policy [3].

1.2 Available energy resources and demand in India

Of the three major energy sources – coal, oil and gas – coal is India's major source of energy. This major fossil fuel deposit in India is about only 75 billion tonnes. With 7%

of the world’s coal deposit, India has the fourth largest coal reserves. Coal and natural gas accounts for ~80% of the annual electricity produced in India [4, 5]. About 65% of the power consumption is contributed by the thermal power generators (which use coal as the energy source) spread all over the country. Coal cannot meet all of India’s energy needs. India’s oil reserves (about 786 Mt: 0.4% of world’s reserve of crude oil) and gas reserves (1,437 billion cubic meters) are also not sufficient to meet its rapidly growing energy needs. Renewable energy sources namely solar, hydroelectric, wind and biomass contribute ~18% of the total electricity production. Nuclear energy contributes only 3% of the share. It has been estimated that India will need 3400 TWh of electricity annually by 2070 [6]. This figure is of importance, despite setting a low benchmark of 2000 kWh per capita per annum for the future. The net potential of the renewable sources in India is estimated to be about 1229 TWh [6]**,** which if realized at all will account for about 36.1% of the total estimated energy demand of 3400 TWh in 2070. Hence, although India has reasonable resources of renewable energy, it is not so well endowed that its future electricity requirements can be fully met by renewable sources. The present rate at which the fossil fuel is being depleted (owing to its high rate of consumption), within 100 years its contribution will also become negligible. Thus the fossil fuel based supply of power for sustaining the industrial activities is meager [7]. Hence, the only sustainable energy resource available in the long run is the nuclear energy, which has the capability to generate sufficient and clean energy to meet India’s growing energy demands. The country has nuclear ores from which a total of about 78,000 tonnes of uranium metal and about 518,000 tonnes of thorium metal can be extracted [8]. Hence, nuclear reserve in India is estimated to serve as the backbone of future energy supply.

1.3 Indian nuclear energy programme

Presently, India occupies a leading place among Asian nations in the indigenous design, development, construction and operation of nuclear power reactors [9]. Nuclear power comprises of about 14% of the total electricity generated worldwide: 440 commercial nuclear reactors operating in 31 countries produce this electricity with a total generating capacity of around 380 GWe [10]. In India presently 20 reactors are under operation and 9 are under construction [11]. This was possible due to the early realization of the limited resources of natural uranium and the abundant availability of thorium in the country. A nuclear power reactor is designed to allow nuclear fission chain reactions to initiate, control and sustain by releasing energy at a controlled rate. Fuel forms the core of the nuclear reactors [12]. The fissile atoms are mainly ^{235}U, ^{239}Pu, ^{241}Pu and ^{233}U. The isotope ^{238}U is not fissile but can be converted to fissile nuclide ^{239}Pu by the nuclear reaction ^{238}U (n, γ) ^{239}U (-β) 239Np (-β) ^{239}Pu process. Hence the isotope ^{238}U is termed as fertile. ^{232}Th is fertile since it can be converted to fissile ^{233}U by a sequential (n, 2β) reaction. Natural uranium constitutes fissile ^{235}U (0.7 wt%) and the remaining, fertile isotope ^{238}U. Plutonium, a man made element, and its other isotopes also undergo fission to varying degrees. Under the guidance of Dr. Homi Jehangir Bhabha a strategy was evolved for the setting up of nuclear power plants for electricity generation in India. This was based on a three-stage plan to eventually make use of the abundant national resource of thorium. To achieve this long-range goal, India had to necessarily start with setting up of heavy water–moderated, natural uranium–fueled power reactors to produce the plutonium required for the subsequent stages.

The first stage involved the setting up of heavy water–moderated, natural uranium-fueled, pressurized heavy water reactors (PHWRs) for electricity generation [13]. Fissile ^{235}U (can sustain a nuclear fission chain reaction by absorbing neutrons) from natural uranium undergoes fission in these thermal reactors, and produces ^{239}Pu from fertile ^{238}U (capable of becoming fissile material after absorbing neutron). Presently all operating reactors in India are based on the use of either natural uranium (0.7% ^{235}U) or enriched uranium containing 3-4% ^{235}U. These reactors are either PHWRs or boiling water reactors (BWRs). The depleted fuel from these first stage reactors contains plutonium and unutilized ^{238}U.

The second stage would comprise fast breeder reactors (FBRs) fueled with the plutonium generated in the first stage along with depleted uranium. ^{233}U would be produced in the thorium-loaded blanket region. Fissile ^{233}U thus produced will be the fuel for the third stage [14]. FBRs are capable of generating more fuel than they consume owing to its high breeding ratio (the average number of fissile atoms created per fission event) and thus are capable of generating nuclear capacity to a very high level.

The third stage of the power program would employ thermal breeders fueled with ^{233}U produced initially from the second stage along with thorium in the blanket region to generate more ^{233}U [14]. In addition thermal or accelerator driven sub-critical reactors exploiting the vast resource of thorium would comprise this stage. Ultimately, the third-stage breeder reactors would produce more fissile material than they burn while providing electricity, thus ensuring the sustainability of nuclear power for several decades to come.

If the entire uranium resources are first used in natural uranium–fueled PHWRs, it is estimated that about 420 gigawatt electric-years (GWe-yrs) of electricity can be produced

[8]. The resulting depleted uranium and separated plutonium from these PHWRs, if used in FBRs, could generate an additional 54,000 GWe-yrs of electricity. In these FBRs, production of ^{233}U can also be achieved by loading thorium sub-assemblies in their blanket and low-power zones. Eventually by transitioning to generations of Th-^{233}U fueled breeder reactors, India should be able to produce an additional 358,000 GWe-yrs of electricity [8]. Thus, even at an installed nuclear power capacity of 500–600 GWe, the country's nuclear resources will be able to sustain its electricity needs far beyond the extinction of its coal deposits. India's flourishing and indigenous nuclear power program projects to have 20,000 MWe nuclear capacity on line by 2020 and 63,000 MWe by 2032. It aims to supply 25% of electricity from nuclear power by 2050. Hence, with these long-term strategies, the nuclear industry is expected to undergo a paradigm shift from a mere electricity producer to being an indispensable part of India's energy policy.

1.4 Different types of Indian nuclear reactor

The nuclear reactors can be broadly divided into two types namely power reactors used for electric power production and the other, research reactors used mainly for materials research, testing and training. The power reactors are divided into the following categories as presented in Table 1.1 [12].

Table 1.1 Type and characteristics of Indian nuclear power reactors [12].

Reactor type	Characteristics
PWR (Pressurized Water Reactor)	Circulating water at about 140 atm and 573 K transfers heat from the fuel elements to steam generators.
BWR	Circulating water transfers heat from the fuel rods, boils and furnishes steam at about 573 K and 70 atm directly to turbines.
PHWR - CANDU (PHWR - Canada Deuterium Uranium)	Pressurized heavy water (at 100 - 150 atm) in a calandria moderates neutrons. Transfers heat from natural UO_2 fuel rods to steam generators.
FBR	Liquid sodium at 673 – 873 K and 2 – 3 atm transfers heat from $(U,Pu)O_2$ fuel rods to intermediate heat exchangers from which sodium transfers heat to steam generators.

1.5 Reactor components

1.5.1 Fuel

UO_2 forms the fuel of thermal reactors. Natural uranium oxide mixed with plutonium oxide (MOX) is used as a fuel for fast reactors since the technology with respect to the oxide form of fuel has evolved. Oxide might not be the best choice as the fuel as metallic form of the fuel is rather preferred. Metallic fuels have highest fissile atom density and high thermal conductivity [15]. Apart from the oxide, the carbide and nitride forms of uranium and plutonium were also developed.

1.5.2 Clad

Clad is the outer jacket of the nuclear fuel and serves as a barrier to the release of fission products [12]. The clad is subjected to very hostile environment of high neutron flux and high temperatures. The desirable properties of clad are:

1. Maintain integrity and geometry of the fuel pin.
2. Retain the fission products.
3. Low neutron absorption cross-section.
4. High thermal conductivity and low thermal expansion coefficient.
5. Chemical compatibility with the fuel and coolant.
6. High strength, ductility, resistance to creep and fatigue.
7. Resistant to irradiation.

1.5.3 Moderator

A moderator is one of the important components of thermal reactors. It helps to maintain neutron population in the thermal energy range [12]. Whenever a neutron causes fission it also leads to the release of fast neutrons. These fast neutrons have to be stalled and brought to lower energy levels if they have to cause successful fission in turn. It is here that the concept of a moderator comes in to picture. A moderator is a medium that is used to absorb a portion of the kinetic energy of fast neutrons so that they come in the category of thermal neutrons, which help to sustain a controlled chain reaction. The mechanism of speed control works in such a way that the fast moving neutrons strike the nuclei (uncharged) of moderator material which is not efficient at absorbing them but simply slows them down with repeated collisions thus bringing them into the thermal zone. Light water, heavy water, graphite, beryllium and lithium are used in different types of reactors as moderators.

1.5.4 Reflector

The purpose of a reflector is to reflect the leaking neutrons back into the core of a nuclear reactor [12]. A reflector material is used to ensure that neutrons do not simply fly off the reactor leaving little room for the chain reaction to continue. The moderator controls the speed of neutrons so that they act usefully in creating more fission, but many of these neutrons may simply get lost, by flying off the reactor core, thus serving no useful purpose. This might hinder the progression of a chain reaction that is essential for the nuclear reactor. In order to reduce this process of neutron loss, the reactor core is surrounded by a material that helps to reflect these escaping neutrons back towards the core of the reactor and these materials are known as reflecting materials. A reflector should posses low neutron absorption cross-section, high reflection and radiation stability. Light water, heavy water and carbon are mostly used as reflectors.

1.5.5 Coolant

A nuclear reactor is a source of intense heat that is generated through the fission reactions taking place inside the core. Therefore, a coolant is needed to ensure that this heat is captured and utilized in a proper manner [12]. This also helps to keep the working temperature of the core within the safe limits for the materials used in the construction of the reactor. Hence, a coolant plays an important role in nuclear power plant and serves the dual purpose of removing the heat from the reactor as well as transferring it to the electricity generation circuit. A coolant should have the following desirable properties,

1. Should have a minimum neutron absorption cross-section.

2. Excellent resistance to high temperature and high level of radiation.
3. Low viscosity.
4. Should be non-corrosive.
5. Liquid coolant should have high boiling point and solid coolant (e.g. Na) should have low melting point.
6. Easy and safe handling.
7. Commercial availability in large quantities at an acceptable cost.
8. Minimum pumping power to remove heat at a given rate from core to boilers.

1.5.6 Control rod

The rate of neutron generation and loss are directly related to the reactivity (rate of change of reactor power) and control of a nuclear reactor. The most effective control materials for the fission reactors are strong neutron absorbers [12]. The control rods should have the following properties.

1. Good mechanical, structural and dimensional stability.
2. Availability at a reasonable cost.
3. Stability under steep and cyclic heating.
4. Relatively low mass to allow rapid movement.
5. Corrosion and wear resistant.
6. High thermal conductivity.
7. High melting point for solids or high boiling point for liquids.

1.5.7 Shielding

A nuclear reaction is a source of intense radiation apart from the heat generated in the exothermic process. Radiation shielding is required to prevent this harmful radiation from leaving the reactor and affecting the environment. This necessitates for having a proper shield so that these radiations get absorbed within the reactor without having a chance to escape into the environment [12]. This is done by using materials that are good absorbents of the nuclear radiations. Concrete and steel are very good at absorbing radiation and they are equally strong as well, hence used as the shielding material. Boron carbide is the choice for fast reactors. Boral, which is essentially a dispersion of B_4C in aluminum, and Bocarsil (B_4C in silicon rubber) also find extensive applications in nuclear reactors as shielding materials.

1.5.8 Pressure vessel

The pressure vessel contains most materials of the primary components of a nuclear fission reactor [12]. They are nuclear fissile and fertile fuels, structural materials, reflector, moderator, blanket materials, control element, shielding and safety systems.

1.5.9 Steam generator

Steam generators are heat exchangers, used to convert water into steam from heat produced in a nuclear reactor core [12].

The major reactor components are given in Table 1.2.

Table 1.2 Components of major nuclear reactors [12].

Components	**Reactor Type**					
	PWR	**BWR**	**PHWR-CANDU**	**FBR**	**HTGR**	**GCFR**
Fuel	UO_2 pellets	UO_2 pellets	UO_2 pellets	UO_2-PuO_2 pellets	UC_2-ThC_2 pellets	U-Pu oxide (or carbide) pellets
Clad	Zircaloy-4	Zircaloy-2	Zircaloy-4	Steel, FeNi alloy	Graphite	SS
Moderator	Light water	Light water	Heavy water	-	Graphite	Graphite
Reflector	Light water	Light water	Heavy water	ThO_2 or UO_2 blanket	Graphite	Graphite
Coolant	Water	Water	Heavy water	Liquid sodium	Helium	Helium

***HTGR**: High-Temperature Gas-Cooled Reactor, **GCFR**: Gas-Cooled Fast Reactor

1.6 Fast breeder reactors

Reactors with conversion ratio (ratio of the rate of production of fissile nuclei to the rate of consumption of it) more than unity is termed as breeder reactors. It is not possible to breed fuel in thermal reactors whereas fast reactors are capable of producing more fissile material than consumed and are therefore called fast breeder reactors (FBRs). In the fast neutron induced fission, it is found that the number of neutrons produced per fission is more than that produced in thermal neutron induced fission. In other words, fast reactors have extra neutrons around than that is necessary for maintaining the chain reaction. In addition, ^{238}U also undergoes fission in the fast neutron regime, unlike in a thermal reactor and therefore there are extra neutrons and energy produced from the fertile material. Further in the fast neutron spectrum, the absorption cross-section of ^{238}U is comparable to that of the ^{239}Pu fission cross-section. The neutron energy and fission cross-sections (probability to undergo nuclear fission) of the fissile material are inversely related. To compensate for the small cross-sections in fast energy regions, highly enriched fuel (enriched in fissile isotope) is used in the core from criticality consideration. Blankets of thorium or natural U are used to capture the neutrons leaking from the core and thus to produce fissile material ^{233}U or ^{239}Pu. The fast reactors use liquid sodium as coolant owing to its highly favourable nuclear, physical and chemical properties. Sodium does not moderate neutrons. It has low melting point, which makes it easy to maintain in liquid form.

1.7 Prototype fast breeder reactor (PFBR)

PFBR is a sodium cooled, mixed oxide (MOX) fuelled, pool type Indian fast reactor. The reactor core constitutes 181 fuel subassemblies (FSA). Each fuel subassembly consists of 217 helium bonded fuel pins of 6.6 mm diameter. Each pin has 1000 mm column of annular MOX fuel pellets and 300 mm each of upper and lower blanket columns. The clad material is 20% CW (cold worked) 15Ni–14Cr–2Mo + Si + Ti (D9). There are 2 rows of radial blanket subassemblies. 12 absorber rods viz., 9 control and safety rods (CSR) and 3 diverse safety rods (DSR) are arranged in two rings. Enriched boron carbide ($^{10}B_4C$, $^{10}B > 67$ at.%) is used as the absorber material for reactor control and shutdown [16]. A single grid plate is used to support all the core subassemblies (CSA) and to distribute coolant to the CSA. The coolant is pumped by two sodium pumps into the grid plate for heat removal from the reactor core. Molten sodium flows under gravity through the four intermediate heat exchangers to transfer heat to the secondary sodium which in turn transfers heat to water in the steam generators to produce steam. High-density concrete is used as the shielding material. The core thermal power is 1253 MW and the gross electrical output is 500 MWe [17].

1.8 Reactors and their control

Four general methods have been used or proposed for changing the power or neutron flux in a nuclear reactor; each involves the temporary addition or removal of any one of the following:

- fuel
- moderator
- reflector
- a neutron absorber or poison.

The most commonly used method to control the nuclear reaction, especially in power reactors, is the insertion or withdrawal of control rods made out of materials having a large cross section for the absorption of neutrons.

1.8.1 Mechanism of control

Nuclear reactors operate by means of sustained chain reactions between neutrons and fissile isotopes. The process is self sustaining in the form of chain reaction. The effective neutron multiplication factor, k_{eff}, is the average number of neutrons from one fission that cause another fission. In order to sustain the chain reaction (the condition of reactor criticality), k_{eff} must be at least unity. When k_{eff} is greater than unity, the chain reaction increases and when it is less the chain reaction dies out. A reactor is said to be critical when $k_{eff} = 1$, supercritical when $k_{eff} > 1$ and subcritical when $k_{eff} < 1$ [18]. To ensure that the reactor does not operate in the supercritical mode, even though k_{eff} is greater than unity, neutron absorbers are intentionally introduced into the reactor core as a part of the control system. Control systems are necessary to vary the power in response to demands and to shut down the reactor. Several types of control elements are used in a given system to perform specific functions. These can be bundles of rods or plates of various shapes.

1.8.2 Characteristics of absorber materials

Neutron absorbers are elements in which the nuclei capture neutrons without generating or emitting new neutrons [18]. The two most common types of reactions involve neutron absorption by the target nucleus followed by the emission of gamma radiation (n, γ) or the ejection of an alpha particle (n, α). A neutron is not re-emitted or produced in either case. The rate at which nuclear reactions proceed is determined largely by a quantity called the nuclear cross-section, σ, which is a measure of the probability of occurrence of that reaction. It is a property of the nucleus as defined for a particular reaction with incident particles e.g. neutrons of a given energy. The dimensions of cross-sections are cm^2. Since the absolute values are very small, the unit barn, 10^{-24} cm^2, is used in common terminology. Cross-sections are highest in the slow neutron energy range and in general, decrease as neutron energy increases. Effective absorber materials have cross-sections of at least 1000 barns in the neutron energy range below 1 eV. In the fast neutron range (~1 MeV), the cross-sections for all reactions are low and an absorber having a cross-section of ~1 barn is very effective.

The cross-section, σ, applies to a single nucleus and is called the microscopic cross-section. Since the target material contains "N" nuclei/cm^3, the quantity $N\sigma$ is equivalent to the cross-section of the material per cm^3 for a particular reaction. This is called the macroscopic cross-section and is the quantity used in evaluating absorber materials and calculating their effects. The macroscopic cross-section is given as,

$$\Sigma = N\sigma \qquad 1.1$$

It has the dimensions of reciprocal length.

The neutron absorber should have the following properties.

1. High neutron absorbing cross-section.
2. Capability of capturing neutrons efficiently to the degree required for reactivity control.
3. The absorber material must retain this capability throughout its life time in the core to ensure that the reactor can be shut down at all times.
4. Should be chemically compatible with clad.
5. Should exhibit compatibility with the reactor coolant.
6. Its performance should not impose operational limitations on the control system.
7. It must be inexpensive to procure and fabricate such that the cost of controlling the reactor is economical.

1.8.3 Overview of neutron absorbers

The most widely used neutron absorbers are hafnium, silver, indium, cadmium, and boron. These materials are briefly discussed below.

1.8.3.1 Hafnium

Because of its neutronic, mechanical and physical properties, hafnium is an excellent control material for water-cooled, water-moderated reactors. It is found together with zirconium and the process that produces pure zirconium produces hafnium as a by-product [19]. Hafnium is resistant to corrosion by high-temperature water, has adequate mechanical strength and can be readily fabricated. Hafnium consists of four isotopes each of which has appreciable neutron absorption cross-section. The capture of neutrons by the isotope ^{177}Hf leads to the formation of ^{178}Hf; the latter forms ^{179}Hf, which leads to ^{180}Hf. The first three have large resonance-capture cross-sections, and ^{180}Hf has a moderately large cross-section. Thus, the element hafnium in its natural form has a long, useful lifetime as a neutron absorber. Because of the limited availability and high cost of hafnium, its use as a control material in civilian power reactors has been restricted [12].

1.8.3.2 Silver-Indium-Cadmium alloys

By alloying cadmium, which has a thermal-absorption cross-section of 2450 barns, with silver and indium, which have high resonance absorption, a highly-effective neutron absorber is produced [12].

The control effectiveness of such alloys in water-moderated reactors can approach that of hafnium and is the control material commonly used in pressurized-water reactors. The alloys (generally 80% silver, 15% indium, 5% cadmium) can be readily fabricated and have adequate strength at water-reactor temperatures. The control material is enclosed in a stainless steel or aluminum tube to protect it from corrosion by the high-temperature steam.

1.8.3.3 Boron containing materials

Boron is a useful control material for thermal (and other) reactors [12]. The very high thermal absorption cross-section of ^{10}B and the low cost of boron have led to wide use of boron-containing materials in control rods and burnable poisons for thermal reactors. The absorption cross-section of boron is large over a considerable range of neutron energies, making it suitable for not only control materials but also for neutron shielding. Boron is non-metallic and is not suitable for control rod use in its pure form. It is due to the fact that boron powder is hard to sinter due to the presence of rigid covalent bonds and corresponding low diffusion mobility. For reactor use, it is generally incorporated into a metallic material. Stainless-steel alloys or dispersions with boron have been employed to some extent in reactor control. The performance of boron-stainless-steel materials is limited because of the ^{10}B (n, α) reaction.

1.8.3.4 Rare earth based materials

Among the rare earth elements, europium, samarium, gadolinium and dysprosium can be used as control rod materials because of their outstanding neutron absorption cross-section [20]. These rare earths are weakly resistant to corrosion and are easily oxidized. Thus rare earth oxides and dispersions in metallic matrices are employed. Eu_2O_3 (50 wt%) dispersed in SS is used as a control rod material for reactors that require a small core. EuB_6 has a reactivity worth equivalent to approximately 25% ^{10}B enriched B_4C, and it is worth about 10% more than europia. Furthermore, the loss of reactivity is lower than boron carbide.

^{149}Sm by neutron capture transforms to ^{150}Sm and its cross-section drops by a factor 10^2 to 10^3. This implies that the element is a consumable absorbent. Like samarium, gadolinium is also a consumable absorbent [12].

1.8.4 Advantages of boron as neutron absorber

Boron and its compounds such as B_4C are the most effective neutron absorbers in most types of reactors. ^{10}B exhibits high neutron absorption cross-section in the low neutron energy range (thermal neutrons). The variation of cross-section as a function of kinetic energy of the neutron plays an important role in control stability. At higher energy region, the cross-sections of most other absorbers (Cd, AIC etc.) become very small, often it decreases abruptly as in the case of Cd, whereas ^{10}B decreases monotonically with energy [18]. This variation is regular across the whole neutronic spectrum, from thermal neutrons to fast neutrons for the ^{10}B nuclide, but for other nuclides the variation of cross-section with neutron energy has numerous resonances for given values of the kinetic energy of the neutrons. Absolute value of the cross-section in the entire energy spectrum is of sufficient magnitude to make it very effective in thermal and fast reactors [21]. The variation of neutron absorption cross-section of various elements with the neutron energy is shown in Fig. 1.1a and b.

Another advantage of boron as control rod material is that the worth (measure of the effectiveness of the absorber rod) of a control rod containing boron as neutron absorber can be increased by nearly a factor of 4.5 by enriching boron with respect to B^{10} (up to 92%) without changing the dimensions of the control rod.

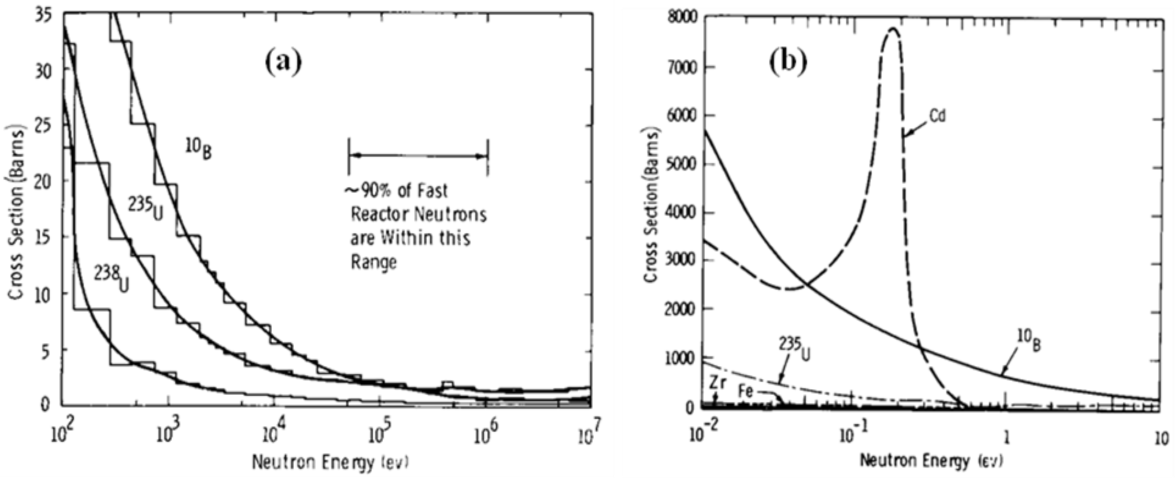

Fig. 1.1 Neutron absorption cross-section at low (a) and high energy (b) region [18].

Boron produces stable, non radioactive isotopes upon absorbing neutron according to the following reaction.

$$^{10}_{5}B + {}^{1}_{0}n \rightarrow {}^{7}_{3}Li + {}^{4}_{2}He + 2.79 \text{ MeV} \qquad 1.2$$

The reaction products are nonradioactive. Thus decay heating problems during reactor shutdown and transfer of depleted control rods are minimized.

Another reaction product generated by neutron absorption by ^{10}B is tritium ($^{3}_{1}H$) according to the following reaction.

$$^{10}_{5}B + {}^{1}_{0}n \rightarrow {}^{3}_{1}H + 2\,{}^{4}_{2}He \qquad 1.3$$

The cross-section for this reaction exists only above about 1 MeV and has a spectral average value of about 0.01 barn in fast spectra. In fast reactor, the amount of tritium generated by boron is small. It is partially retained in boron carbide and the remainder trapped.

1.9 Abundance and occurrence of boron

Boron is a relatively rare element in the Earth's crust, representing only 0.001% [12]. Boron exists in Earth's crust and sea water as borax ($Na_2B_4O_7.10H_2O$), boric acid (H_3BO_3), colemanite ($Ca_2B_6O_{11}.5H_2O$), kernite ($Na_2B_4O_7.4H_2O$), ulexite ($NaCaB_5O_9.8H_2O$) and borates [22]. Boron has two principal isotopes ^{10}B and ^{11}B, which are chemically identical but have distinctive nuclear properties. ^{10}B and ^{11}B are naturally present at an abundance of 19.10 – 20.31% and 79.69 – 80.90% respectively. Elemental boron is a dark brown powder in its amorphous form and a dark grey, hard, brittle solid in its crystalline form. Its physical properties are depicted in Table 1.3.

Table 1.3 Physical properties of boron [12].

Properties	**Magnitude**
Density (kg m^{-3})	2.48×10^3 (Crystalline boron)
Melting Point (K)	2273 – 2348
Boiling Point (K)	2823
Knoop Hardness	3300
Specific Heat (J kg^{-1} K^{-1})	
At 273 K	600
At 573 K	651
At 1073 K	1760
Thermal Expansion Co-efficient at 293 – 1023 K (10^{-6} K^{-1})	8.3

1.9.1 Boron for non-nuclear applications

Boron and its compounds find various industrial applications [23 – 32]. For example, boron deoxidizes and degasifies the steel and other alloy melts for the improvement of hardness and facilitates annealing of these alloys [23]. The compounds of boron, viz., aluminum-boron-carbide cermet, boron nitride, boron doped in silicon etc., find their application as advanced materials in automotive [24] as well as electronic industries [25, 26]. Metallic borohydrides [27, 28], boron nanostructures [29] and ammonia–borane complexes [30, 31] are used for hydrogen storage. Boron-metal composite, owing to its high thermal conductivity, high specific stiffness (elastic modulus per unit density of a material) and low co-efficient of thermal expansion, is used in aerospace industries [31, 32].

1.9.2 Methods of production of elemental boron

Elemental boron can be produced by pyrometallurgical and pyroelectrolysis processes.

1.9.2.1 Pyrometallurgical Process

1.9.2.1.1 Metallothermic reduction of boric oxide

Feasibility of reduction of boric oxide to boron by magnesium, calcium and aluminum was reported by Efremkin [33 – 35] through thermodynamic calculations over the temperature range 298 – 2000 K. Powdered magnesium was found to be a suitable reductant due to its abundance and cost effectiveness. In 1892 Moissan [36] developed a process (Moissan’s process) for producing elemental boron, based on magnesiothermic reduction of boric oxide. The reaction is represented as Eqn. 1.4.

$$B_2O_3+3Mg \rightarrow 2B+3MgO \qquad 1.4$$

During the course of the reaction excess of boric oxide binds with the formed magnesium oxide in the form of borates [37, 38].

$4B_2O_3+3Mg \rightarrow 2B+3MgO.B_2O_3$ 1.5

$4B_2O_3+3Mg \rightarrow 2B+3(MgO.B_2O_3)$ 1.6

This reduction process is highly exothermic and the reaction mixture attains temperature as high as 2813 K [33]. Impurities such as magnesium borides and subborates [39] are the by-products of the process. The process yields amorphous boron (< 92% purity). It is limited by the boron loss in the form of boric oxide vapour due to excess heat generation.

1.9.2.1.2 Metallothermic reduction of boron halides

Boron can be produced by the reduction of its halogenides (BCl_3 and BF_3) by different metals [33 – 35]. Reduction of BCl_3 with a liquid alloy of K-Na at about 673 K yields 98.8% pure amorphous boron [39]. BCl_3 reduction by Zn vapours over the temperature range 1123 – 1223 K was significant due to the absence of stable boride formation [40, 41]. These processes are very expensive and industrially not viable.

1.9.2.1.3 Hydrogen reduction of boron halides

Thermodynamic calculations on hydrogen reduction of boron halides (BF_3 and BCl_3) reveal that the process is endothermic and should be carried out over a very high temperature range 1273 – 2273 K [42, 43].

$BX_3(g) + 1.5\ H_2 \rightarrow B(s) + HX(g)$ 1.7

(X= F, Cl, Br)

BBr_3 is reduced by hydrogen more easily than BCl_3 over the temperature range 1023 – 1123 K. The bromide and iodide of boron are scarce and very expensive. Gaseous mixtures of BF_3 and H_2 were passed over an electrically heated filament (molybdenum, tungsten, tantalum, graphite and titanium) suspended in a pyrex reaction tube [42]. High deposit to filament diameter ratio is obtained with titanium as a core and thus it minimizes metal contamination. Crystalline boron of 99.0 – 99.6% purity could be obtained through this process. Crystallinity appeared to be a function of temperature and filament material.

1.9.2.1.4 Thermal reduction of boron halides

Fine crystalline red α-rhombohedral boron [44, 45] can be formed by thermal decomposition of $BI_{3.}$ Amorphous boron may be formed only as an intermediate phase, which turns crystalline at temperatures above 1273 K. Other crystalline boron modifications can also be formed during thermal decomposition in the arc discharge [46] or on the incandescent tungsten wires [47]. A mixture of polycrystalline and amorphous boron is deposited when tungsten filament is heated at 1473 K [44].

1.9.2.1.5 Thermal reduction of boron hydrides

Amorphous boron of a wide range of purity can be obtained by decomposition of diborane, pentaborane and decaborane over the temperature range 573 – 1173 K [48 – 51]. Decomposition is carried out by passing the gaseous hydride, usually diluted with hydrogen, through a heated quartz tube as well as by heating solid boron hydrides over the temperature range 1073 – 1173 K in boron nitride boats. Pyrolysis of diborane on an incandescent tungsten and tantalum [52] filament results in the formation of boron rods or films of crystalline nature. Diborane has the disadvantage of toxicity, flammability and under some conditions spontaneously explosive.

1.9.2.2 Pyroelectrolysis Process

It is well known that metals residing below manganese in the electrochemical series cannot be electrodeposited from aqueous solutions of their salts [53]. As boron is placed below manganese in the electrochemical series, it cannot be electrodeposited from aqueous electrolytes. Pyroelectrolysis which uses molten salts as electrolytes is the only process suitable for boron deposition. Molten salt electrolysis is used in the primary extraction of metals (electrowinning), purification and recycling of metals (electrorefining) and in the formation of metal coatings (electrocoating). The microstructure of electrodeposited product could be tailored by using molten salt electrodeposition [54].

Electrochemistry of boron is being studied since 1925 [55 – 57]. Electrodeposition of elemental boron from molten salts is the only process available to get high-purity elemental boron. Cooper *et al.* [58, 59] have successfully deposited elemental boron of high purity in plant scale by using a molten salt based electrolysis process containing electrolytic mixture of alkali metal oxides and boron compounds over the temperature range 1023 – 1223 K. Till date various researchers have tried to deposit elemental boron from different boron containing salts [55 – 66]. This molten salt based electrodeposition has been explored by researchers in laboratory scale as well as in industrial scale. There are a number of patents [58 – 65] for this electrodeposition process. These electrochemical deposition processes could be broadly classified into the following categories as represented in Table 1.4.

Table 1.4 Different types of melt systems explored for boron deposition.

Sl. No.	Classification	Melt Constituents	Reference
1.	Electrodeposition from fluoroborate containing melts.	LiF-NaF-KF-KBF_4	[66]
		LiF-KF-KBF_4	[72]
		NaCl-KCl-NaF-KBF_4	[67]
		NaCl-KCl-KBF_4	[67]
		KCl-KF-KBF_4	[68]
		KCl-NaCl-$NaBF_4$	[69]
		BF_3-LiF-KF	[70]
		B_4C-NaCl-KF-KBF_4	[71]
		KBF_4-KCl	[73, 74]
		KI-KBF_4	[75]
2.	Electrodeposition from melts containing a mixture of boric oxide and fluoroborate.	KF-KBF_4-B_2O_3	[59]
		KCl-KBF_4-B_2O_3	[59]
		K_2CO_3-B_2O_3-KBF_4	[61]
		Na_2CO_3-$NaBF_4$-B_2O_3	[61]
		HPO_3-$NaPO_3$-NH_4BF_4-B_2O_3	[64]
		B_2O_3-KBF_4	[76, 77]
		KBF_4-KCl-KHF_2-B_2O_3	[78]
3.	Electrodeposition from boric oxide containing melts.	LiF-KF-B_2O_3	[72]
		KCl-KF-B_2O_3	[65, 79]

When oxygen containing melts are used the process does not give high purity boron [72] for the product is contaminated by substantial amount of oxygen. The use of fluoride electrolytes is limited because these melts are corrosive and toxic.

The use of mixed chloride–fluoride melts presents considerable interest as high purity boron free from oxygen impurity can be obtained at relatively lower temperatures (melt is relatively less corrosive). The stability of BF_4^- in molten alkali chloride increases in the following order LiCl< NaCl< KCl [69].

Miller [68] has reported the electrodeposition of boron from KCl-KF-KBF_4 melt (70wt% KCl, 12 wt% KF and 17.8 wt% KBF_4) over the temperature range 1023 – 1073 K. This author has described the overall reaction with the help of Eqn. 1.8 which involves the simultaneous evolution of Cl_2 and F_2.

$$0.5KCl + KBF_4 \rightarrow B + 1.5KF + 0.25Cl_2 + 1.25F_2 \tag{1.8}$$

The electrodeposition was carried out on a monel cathode and a fine grained graphite crucible was used as a container for the melt as well as the anode. Electrolysis was carried out at a current density of 80 A/dm^2 and at 5 – 6 V DC supply. The current yield was about 74% with a consumption of about 55 $kWh^{-1}kg^{-1}$. Boron was deposited on monel cathode with the evolution of chlorine on graphite anode. After processing the deposit a 94 - 96% purity product was obtained. The effects of anode, cathode material and salt impurities on boron yield as well as drying conditions were also investigated.

Nelson *et al.* [61] have used a fused salt containing boric oxide, alkali metal fluoroborates and alkali metal oxides (K_2CO_3 or Na_2CO_3) over the temperature range 1023 to 1148 K. Sodium and potassium oxide salts could be used effectively in the process. The merits of the process are:

i) Chlorine gas is not evolved at anode.

ii) Potassium salts are not essential for the process.

iii) Sodium salts are less hygroscopic.

iv) Sodium salts are less corrosive.

Ellis [64] has used various phosphate mixtures as electrolytes for the deposition of boron at a relatively lower temperature of 523 K. The electrolyte constituted HPO_3 (80 wt%), $NaPO_3$ (15 wt%) and NH_4BF_4 (5 wt%) in 185 g melt. About 7 g of B_2O_3 was added in the melt at 523 K and electrolysis was carried out using copper as the cathode and graphite as the anode. Deposition was carried out at a potential of 2 V for 3 h.

Kahlenberg [55] has studied various melts containing (NaCl, KCl, $CaCl_2$, KF, K_2CO_3 and K_2SO_4) which have B_2O_3 solubility. A melt containing KCl-KBF_4-B_2O_3 was found to be suitable for boron electrodeposition. However poor miscibility, low conductivity, corrosion of electrodes and contamination of the product were major hurdles for the industrial utilization of the process.

Nies *et al.* [65, 80 – 81] have developed a process for the electrodeposition of 97.5% pure boron on a steel cathode, in fairly large quantities by the electrolysis of B_2O_3-KCl-KF at 1123 K. The melt was contained in a graphite crucible. These authors [65] have emphasized on the alkalinity of the melt to the product purity and yield. Gaseous HCl and HF at the melt temperature were used to maintain the pH in the range of 4.5 to 7.5. They have also suggested that the melt should be devoid of KCl such that the alkalinity of the bath was controlled.

Jain *et al.* [82 – 84] have reported that elemental boron powder with a purity of 95 - 99% could be produced by electrodeposition from KCl-KF-KBF_4 melt (70wt% KCl, 12 wt% KF and 18 wt% KBF_4) on mild steel cathode at 1073 K [82]. The electrodeposit was found to be an amorphous mass of B with distinct β-rhombohedral crystallites of B embedded in it. In the molten salt medium B particles grew on the surface of the mild steel cathodes as spheres and the spherical morphology was found to be uniform throughout the particle [82 - 84].

A meaningful study of the electrodeposition of boron from melts is a challenge due to the higher operating temperature. A good understanding of the electrochemical process requires electroanalytical studies on the melt systems. Electroanalytical studies involve a three electrode system consisting of working, reference and counter electrodes. Redox potentials are obtained with respect to the reference electrode.

1.9.3 Reference electrode

It is difficult to find a suitable reference electrode for chloride-fluoride and fluoride melts [85]. Several attempts have been reported towards the development of a reference electrode suitable for use in these melt systems, allowing accurate electrochemical measurements. Some reference electrodes suitable for molten fluorides have been suggested in the literature [85 – 87]. Different reference electrodes such as Ni/Ni^{2+} with a LaF_3 diaphragm [88], Ag/Ag^+ [89] and a dynamic chlorine electrode [90] have been used in the study of melts containing KBF_4. Many difficulties were encountered in using these electrodes that include contamination of the melt by the constituents of the material of construction [91], viz., porous oxide diaphragms [91] or the electrode metal [69]. In the dynamic chlorine electrode the fluoride ions present in the mixed chloride-fluoroborate melt was found to affect the equilibrium potential [92]. Freon evolution due to the reaction between fluorides and graphite (used as a cathode) as well as the presence of Cl_2 in the melt affected the formation of the complex and redox equilibria in these reference electrodes [92]. Polyakova *et al.* [93], have studied an Ag/AgCl reference electrode. This reference electrode comprised a silver wire immersed in molten AgCl-KCl-NaCl (2 wt% AgCl in equimolar NaCl-KCl), enclosed in an alumina tube. This assembly was in turn held in a glassy carbon tube containing NaCl-KCl melt. The latter was fitted with a graphite diaphragm at its lower end. The portion of the alumina tube in the hot zone above the melt exposed to the electrolyte vapour reacted with the latter and contaminated the melt. Coriou *et al.* [94] have described an Ag/Ag^+ reference electrode suitable for use with chloride-fluoride melts at 1123 K. This electrode consisted of a silver wire immersed in molten AgCl contained in a fused silica tube and in equilibrium with molten NaCl (contained in a graphite outer casing) through a porous barrier. This electrode was found to be reversible and yielded a reproducible emf in molten NaCl at 1123 K. However the suitability of this electrode for use with a melt containing chloride and fluoride has not been reported so far. Often the use of a quasi-reference electrode could help overcome some of the difficulties described above [90]. However a quasireference electrode cannot be used to generate accurate values of the equilibrium half cell potentials for the latter would be influenced by the composition of the melt. Hence, there is a need to develop a suitable reference electrode for studying chloride-fluoride melts.

1.9.4 Electroanalytical studies on boron containing melts

The electrochemical behaviour of boron in various melt systems has been studied by various researchers using electroanalytical techniques. The mechanism of cathodic boron deposition in fluoride and fluoride-chloride melts has been studied extensively. The electroreduction of KBF_4 in molten eutectic mixture of LiF-NaF-KF as reported by Brookes *et al.* [66] and Makyta *et al.* [72], followed a single-step reversible three-electron reduction process. Later Makyta *et al.* [95] reported that boron reduction in this eutectic mixture occurred reversibly upto a polarization rate of 1.0 Vs^{-1} and became quasireversible at a higher polarization rate. Using LiF-KF-NaF (FLINAK) melt, Polyakova *et al.* [96] reported that the deposition of boron from BF_4^- on a silver electrode was accompanied by an irreversible three-electron transfer process. Cyclic voltammetric measurements of FLINAK melt on silver electrode had a wide electrochemical window. The electroreduction of boron from fluoroborate salt in an equimolar mixture of NaCl-KCl was assumed [97, 98] to involve a preceding reaction of complex dissociation, which resulted in the formation of fresh electrochemically active species in the form of boron trifluoride. The LiF-KF-KBF_4 system [99] showed a similar reduction involving three-electron. LiF-KF-B_2O_3 system [72] gives rise to BF_4^- and an unspecified oxofluoro complex(es) with a mean oxygen to boron ratio of 1.66. Kuznetsov [67] has studied the electroreduction of BF_4^- complexes on silver and glassy carbon electrodes in NaCl-KCl and NaCl-KCl-NaF melts. The electroreduction of boron complexes was reported to follow a three-electron irreversible process. An excess fluoride ion in the melt restricts the evolution of BF_3 and stabilizes the melt. If the condition $[B^{3+}]:[F^-] < 1:2$ is fulfilled in the melt, the rate of BF_4^- reduction remains unchanged indicating the stability of the melt [67, 69]. The transfer and diffusion coefficient of BF_4^- were found to be similar in case of silver and glassy carbon electrodes. Cyclic voltammetry (CV) indicated the formation of B_4C due to cathodic incorporation of boron on glassy carbon electrode but Taranenko *et al.* [69] did not observe the formation of B_4C using glassy carbon electrodes. Kuznetsov [67] pointed out that the use of chloride-fluoride melt made the peak potential shift to a more negative value and decreased the value of diffusion coefficient because of an increase in the basicity of the melt. In the melt KCl-NaCl-NaF (5 wt%)-KBF_4 (0.2 – 2×10^{-4} mol cm^{-3}) the KBF_4 concentration was reported [67] to be virtually constant for several hours. In a typical CV of the melt two peaks were observed in the anodic cycle whereas only one peak was observed in the cathodic cycle. This behavior was described by the author [67] as during cathodic polarization the near-electrode space contained an excess of F^- ions. The presence of excess fluoride ions was due to the cathodic process (Eqn. 1.9) followed by the exchange reaction (Eqn. 1.10) as depicted below.

$$BF_4^- + 3e \rightarrow B + 4F^- \qquad 1.9$$

$$BF_3Cl^- + F^- \leftrightharpoons BF_4^- + Cl^- \qquad 1.10$$

Appearance of multiple peaks during anodic polarization was due to the lack of fluoride ions in the near electrode space which resulted in the dissolution of boron within heteroligand complexes.

The reduction of B(III) in NaCl-KCl was studied by Taranenko *et al.* [69] within the MBF_4 (M = Na, K) concentration range of 3×10^{-5} to 8×10^{-4} mol cm^{-3}. The voltammograms were recorded on a glassy carbon electrode at 973 K. The reduction potential of B from B(III) involving a single-step three-electron transfer process was reported to start at a potential of about -2.35 V with respect to a Ag/AgCl reference electrode. The peak potentials were found to shift towards negative potential with increasing scan rates above 0.1 V s^{-1}. The difference between the cathodic and anodic peak potential was found to vary between 0.7 to 1.1 V at different scan rates. The redox peak current density was observed to decrease with time. It thus indicated the decrease of concentration of the electrochemically active species in the melt. This was explained by the authors as a result of chemical reaction of tetrafluoroborate with the chloride melt and (or) the thermal decomposition of tetrafluoroborate. According to Danek *et al.* [100], the dissolution of KBF_4 was supposed to follow the exchange reaction.

$$4MCl + KBF_4 \rightleftharpoons 4MF + KBCl_4 \qquad 1.11$$

The $KBCl_4$ thus formed could again decompose according to Eqn. 1.12.

$$KBCl_4 \rightleftharpoons BCl_3\uparrow + KCl \qquad 1.12$$

The stability of BF_4^- anions in molten alkali chlorides was reported to increase as LiCl < NaCl < KCl due to the strong polarizing effect of the cation ($Li^+ > Na^+ > K^+$) [69]. Decomposition of BCl_4^- ions was not observed in NaCl and KCl melt systems. It was assumed that MBF_4 thermally decomposed to gaseous BF_3 according to Eqn. 1.13.

$$MBF_4 \rightleftharpoons BF_3\uparrow + MF \qquad 1.13$$

From thermodynamic analysis it was inferred that addition of F^- ions to the chloride melts shifted the equilibrium of Eqns. 1.11 and 1.13 to the left and consequently suppressed the decomposition of the electrochemically active species. Thus chloride-fluoride supporting electrolyte was better suited compared to pure chloride melts.

The electrodeposition of boron from LiF-NaF-KF–KBF_4 melt was studied in detail by Polyakova *et al.* [96]. At low KBF_4 concentrations ($<5.7\times10^{-2}$ mol%) the cathodic process was shown to proceed irreversibly. At higher concentrations B(III) electroreduction was dictated by the surface ohmic control.

The mechanism of electroreduction and nucleation process of B on platinum electrode was studied by Jun *et al.* [99] using CV and chronoamperometry in a melt containing LiF, NaF, KF and KBF_4 at 973 K. This reduction process involved a three-electron reversible step. The nucleation process was reported to follow instantaneous nucleation confirmed through chronoamperometry studies.

1.9.5 Determination of oxide ion in melts

Industrial metallurgical extraction processes using high temperature molten salt as electrolytes are influenced by the oxide ion content in the electrolytes at the operating conditions [101, 102]. According to White [103], among various methods for oxide determination, linear sweep voltammetry (LSV) is probably the most acceptable technique. Potentiometric titration of oxide ions in chloride melts using Yttria Stabilized Zirconia Electrode (YSZE) was proposed by several authors [104 – 108]. In mixed chloride-fluoride melts the YSZE could not be used because of the instability of ZrO_2 and Y_2O_3 in these media.

Polyakova *et al.* [109] have carried out voltammetric studies using glassy carbon electrode to determine the concentration of oxide ion in CsCl-KCl-NaCl eutectic melt. These authors have reported a two-step anodic process for the oxidation of oxide ions in the melt. The mechanism of electrode process and some kinetic parameters have also been established. Similar observations have also been reported by Nekrasov *et al.* [110] for oxochloride melts. Barbin *et al.* [111] have reported a detailed study on the physicochemical and electrochemical behaviour of oxide in NaCl-KCl-Li_2O melts. The anodic process on a glassy carbon electrode in the said oxide-chloride electrolyte was studied using linear sweep voltammetric method. Electrochemical and diffusion parameters characterizing the electrode process were also evaluated.

1.9.6 Determination of electroactive species in KCl-KF-KBF_4 melts

Miller [68] electrodeposited boron from a melt containing KCl (70 wt%),

KF (12 wt%) and KBF_4 (17.8 wt%) in the temperature range 1023 – 1073 K. This author described the overall electrochemical reaction based on the composition of the electrolyte and analysis of the effluent gas (Eqn. 1.8) and proposed that Cl_2 and F_2 evolved simultaneously during the electrodeposition. However the actual composition of the effluent gas and its time dependent variation with the progress of the electrodeposition were not described by this author. Further, this author had stated vividly that the electrode processes pertaining to his experiments had not been resolved [68].

Nair *et al.* [71] carried out electrodeposition of boron from a melt containing KCl (70 wt%), KF (12 wt%) and KBF_4 (18 wt%) at 1073 K and proposed a reaction mechanism similar to the one reported by Miller [68].

IR emission spectroscopy of melts has been utilized for establishing the ionic species in the melt by Bezarashvili *et al.* [112] and Solovev *et al.* [113]. These investigators employed custom made attachments and cells for high temperature IR investigations of a molten mixture of $NaCl$, KCl and KBF_4. They reported this system to be comprised of the species BF_4^-, BCl_4^- and $[BF_{4-n}Cl_n]^-$ (n = 1 - 3). These authors arrived at the conclusion that the concentration of BF_4^- in the melt increased with an increase in KBF_4 concentration. The concentration of the “chloride-fluoride” complexes $[BF_{4-n}Cl_n]^-$ was found to increase with temperature [112]. Shapoval *et al.* [114, 115] have described the composition of the melts $KCl - KF - KBF_4$ and $KCl - NaCl - KBF_4$. These authors have also suggested a scheme for the formation of the electrochemically active species ($[BF_{4-x}Cl_x]^-$ and $[BF_{4-x}]^{x-1}$ where x= 1 - 3). Danek [116] established (through IR spectroscopy) the substitution of a fluoride ion by a chloride ion in the co-ordination sphere of the BF_4^- anion in $KCl - KF - KBF_4$

melts. However, the author [116] did not obtain any other evidence for the existence of these mixed anions through other methods. From these experiments it is evident that the actual processes involved in the electrodeposition of B from $KCl - KF - KBF_4$ are yet to be understood.

1.9.7 Context of the present work

Sufficient experimental information on the electrodeposition of boron from KCl-KF-KBF_4 melts is not available for the complete understanding of the system. Extensive research has not been carried out on KCl-KF-KBF_4 melts which is an electrolyte for the electrodeposition of boron. A systematic study on other alkali metal fluoroborates in KCl-KF melt also has not been reported yet. The electrochemistry and the mechanism behind the deposition of boron from these melts are yet to be completely understood. Thus there is a significant scope for electroanalytical studies related to the deposition of boron from alkali metal fluoroborates in KCl-KF melt.

1.9.8 Objective of the present study

The effective control of any electrochemical process is feasible only through acquiring knowledge of the structure and properties of the electrolyte and mechanism behind the electrochemical processes involved.

An electrochemical process can be analyzed by employing electroanalytical techniques involving a three electrode system consisting of a working, reference and counter electrode. The values of the electrochemical potential of the redox process are obtained with respect to the reference electrode. Development of a suitable reference electrode is necessary to study the electrochemistry of deposition of boron from chloride-fluoride melt systems.

Electrodeposition of boron from molten salts is yet to be understood fully. In spite of a large number of reports published on the electrochemical properties of boron, clear understanding of the mechanism and kinetics of the electrodeposition of boron from halide electrolytes has not been evolved. Studies related to the electrokinetic parameters such as electron transfer coefficient, electron transfer rate constant, diffusion coefficient and nucleation of the electroactive species would draw some more insight into the process. These electrokinetic parameters for the electrodeposition of boron from KCl-KF-KBF_4 melts at different temperatures and composition of melts are reported in this study.

The presence of oxide ions affects the quality of deposition of any element. For industrial applications it is extremely difficult to prepare a melt free from oxide ions. Periodic monitoring of oxide ion content of the melts during the process is of great industrial importance. Preferably an on-line monitoring of the oxide content is highly desirable. Electrochemical detection of the oxide ion in melts was explored for on-line monitoring.

The concept of complexation in molten salt mixtures is supported by a series of spectroscopic investigations. The progress of the electrowinning of boron from the melt $KCl - KF - KBF_4$ would be influenced by the nature of the complex boron containing electroactive species. Based on the type of complexes existing in the melt during the electrodeposition process, a plausible scheme of reaction(s) that is consistent with the experimental observations was elucidated for better understanding of the process.

1.9.9 Overview of the doctoral work

The organization of the chapters in the thesis and its brief contents are presented below.

Chapter II: Experimental techniques, principle and procedure

Chemicals, fabrication of the electrochemical cell, construction, validation of the reference electrode and experimental methods employed in this study for the deposition of boron from alkali metal fluoroborates in KCl-KF melt are explained. Brief description of various analytical methods and tools such as cyclic voltammetry, linear sweep voltammetry, chronoamperometry, emf technique, X-ray diffraction, scanning electron microscopy (SEM), inductively coupled plasma-mass spectrometry (ICP-MS) and chemical analyses by ion-selective electrodes are presented in this chapter.

Chapter III: Results and discussion

The performance of the Ag/AgCl reference electrode developed in this study for use in chloride-fluoride melts and the electrochemistry of deposition of boron from KCl-KF-MBF_4 (M= K and Na) melts studied by cyclic voltammetry, chronoamperometry and convolution voltammetry at different temperatures are described in this chapter. Linear sweep voltammetric studies carried out to determine the concentration of oxide ion in KCl-KF melts are also elaborated. A plausible scheme of reaction(s) that governs the electrodeposition of boron from melts containing KCl, KF and KBF_4 (at 1073 K) is described on the basis of analyses of the melts.

Chapter IV: Conclusions

Important findings and results obtained by carrying out the above mentioned experiments are summed up in this chapter.

Chapter V: Scope of future studies

This chapter describes the scope for future studies that include the determination of phase diagram of the system KCl-KF-KBF_4 by various experimental techniques, speciation in KCl-KF-KBF_4 system by NMR spectroscopy, TG-DTA analysis of the KCl-KF-KBF_4 condensed phase in conjunction with mass spectrometric analysis of the gas phase and electrochemical synthesis of refractory borides.

CHAPTER II

2.0 Experimental techniques, principle and procedure

Chemicals, electrochemical cell, construction of the reference electrode and various experimental methods adopted in the present study are discussed in this chapter. The handling and purification of salts for the preparation of the melts is detailed. A brief description of various analytical methods and tools such as X-ray diffraction, SEM, ICP-MS and chemical analysis by using ion-selective electrodes are presented. A detailed description of instrumentation for the voltammetric measurements and the electrochemical transient techniques employed in the present study are also presented.

2.1 Materials and chemicals used

All the reagents used in this study were of analytical grade. AgCl (99.998% purity) was procured from M/s. Alfa Aesar, Lancashire, UK. Silver wire (99.99% purity 1 mm diameter) and nickel wire (99.99% purity 1 mm diameter) were obtained from M/s. Goodfellow Metals Inc., UK. Platinum wire (1mm dia, 99.99% purity) was procured from M/s. Sevantilal Mahasukhlal, Mumbai, India. KCl (99.5% purity), KBF_4 (99% purity) and KF (99% purity) were supplied by M/s. Loba Chemie, Pvt. Ltd., Mumbai, India. $NaBF_4$ (> 98% purity) was obtained from M/s. Sigma Aldrich, USA. High-density (1.85 g cm^{-3}, grade G347) graphite was procured from M/s. Purelec India Pvt. Ltd., Pondicherry, India. Fused silica tubes (99.9% pure) that formed the body of the reference electrode was obtained from M/s. ILE Co., Chennai, India. A porous graphite plug (30% porosity, 1.6 g cm^{-3} density, grade GLM50) was supplied by M/s. Graphite India Ltd., Nasik, India. Torr seal® was obtained from M/s. Varian Vacuum Technologies, USA. Iron wire (99.9% purity, 3 mm diameter) was obtained from M/s. Mishra Dhatu Nigam Ltd., Hyderabad, India.

Inconel 600 (99.9% purity) which formed the structural material of the electrochemical cell was supplied by M/s. Kalapurna Engineering, Mumbai, India. Stainless steel (SS) flanges were procured from M/s. M. S. Enterprises, Secunderabad, India.

2.2 Description of the electrochemical cell for the laboratory scale experiments

The electrochemical cell (Fig. 2.1 and Fig. 2.2) essentially consisted of a cylindrical inconel retort (OD: 89 mm, ID: 82 mm and height: 300 mm) made out of inconel 600. This one-end-closed inconel retort was provided with a SS knife edge flange (CF 100) at the other end. A high-density graphite crucible (OD: 80 mm, ID: 60 mm and height 295 mm) (Fig. 2.3) was used as a container for ~200 g of molten salt. This crucible was the anode and was placed inside the inconel retort. The height of the graphite crucible was equal to the height of the inconel vessel in order to prevent the corrosion of the inconel retort by salt vapours. An air-cooled SS knife edge flange (CF 100) with provision for inlets for the working as well as the reference electrodes, vacuum degassing port, argon inlet and an outlet for gaseous products was placed on the inconel retort. A copper gasket was placed between the two flanges for leak tightness of the vessel. The temperatures of the cell and the furnace were monitored by K type thermocouples. The difference between the temperature of the cell and the furnace was found to be about 2 K. During the actual experiments this temperature difference was taken into consideration. Forced air cooling of the flange was essential to maintain the skin temperature of the cell below 313 K.

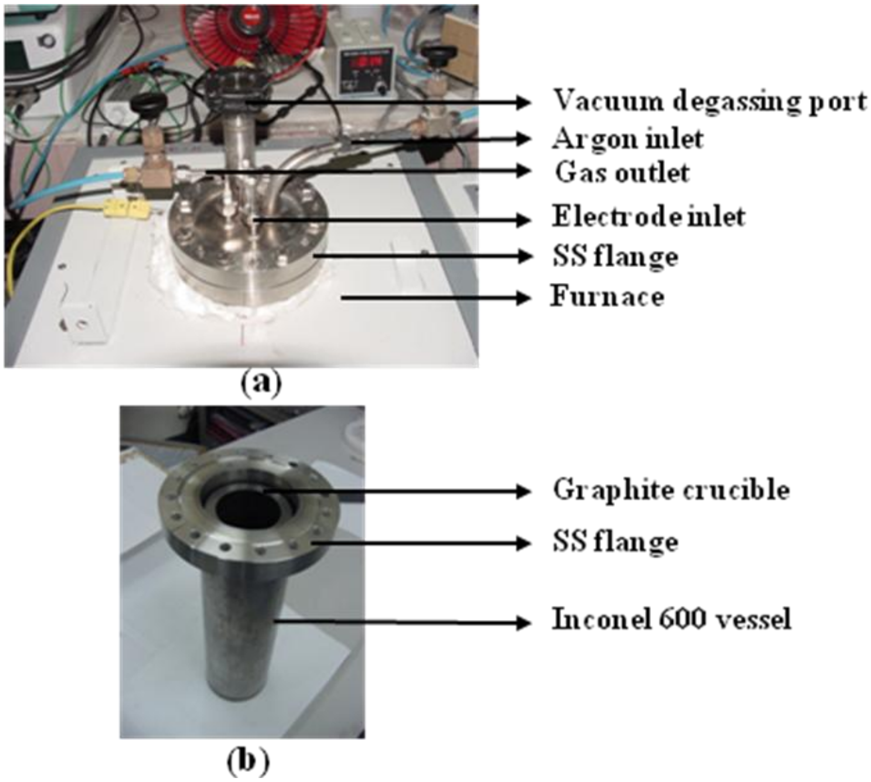

Fig. 2.1 Photograph of the electrochemical cell assembly: (a) Top flange with fittings (b) Inconel 600 retort.

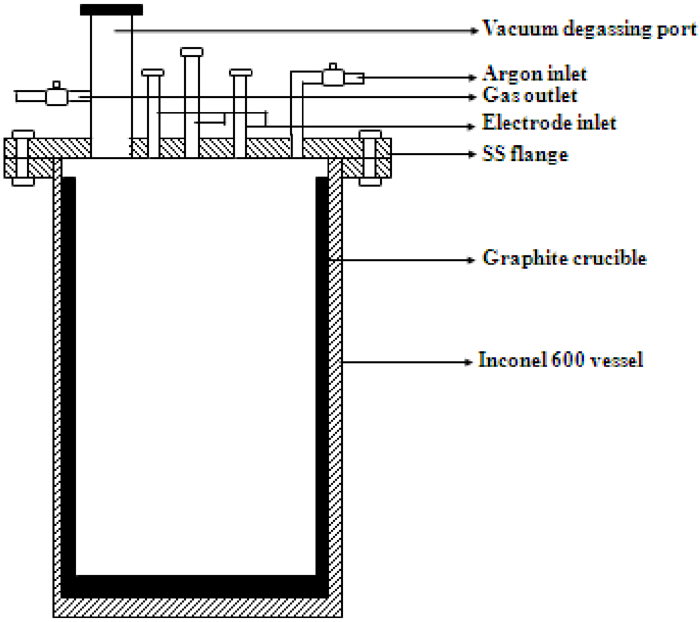

Fig. 2.2 Schematic of the electrochemical cell assembly.

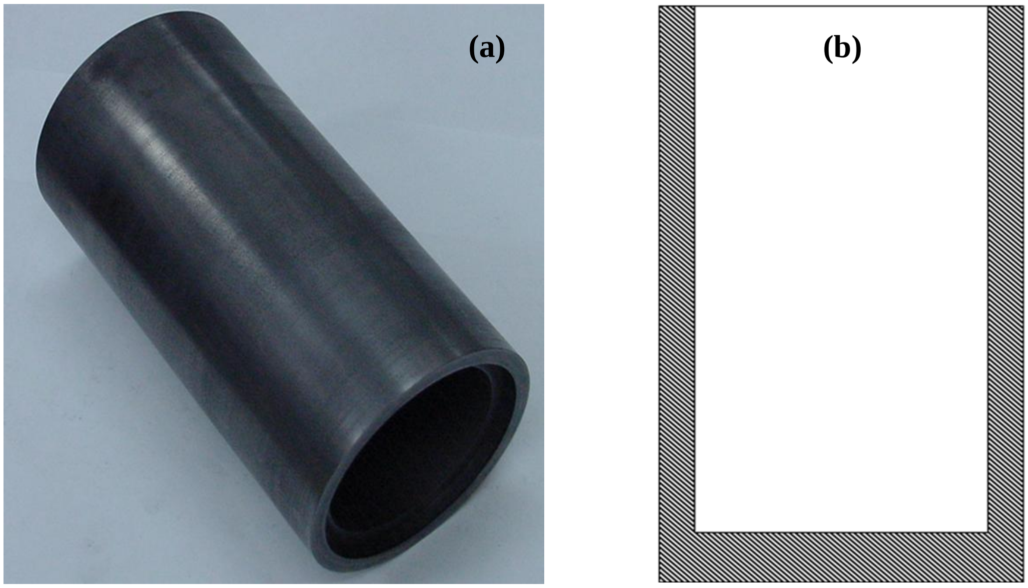

Fig. 2.3 High-density graphite crucible: (a) Photograph and (b) Schematic.

2.3 Construction of the Ag/AgCl reference electrode

The reference electrode essentially comprised of a fused silica tube filled with silver chloride into which a silver wire was inserted. This tube was closed at the bottom with a 5 mm thick graphite sleeve. The top end of this tube was closed with a high vacuum sealant (Torr seal®). This assembly in turn was placed inside a (100 mm long) high-density graphite tube provided with a threaded porous graphite plug at the bottom containing vacuum dried KCl. This graphite outer casing served as a protective sheath for the fused silica tube (Fig. 2.4). The top portion of the fused silica tube was covered with another graphite tube (about 120 mm long) in order to protect it from fluoride vapours. AgCl and KCl powders were filled into the electrode compartments inside an argon atmosphere glove box at room temperature.

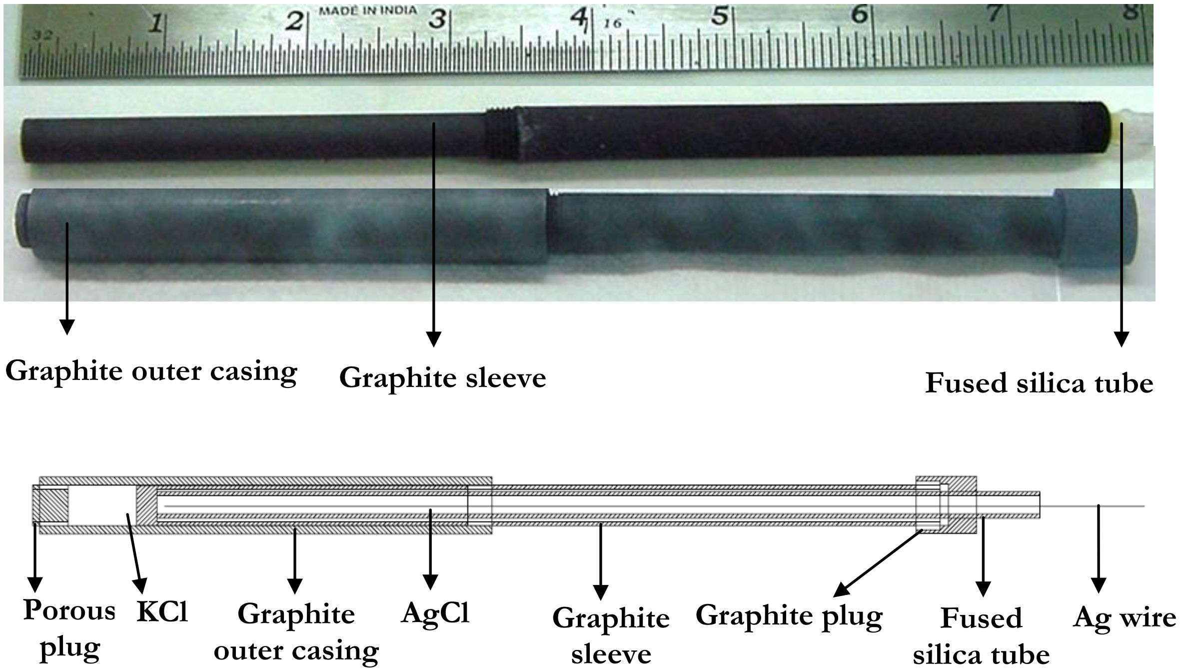

Fig. 2.4 Reference electrode assembly with schematic.

2.4 Glove box

KCl, KF, KBF_4, $NaBF_4$ and Na_2O salts absorb moisture. On exposure to moist air these salts become deliquescent. These salts are handled in a high-purity inert atmosphere (argon) glove box. The glove box is a cubical box made of stainless steel and provided with laminated safety glasses for viewing. The box is designed to be leak tight. Glove ports fitted with butyl rubber gloves with neoprene “O” ring seal are arranged laterally on both sides of the box. Material movement into the glove box is allowed through a transfer port, which is filled with argon gas. A photohelic gauge is used for automatic filling and venting of argon in and out of the glove box thus maintaining the pressure of the glove box between the set limits. The box is maintained at a positive pressure of 2 - 4 mbar of water column restricting entry of air into it.

2.5 Melt preparation for laboratory scale experiments

2.5.1 Melt preparation for validation of Ag/AgCl reference electrode

KCl was pre-dried under flowing argon for 48 h at 393 K and then vacuum dried for 48 h at 393 K. KF was vacuum dried for 48 h at 503 K. A 172 g charge of vacuum dried KCl (81.54 mol%) and KF (18.45 mol%) was poured into the cell at 548 K under argon flow. In-situ vacuum (3×10^{-3} mbar) degassing of the salt mixture was carried out for 12 h at 548 K. A liquid nitrogen cooled moisture trap (Fig. 2.5) was used along with the vacuum system for vacuum degassing of salts. The vacuum dried salt mixture was then heated (pit type kanthal resistance furnace) to 1073 K, under flowing high-purity argon, at a heating rate of 3 K min^{-1}.

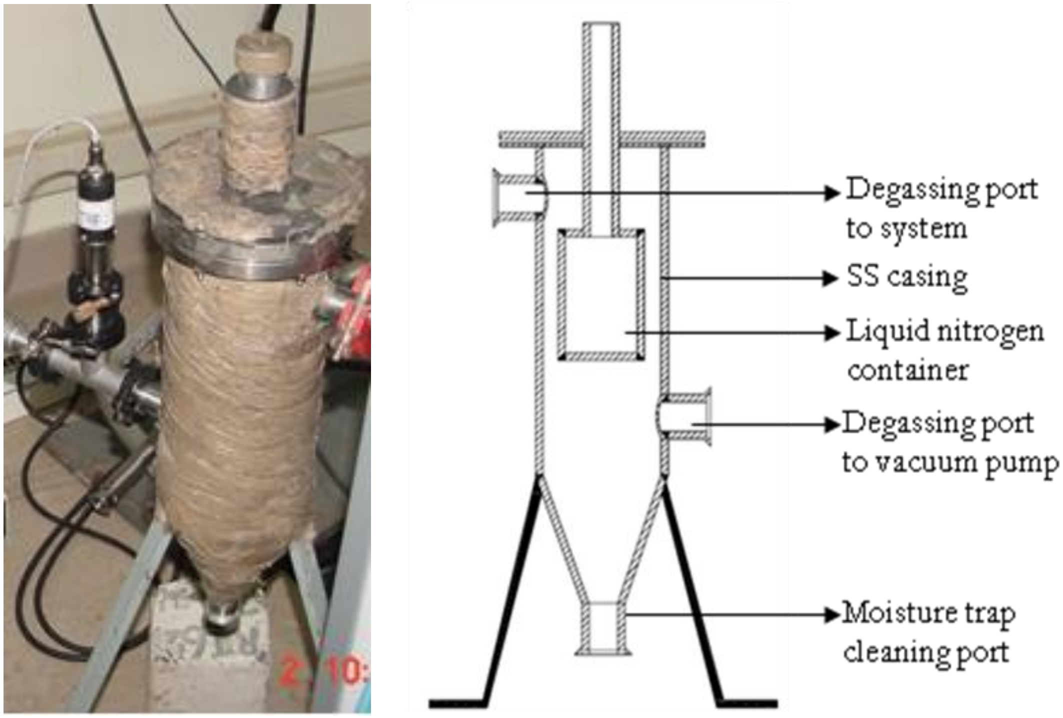

Fig. 2.5 Liquid nitrogen moisture trap with schematic.

2.5.2 Melt preparation for studies on electrodeposition of boron from fluoroborate melts

Drying of KCl and KF salts were performed as mentioned in Section 2.5.1. KBF_4 salt was pre-dried under flowing argon for 48 h at 393 K and then vacuum dried for 48 h at 393 K. Melts containing 1.6×10^{-4}, 4.1×10^{-4} and 7.73×10^{-4} mol cm^{-3} of KBF_4 in KCl-KF were prepared. Required amounts of KBF_4 were added in a 172 g of KCl-KF charge for preparing the above mentioned compositions. Required amount of $NaBF_4$ was added into 172 g of KCl-KF melt for the preparation of 1.67×10^{-4} mol cm^{-3} of $NaBF_4$ melt.

2.5.3 Melt preparation for studies on the determination of oxide ion

Melt preparation was similar as stated in Section 2.5.1. Sodium oxide samples required for the experiments were weighed and sealed in polypropylene ampoules inside a glove box filled with high-purity argon. These samples were added into the melt under argon flow. The melt was equilibrated at the temperature of measurement for 0.5 h after each additions of Na_2O.

2.6 Description of the electrochemical cell used for the large-scale synthesis of boron

The electrowinning cell (Fig. 2.6) essentially consisted of a cylindrical retort (OD: 273 mm, height: 710 mm) made out of inconel 600. A liner made out of nickel was placed inside this vessel. A high-density graphite crucible (OD: 240 mm, height 300 mm) was used as the container for ~12 kg of molten salt and also as the anode. This crucible in turn was placed inside the nickel liner. In order to protect the upper portion of the nickel liner from corrosion, a graphite liner was placed on top of the crucible such that it completely covered the internals of this liner.

A cooling collar was placed over the inconel retort. A water-cooled top flange having provisions for an inlet for the mild steel cathode, a sight port, argon inlet and an outlet for gaseous products was placed on the cooling collar. The circulation of chilled water through the collar and flange is essential in order to maintain the skin temperature below 313 K.

Boron was electrodeposited on a mild steel, “cruci-form” cathode. In order to facilitate its immersion into the melt and subsequent withdrawal, the cathode was connected to a long shaft made of nickel. This shaft was introduced into the retort through a hermetically sealed feed through provided on the top flange. The electrolysis was initiated by lowering and dipping it into the molten salt. In order to avoid high temperature gas phase corrosion of the mild steel cathode, its upper portion was covered with a protective sleeve made out of high-density graphite. This retort assembly was lowered into a “pit type” (pit type nichrome resistance furnace manufactured by M/s. Hightemp Industries, Kochi, India) furnace such that most of it, excepting the cooling collar was located inside the pit.

2.7 Process for the large-scale synthesis of boron

KCl and KBF_4 salts were pre-dried under flowing argon for 48 h at 393 K and then vacuum dried for 48 h at 393 K, while KF was vacuum dried for 48 h at 503 K. A charge of about 6 kg of vacuum dried salt mixture (KCl (4.2 kg), KF (0.72 kg) and KBF_4 (1.08 kg)) was poured into the cell at 548 K under flowing argon. In-situ degassing of this salt mixture was then carried out for 12 h at 548 K by using a rotary vacuum pump (0.3 Pa vacuum) coupled with a cryogenic moisture trap maintained at the boiling point of liquefied N_2. The dried salt mixture was then heated under flowing argon at a rate of 3 K min^{-1} to 1148 K. In order to ensure the complete melting of the salt mixture, the same was held at this temperature for about 2 h and then cooled to 548 K. Subsequently yet another (6 kg)

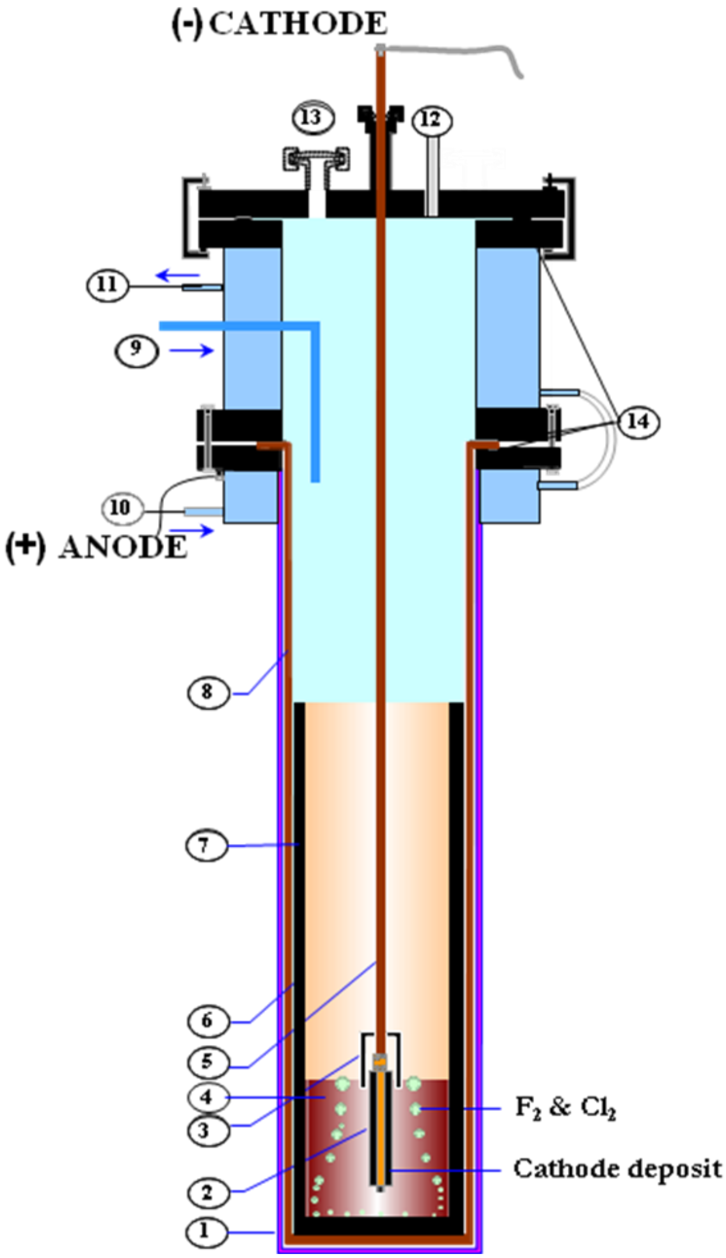

1. Inconel vessel
2. Mild steel cruciform cathode
3. Protective graphite cup
4. Molten salt
5. Nickel cathode shaft
6. Graphite crucible (Anode)
7. Graphite sleeve
8. Nickel liner
9. Argon inlet
10. Cooling water inlet
11. Cooling water outlet
12. Argon outlet
13. Sight port
14. Gaskets

Fig. 2.6 The electrowinning assembly [82, 83].

charge was loaded into the crucible and the same sequence of operations described above was repeated. After the consolidation of the charge, the same was maintained at 1073 K. A mild steel cathode was dipped into it and pre-electrolysis was carried out at 1.5 V (by using a DC power supply manufactured by M/s. Digitronics, Pune, India) until the cell current reached a value below 1 A. A fresh mild steel cathode was then lowered into the melt. The cell voltage was increased from an initial value of 1.5 to 3.5 V with an increment of 6.6×10^{-4} Vs^{-1}**.** After it attained a value of 3.5 V the cell voltage was increased to 4.5 V with an increment of 3.3×10^{-4} Vs^{-1}**.** The cell voltage was maintained at 4.5 V for 6 h in order to facilitate the electrolysis. After carrying out three such electrodepositions a "make-up" charge containing KCl (2 kg) and KBF_4 (1.12 kg) was added to the solidified salt mixture at 548 K. After vacuum degassing and melting this replenished charge, two more electrodepositions were carried out. Another "make-up" charge containing KCl (2 kg) and KBF_4 (1.12 kg) was then added to the solidified salt mixture at 548 K. Two more electrodepositions were carried out subsequently after vacuum degassing and melting. Each electrodeposition was carried out for 6 h. After each of these, the cathode was withdrawn from the melt and was held at a certain height above the melt inside the cell and allowed to cool under flowing argon. The cathode along with the deposit was subsequently quenched by immersion in water. The quenched deposit was washed with water and stored in 0.2 N HCl solution. Each deposit contained ~54 g of elemental boron, indicating the rate of boron deposition to be 9 g h^{-1}. The process flowsheet is depicted in Fig. 2.7.

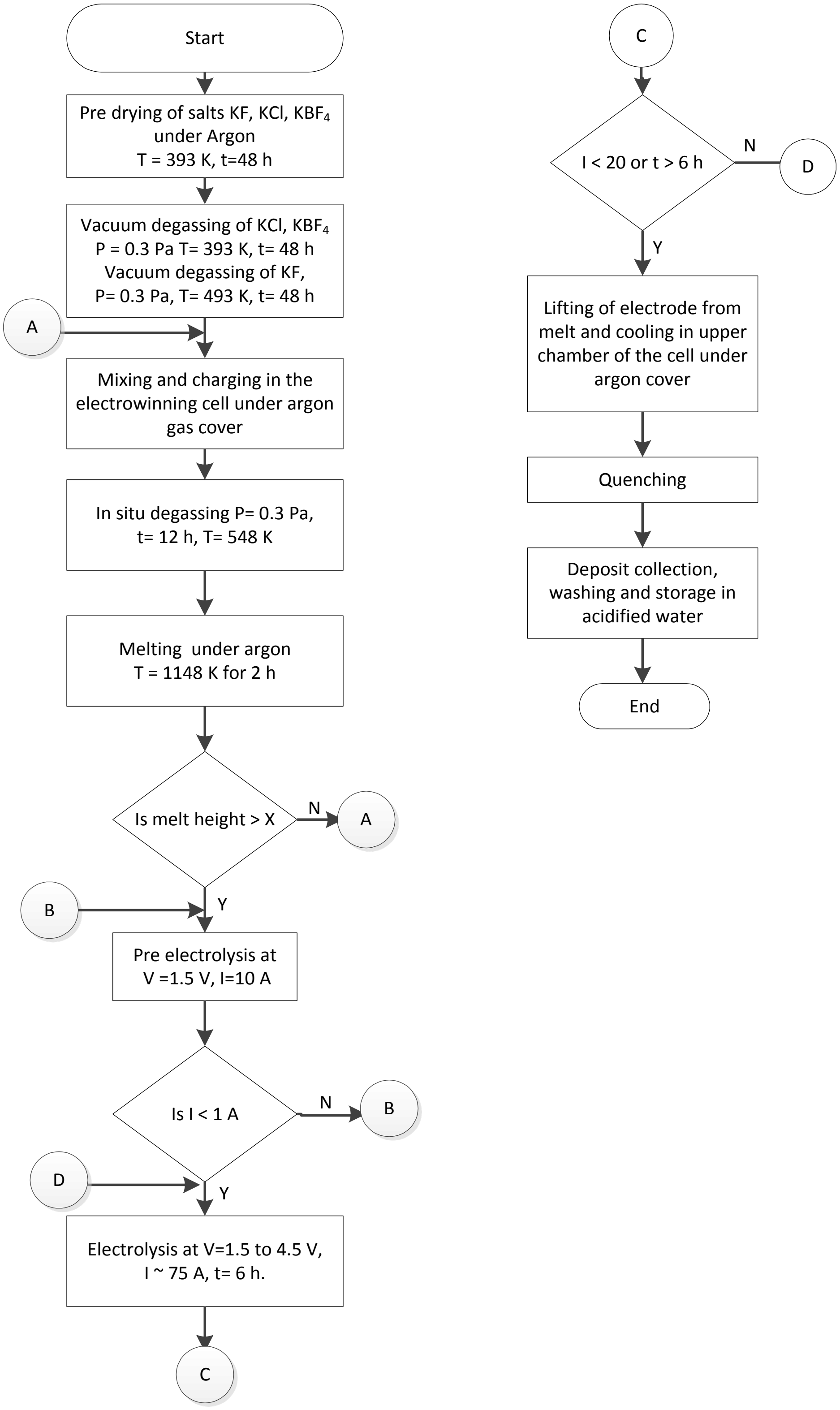

Fig. 2.7 Flowsheet depicting the elemental boron electrodeposition process [82, 83].

2.8 Elucidation of electrode process using three electrode system

The electrode processes can be broadly classified as faradaic and nonfaradaic processes. The process in which charge (i.e. electrons) is transferred across the electrode-electrolyte interface is known as faradaic process. The processes such as adsorption, desorption and double-layer charging/discharging are known as nonfaradaic processes. The presence of adsorption, multiple charge-transfer reactions and coupled chemical reactions can be determined by a cyclic voltammogram which involves a three electrode system. These are the working electrode, reference electrode and counter electrode.

2.8.1 Working electrode

The working electrode possesses the interface of interest under study. It should be a polarizable electrode. The electrochemical reaction of interest occurs at the working electrode at a potential that is either controlled or measured with respect to a reference electrode. The working electrode must be electroinactive within the potential range of interest [117].

All the electroanalytical experiments were carried out using platinum and glassy carbon as the working electrode.

2.8.2 Reference electrode

Cyclic voltammetric, chronoamperometric and other electrochemical experiments are based on the electron transfer reaction that occurs at the working electrode. Thermodynamic and kinetic measurements require that the potential of the working electrode to be known and controlled with respect to the fixed potential of a reference electrode [117]. A suitable reference electrode must be electrochemically reversible, stable and unreactive with respect to other species in the solvent-electrolyte system and return to the equilibrium potential after polarization in either direction. In other words a reference electrode should be non-polarizable. The most widely used nonaqueous reference electrode is based on the Ag/Ag^+ couple. Ag^+ is normally furnished by a silver salt (e.g. AgCl). As long as the components of the solvent-electrolyte system are not oxidized by Ag^+, stable, reversible behaviour for the Ag/Ag^+ couple is observed in most solvent systems.

2.8.3 Counter (or auxiliary) electrode

It is the third electrode. Current passes between the working and counter (or auxiliary) electrode. Its electrochemical properties do not affect the behavior of the electrode of interest. It is usually chosen to be an electrode that does not produce substances by electrolysis that will reach the working electrode surface and cause interfering reactions [117]. Thus a counter electrode should also be non-polarizable.

2.8.4 Background of voltammetric studies

During voltammetric studies involving a three electrode assembly, the electrochemical response is dependent on the mode of mass transport. These mass transport phenomena are diffusion, migration and convection [118]. Convection is eliminated by carrying out the experiment under quiescent conditions. Migration is eliminated by adding large excess of inert supporting electrolyte (e.g. KCl). In voltammetric studies the species that responds to the applied potential or current are known as electroactive species. Thus, the essential mode of mass transfer occurs only by diffusion of electroactive species. Such electrode reactions are known as diffusion controlled processes.

2.8.5 Potentiostat

A potentiostat is an electronic amplifier which controls the potential drop between the working electrode and the electrolyte [119]. All the three electrodes as mentioned earlier are controlled by a potentiostat which acts in the manner shown in Fig. 2.8.

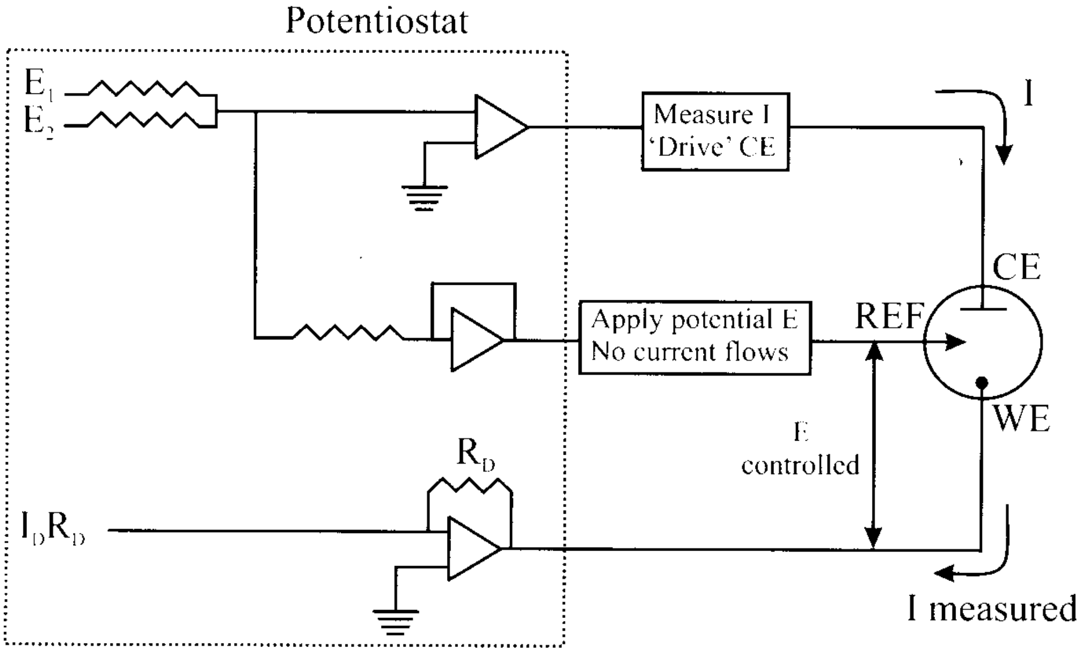

Fig. 2.8 A schematic of a potentiostat connected to a three electrode assembly. R_D is variable resistance, CE is counter electrode, WE is working electrode and REF is reference electrode [119].

The potentiostat imposes a fixed potential, E, between the working (WE) and the reference (REF) electrode and draws negligible current through the latter electrode.

$$E = (\phi_M - \phi_S)_{working} - (\phi_M - \phi_S)_{reference} \qquad 2.1$$

where ϕ_M is the electrical potential and ϕ_S is the solution potential.

Since the reference electrode serves to provide a constant value of $(\phi_M - \phi_S)_{reference}$ any changes in E are reflected as changes in $(\phi_M - \phi_S)_{working}$. The imposition of the potential drop $(\phi_M - \phi_S)_{working}$ on the working electrode-solution interface will typically cause a current to flow. The counter electrode (CE) serves to pass the same current as that induced to flow through the working electrode. Accordingly, the potentiostat drives the counter electrode to whatever voltage is required to pass this current. The introduction of the third electrode is the only reason why a controlled potential can be applied to the working electrode as expressed by the Eqn. 2.1.

Autolab, PGSTAT 302N manufactured by M/s. Eco Chemie, Utrecht, The Netherlands was employed for the present studies. The data were processed by using appropriate software (GPES 4.9).

2.8.6 Cyclic voltammetry (CV)

Principle: Cyclic voltammetry involves applying a potential to the working electrode which changes with time as shown in Fig. 2.9 [119].

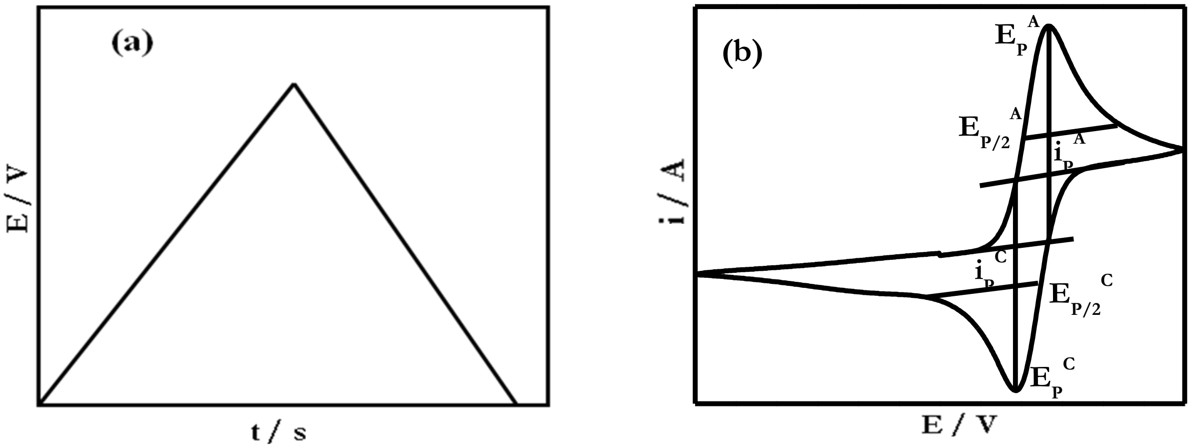

Fig. 2.9 Potential simulation (a) and resulting current response (b) in a cyclic voltammetry experiment.

The current flowing through the working electrode as a function of the applied potential and a plot of current versus potential is recorded which is known as the voltammogram. The initial voltage is selected such that the chemical species under investigation are not initially oxidized or reduced. The potential is swept in a linear manner to a certain value and then the direction of scan is reversed usually to its original value. The potential range is usually selected such that the range contains an oxidation or reduction process of interest. The observed voltammogram depends on the parameters such as the electron transfer coefficient, standard electrochemical rate constant (k_s), formal potential of the redox couple, diffusion coefficient (D) of the redox species and the voltage scan rate (ν).

Procedure: In the present study, voltammetric studies were carried out over the temperature range 1073 – 1123 K. The electrochemical cell was operated under argon during the measurement. The experiments were conducted using a three-electrode assembly, where the graphite crucible served as the container for the electrolyte as well as the counter (auxiliary) electrode. Platinum wire (1 mm diameter) served as the working electrode. The surface area of the Pt electrode dipped in the melt was kept constant (0.196 cm^2) for each measurement in KCl-KF-KBF$_4$ melts. Pt working electrode (area: 0.23 cm^2) was employed for KCl-KF-NaBF$_4$ melt. The potentials were measured against an Ag/AgCl reference electrode explained in Section 2.3.

2.8.7 Electron transfer coefficient

The electron transfer coefficient (α) gives the ratio of the change of the height of the energy barrier the electron has to surmount during charge transfer with respect to the change of electrode potential ΔE [119]. A value of $\alpha = 0$ implies no influence of the electrode potential change on the barrier height. $\alpha = 1$ implies that the change of electrode potential causes an exactly equal change of barrier height. The value of αn_α (where n_α is the number of electrons transferred for the reduction process in the rate determining step) can be determined from the equation given by Matsuda and Ayabe (Eqn. 2.2) [120, 121].

$$E^C_{P/2} - E^C_P = \frac{1.857RT}{\alpha n_\alpha F} \qquad 2.2$$

where, E^C_P is cathodic peak potential, $E^C_{P/2}$ is cathodic half peak potential, R is the molar gas constant, T is the absolute temperature and F is the Faraday constant.

The αn_α also can be evaluated from the following equation [118].

$$\frac{\Delta E^C_P}{\Delta \log \nu} = \frac{2.3RT}{2\alpha n_\alpha F} \qquad 2.3$$

where $\frac{\Delta E^C_P}{\Delta \log \nu}$ is determined from the slope of E^C_P vs. $\log \nu$ plots.

The current function ($i^C_P / \nu^{1/2}$) i.e., the ratio of cathodic peak current (i^C_P) to the square root of scan rate ($\nu^{1/2}$) can be measured as a function of scan rate to determine the mechanism of electrochemical reactions. If the current function and the peak potential (E_P) are independent of scan rate then the electrode process is said to be reversible, otherwise the process may be quasi-reversible or irreversible. In the case of a quasi-reversible process, the current function is virtually independent of scan rate but the peak potential shifts with the scan rate. The difference between E^A_P (anodic peak potential) and E^C_P, (ΔE_P), is a useful criterion for nernstian behaviour. The electrochemical behaviour is said to be nernstian if ΔE_P is very close to $2.3RT/nF$ and the ratio of i^A_P / i^C_P is approximately 1 regardless of scan rate and switching potential. A relationship between the cathodic peak current (i^C_P)

and square root of the scan rate for an insoluble deposit in irreversible/quasireversible system is given by the following expression [122].

$$i_P^C = 0.496nFAC_O^* \sqrt{D_O} \sqrt{\left(\frac{\alpha n_\alpha F \nu}{RT} \right)} \tag{2.4}$$

where A is the surface area of the electrode in cm^2 , C_O^* is the concentration of the electroactive species in mol cm^{-3} and D_O is the diffusion coefficient in cm^2 s^{-1}.

2.8.8 Electron transfer rate constant

Klingler and Kochi [123] have derived the following expression (Eqn. 2.5) for obtaining the electron transfer rate constant (k_s) by assuming that the electron-transfer reaction is irreversible.

$$k_s = 2.18(\alpha n_\alpha)^{1/2} \left(\frac{D_O F \nu}{RT} \right)^{1/2} e^{\frac{\alpha^2 nF(E_P^C - E_P^A)}{RT}} \tag{2.5}$$

2.8.9 Logarithmic analysis of convolution voltammetry

A working electrode is cathodically polarized to initiate the reduction process as expressed by the following Eqn. 2.6.

$$Ox + ne \rightarrow \mathrm{Re} \tag{2.6}$$

where Ox is the oxidized species and Re represents the reduced species.

If transport of Ox to the working electrode is solely as a result of semiinfinite linear diffusion with *D* being the diffusion coefficient, then the following equations are obeyed [124 – 127].

$$\frac{\partial}{\partial t} C(r,t) = D \frac{\partial^2}{\partial r^2} C(r,t) \tag{2.7}$$

$$C(\infty, t) = C \tag{2.8}$$

$$C(r,0) = C \qquad 2.9$$

where *C(r,t)* denotes the concentration of Ox at distance *r* from the electrode surface at time *t* and *C* is the concentration of Ox in the bulk. Moreover, the flux of Ox at the surface of the working electrode is given by,

$$D\frac{\partial}{\partial r}C(0,t) = \frac{i(t)}{nAF} \qquad 2.10$$

where $i(t)$ denotes the cathodic faradaic current. From Eqns. 2.9 and 2.10 we get,

$$C(0,t) = C - \frac{m(t)}{nAF\sqrt{D}} \qquad 2.11$$

where $m(t)$ denotes the semiintegral of faradaic current, $i(t)$ with respect to time which is represented as,

$$m(t) = \frac{d^{-1/2}}{dt^{-1/2}}i(t) \qquad 2.12$$

The equation governing the semiintegral convolution analysis for a process involving reversible deposition of an insoluble species is given by Eqn. 2.13, the details of which are given elsewhere [124 – 127].

$$E(t) = E_{1/2} + \frac{RT}{nF}\ln\left\{\frac{2[m^*(\infty) - m(t)]}{m^*(\infty)}\right\} \qquad 2.13$$

where, $E(t)$ is the time dependent applied potential, $m^*(\infty)$ is the semiintegral of cathodic current limit, $m(t)$ is the semiintegral of cathodic current and $E_{1/2}$ is the average of cathodic and anodic peak potential.

$E_{1/2}$ for a reversible voltammetric wave is given by Eqn. 2.14 [125].

$$E_{1/2} = \frac{E_P^A + E_P^C}{2} \qquad 2.14$$

Eqn. 2.13 predicts that a plot of $\ln\left\{\frac{2[m^*(\infty)-m(t)]}{m^*(\infty)}\right\}$ vs. $E(t)$ should yield a straight line whose slope is $\frac{RT}{nF}$.

Similar equations have been derived by Oldham *et al.* for irreversible and quasireversible processes [125].

For a quasireversible process a plot of $\ln\left\{\frac{m^*(\infty)-m(t)\left[1+\exp\left\{\frac{RT}{nF}\left(E-E_{1/2}\right)\right\}\right]}{i(t)}\right\}$ vs. $E(t)$ should yield a straight line whose slope is $\frac{RT}{\alpha nF}$. From the slope α can be calculated.

For an irreversible process a plot of $\ln\left[\frac{m^*(\infty)-m(t)}{i(t)}\right]$ vs. $E(t)$ should yield a straight line whose slope is $\frac{RT}{\alpha nF}$. Thus α can be evaluated from the slope.

2.8.10 Linear sweep voltammetry (LSV)

Principle: In this method the potential is varied linearly with time and the current signal is recorded as a function of potential. Fig. 2.10 (a, b) depicts a typical LSV scan. The scan is carried out at a potential where no electrochemical reaction occurs. At the potential where the charge transfer begins, a current signal can be observed which increases with the potential, however, after a maximum value (peak current) it starts to decrease due to the depletion of the reacting species at the interface. In LSV essentially only the first half-cycle of a CV is executed. Data analysis is similar to the method adopted for CV analysis.

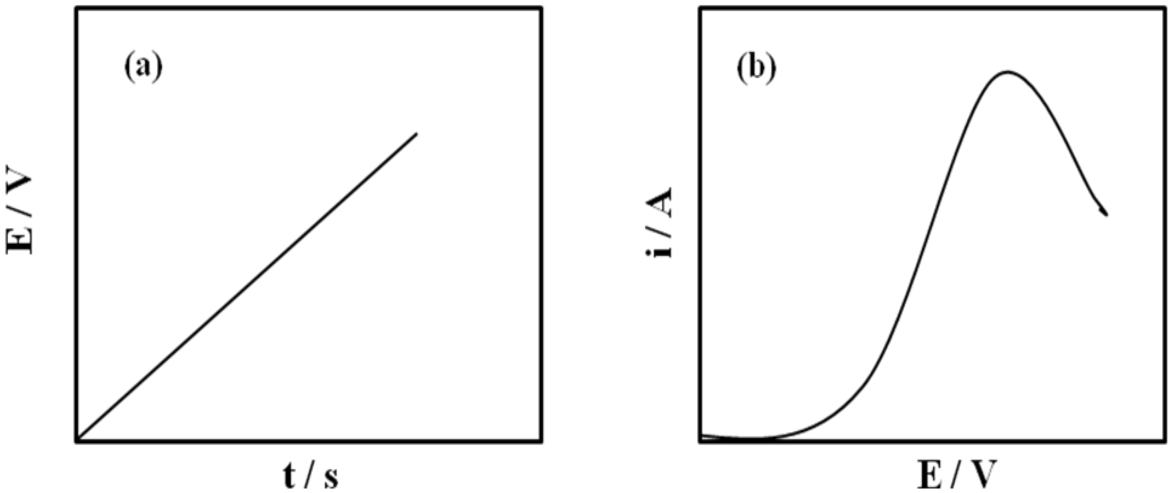

Fig. 2.10 Potential simulation (a) and resulting current response (b) in a linear sweep voltammetry experiment.

Procedure: LSV studies were carried out with KCl (81.54 mol%) – KF (18.45 mol%) melt over the temperature range 1073 – 1123 K. The experiments were conducted using a three-electrode assembly. The graphite crucible served as the container for the electrolyte as well as the auxiliary electrode. A glassy carbon rod (2 mm dia, area of the glassy carbon rod dipped inside the electrolyte: 0.48 cm^2) was used as the working electrode. A fresh glassy carbon electrode was used for each measurement. The potentials were measured against an Ag/AgCl reference electrode developed in this study. Voltammetric scans were recorded at different scan rates varying from 0.1 to 1 V s^{-1} within the potential range of 0 to +1.4 V. All these measurements were carried out by using an electrochemical workstation as mentioned earlier in Section 2.8.5.

2.8.11 Chronoamperometry

Principle: In chronoamperometric method, the current is measured as a function of time after application of a potential step perturbation (Fig. 2.11).

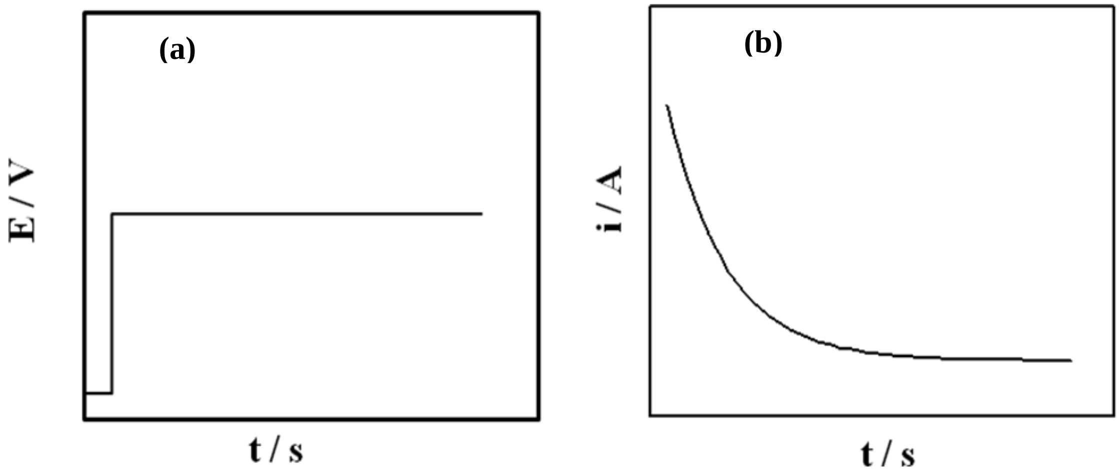

Fig. 2.11 Potential simulation (a) and resulting current response (b) during a chronoamperometric experiment.

In this electroanalytical method the potential is stepped from a value, where no current flows, i.e., the oxidation or reduction of the electrochemically active species does not take place, to a value where the current flows due to a faradaic process. The resultant faradaic current is monitored as a function of time.

The current flowing after the application of the potential step obeys Cottrell equation (Eqn. 2.15) [118]. The current decreases with time due to the fall in concentration gradient of the redox species.

$$i = \frac{nFAD_O^{1/2}C_O^*}{\pi^{1/2}t^{1/2}} \qquad 2.15$$

where i is the current and t is the transition time.

Procedure: Chronoamperometric measurements were carried out employing a platinum electrode (0.2 cm^2 area) by applying potentials ranging from -0.9 to -1 V for a short duration of 10 s for the KCl (81.54 mol%)-KF (18.45 mol%) melt with KBF_4 concentration of 1.6×10^{-4}, 4.1×10^{-4} and 7.73×10^{-4} mol cm^{-3} over the temperature range 1073 – 1123 K. Potentials ranging from -0.88 to -0.85 V were applied for a short duration of 5 s (Pt electrode, 0.23 cm^2 area) for the KCl (81.54 mol%)-KF (18.45 mol%) melt with $NaBF_4$ (1.67×10^{-4} mol cm^{-3}) over the temperature range 1073 – 1123 K. Chronoamperograms were also measured using Autolab (PGSTAT 302N) equipped with an IF 030 interface.

2.9 Emf measurements

The maximum work (non-volume work) obtained from a galvanic cell is given by Eqn. 2.16 [128, 129].

$$\Delta G = -nFE \qquad 2.16$$

where ΔG is the change in Gibbs energy of the electrochemical reaction, n is the number of moles of electron, E is the electromotive force (emf) produced by the cell and F is the Faraday constant (96485 C mol^{-1}). Any meaningful thermodynamic investigation requires that the cell functions in a reversible way i.e., there is no external flow of current. This is usually assured by the use of high-resistance (larger than 10^{10} Ω) measuring devices, resulting in the measurement of an open-circuit potential. Two general classes of cells i.e., chemical and concentration cell may be employed during thermodynamic investigations. In a chemical cell an emf is produced due to chemical reaction occurring within the cell. In a concentration cell emf is generated due to Gibbs energy decrease resulting from the transfer of an element from one electrode to the other through an electrolyte containing the element. Successful cell operation requirements are:

1. A suitable electrolyte which provide purely ionic conductivity at the operating temperature range.
2. Identification of the single reversible process occurring at each electrode.
3. The equilibrium potential at a given temperature should be established within a reasonable time.
4. Equilibrium potential has to be established regardless of whether the temperature has been increased or lowered.
5. Similar values of potential have to be established even after polarization of the cell from its equilibrium value.
6. Reactions between electrodes and electrolyte as well as between electrodes and lead wires must be avoided.
7. Temperature gradients in the cell should be avoided.
8. Reactions between crucible materials and electrodes or electrolyte should be excluded.
9. Concentration changes due to the vapor pressure of the electrodes must be taken into consideration.
10. Direct exchange of matter between the two electrodes (e.g., via the gas phase) has to be excluded.
11. Electrical interference between the furnace in which the cell is heated and the cell itself should be avoided, either by a proper winding of the furnace or by a corresponding grounding.

Under such circumstances the potential E of a given cell

$$A(solid\ or\ liquid)\,|\,ionic\ \ electrolyte, A^{n+}(or A^{n-})\,|\,A_x B_{1-x}(solid\ or\ liquid) \qquad 2.17$$

is related to the partial Gibbs energy or the thermodynamic activity, of A by,

$$\Delta\overline{G}_A = -nFE = RT\ln a_A \tag{2.18}$$

where R is the gas constant and T is the absolute temperature.

The results of emf measurements yield values of E at different T for a fixed composition of the galvanic couple. These data are fitted to the linear Eqn. 2.19.

$$E = a + bT \tag{2.19}$$

where a and b are constants. By using the following relationship:

$$\Delta\overline{G}_A = RT\ln a_A = \Delta\overline{H} - T\Delta\overline{S} = nF(a+bT) \tag{2.20}$$

The thermodynamic activity (a_A), partial enthalpy $\left(\Delta\overline{H}\right)$ and partial entropy $\left(\Delta\overline{S}\right)$ of the alloy component could be determined directly from a and b parameters as:

$$\Delta\overline{S} = nF\left(\frac{\partial E}{\partial T}\right) = bnF \tag{2.21}$$

$$\Delta\overline{H} = nF\left[T\left(\frac{\partial E}{\partial T}\right) - E\right] = -anF \tag{2.22}$$

2.10 Validation of the reference electrode

2.10.1 Polarization test

Galvanostatic chronopotentiometry was employed for the cathodic and anodic polarization tests by using an electrochemical workstation (described in Section 2.8.5). In these tests 1, 2, 3, 4 and 5 mA currents were passed through the cell (300 s duration) maintained at a desired temperature that varied between 1073 and 1123 K. Subsequently the open circuit potential was monitored. This cell could be represented by (Eqn. 2.23),

$$Ag/AgCl/\underset{X}{KCl}^{*},\underset{(1-X)}{KF}/AgCl/Ag \tag{2.23}$$

*In the salt mixture KF-KCl, X_{KCl} (mole fraction) = 0.81

2.10.2 Reversibility test

The reversibility, which is ensured by fast electrode kinetics (i.e. high exchange current density), is the basic requirement for a reference electrode system [130]. The reversibility test involves application of the micropolarization test. In this test, the electrode is polarized within a short potential range, usually less than +5 to –5 mV or +10 to –10 mV. This potential range is the so-called linear polarization response region of the η (polarization) vs. i curve [130]. The ohmic resistance of the cell must be low, or the measured polarization value must be corrected for IR-voltage drop. Criteria for proper functioning of the reference electrode are straightness of the polarization curve. Reversibility has to be tested at several temperatures in the intended temperature range. Any counter electrode that has an invariant potential during the test will be satisfactory. Adequate reversibility ensures fast and perfect recovery of the potential after a short, inadvertent current load.

Micropolarization tests were carried out in the temperature range 1073 to 1123 K for establishing the reversibility of the reference electrode developed in this study. The Ag/AgCl electrode served as the working electrode while the graphite crucible functioned as the counter electrode. The electrolyte was KCl-KF melt. In this test cyclic voltammograms were recorded at a scan rate of 0.5 mVs^{-1} within the potential range +5 to -5 mV.

2.10.3 Reproducibility test

Reproducibility tests were carried out by measuring the potential difference between two similar reference electrodes in equilibrium with the same melt (KCl 81.54 mol% - KF

18.45 mol%) at 1073, 1098 and 1123 K. These electrodes were immersed into the melt to the same height in order to keep their areas of contact identical (0.06 dm^2).

2.10.4 Stability test

The stability of this reference electrode was checked by measuring the cyclic-voltammograms at different time intervals on a 1 mm diameter platinum electrode acting as a working electrode and the graphite crucible containing the melt as the counter electrode in the same KCl-KF melt in the similar temperature range. The cyclic voltammograms were recorded at a scan rate of 250 mVs^{-1} after equilibrating the melt for 2 h prior to the measurements.

2.10.5 Emf measurements

The half cell potentials of Fe/Fe^{2+} and Ni/Ni^{2+} couples in KCl-KF melt were measured over the temperature range 1073 to 1123 K by using a high impedance multimeter (Agilent, 34970A Data acquisition unit, Agilent Technologies, USA). A nickel wire (1 mm diameter) and an iron wire (3 mm diameter) were dipped in the melt and equilibrated for 2 h. The open circuit potential between each of these electrodes with respect to the reference was measured for a period of 1 h at an interval of 300 s. The mean of 12 such measurements were taken to represent the equilibrium redox potential of the respective metals in this melt. These galvanic cells could be represented by Eqns. 2.24 and 2.25.

$$Ni/Ni^{2+}/\underset{X}{KCl^{*}},\underset{(1-X)}{KF}/Ag/AgCl \qquad 2.24$$

$$Fe/Fe^{2+}/\underset{X}{KCl^{*}},\underset{(1-X)}{KF}/Ag/AgCl \qquad 2.25$$

*In the salt mixture KF-KCl, X_{KCl} (mole fraction) = 0.81

2.11 Analysis of boron in the melt by ICP-MS

Principle: Inductively coupled plasma-mass spectrometry (ICP-MS) not only offers extremely low detection limits in the parts per billion (ppb) range but also enables quantification at the parts per million (ppm) ranges. This unique capability makes the technique attractive compared to other elemental analysis techniques [131]. The sample, in a liquid form, is pumped (usually with a peristaltic pump) into a nebulizer, where it is converted into fine aerosol droplets with argon gas. The aerosol droplets, which represent only 1 – 2% of the sample, are separated from larger droplets using a spray chamber. The fine aerosol then emerges from the exit tube of the spray chamber and is transported into the plasma torch via a sample injector. The plasma is produced by the interaction of an intense magnetic field (produced by radio frequency passing through a copper coil) on a tangential flow of argon gas through a concentric quartz tube (torch). This ionizes the gas and when seeded with a source of electrons from a high-voltage spark, forms high temperature plasma (~10,000 K) at the open end of the tube. The ions produced in the plasma are directed into the mass spectrometer via the interface region, which is maintained at a vacuum of 1 - 2 torr with a mechanical roughing pump. This interface region consists of two metallic cones (usually made of nickel), called the sampler and a skimmer cone. Each cone features a small orifice to allow the ions through to the ion optics, where they are guided into the mass separation device. The mass separation device allows analyte ions of a particular mass-to-charge ratio (m/z) through the detector. The non-analyte and interfering matrix ions are filtered out. A detector converts the ions into an electrical signal. The most commonly used detector is a dynode detector. The signal is then processed by the data handling system and converted into analyte concentration using ICP-MS calibration standards.

Procedure: After the completion of the voltammetric scans, melt samples were withdrawn from the cell and analyzed. About 10 mg of the solidified melt was dissolved in 10 ml of 0.02 N HNO_3. The solution was then analyzed for its boron content by inductively coupled plasma mass spectrometer (ICP-MS, Model: Elan 250, M/s. Sciex, Toronto, Canada) after suitable dilution. These measurements had a standard deviation of about 3 to 5% of the reported value. Boron electrodeposit was dissolved in concentrated nitric acid and analyzed using ICP-MS.

2.12 Characterization of the electrodeposit

2.12.1 SEM studies

Principle: Electrons from a thermionic, Schottky or field-emission cathode are accelerated through a voltage difference (0.1 to 50 keV) between cathode and anode [132]. The electron beam is demagnified by a two or three stage electron lens system. An electron probe of diameter 1 – 10 nm carrying an electron probe current of 10^{-9} to 10^{-12} A is formed at the specimen surface. A deflection coil system in front of the final lens field scans the electron probe in a raster across the specimen in synchronization with the electron beam of a separate cathode ray tube (CRT). The intensity of the cathode ray is modulated by one of the signals recorded to form an image. Elastic and inelastic scattering are the elementary atomic interaction processes, though the final signal used for the image formation is, with only a few exceptions, not the result of single scattering process but of the complete electron diffusion caused by the gradual loss of the electron energy and by lateral spreading caused by multiple elastic large-angle scattering. These electron-specimen interactions are used to form the image and furnish qualitative and quantitative information.

Procedure: Boron deposited on the platinum electrode was adhered with carbon tape and mounted on the sample holder. The microstructure of the boron deposit was analyzed by using a scanning electron microscope (SEM) supplied by M/s. Philips XL 30, The Netherlands.

2.12.2 X-ray diffraction (XRD)

Principle: X-rays with energies of about 12 keV have a wavelength of about 1 Å which is comparable with the atomic spacings in a crystal lattice. The interaction of this radiation with matter can provide high-resolution structural information on the atomic scale [133]. In a typical X-ray diffraction (XRD) experiment, a thin layer of a powder sample is spread onto a sample holder and exposed to the X-ray beam. Diffraction patterns resulting from the interference of beams scattered from surface atoms of the sample is in accordance with Bragg's equation (Eqn. 2.26).

$$n\lambda = 2dSin\theta \qquad 2.26$$

where n is the order of reflection, λ is the wavelength, d is the lattice spacing and θ is the angle of scattering.

Procedure: XRD analysis was performed using Ni filtered Cu K_α radiation (154.098 pm) by using a Philips X-ray diffractometer (X'pert MPD system obtained from M/s. Philips, The Netherlands). Electrodeposited boron on the platinum electrode was mounted on to the sample holder. Calibration of the diffractometer was carried out using silicon and α-alumina standards obtained from the National Institute of Standards and Technology (NIST) USA. The crystalline / amorphous nature and the different phases present in the sample were identified by comparing the XRD pattern obtained for the sample with the relevant JCPDS files.

2.13 Ion-selective electrode

Membrane electrodes permit the rapid and selective determination of numerous cations and anions by the direct potentiometric measurements. The membrane electrodes are called ion-selective electrodes (ISEs) because of high selectivity of these electrodes for a specific ion [134]. ISEs typically use an ionophore as the sensing platform to ensure selectivity toward a specific ion of interest.

***Principle*:** LaF_3 is used for the preparation of crystalline membrane electrode for the determination of fluoride ion [134]. The fluoride ion is the mobile species in the crystal. The excellent selectivity arises from the low K_{sp} (solubility product) and the inability of most anions to duplicate the F^- lattice mobility. At the two interfaces of the membrane, ionization creates a charge on the membrane surface as shown by the following equation.

$$LaF_3(s) + e = LaF_2^+(s) + F^-(sol) \qquad 2.27$$

The magnitude of the charge is dependent upon the fluoride ion concentration in the solution. Thus, the side of the membrane encountering the lower fluoride ion concentration becomes positive with respect to the other surface; it is this charge difference that provides a measure of the difference in fluoride concentration of the two solutions. The potential of the cell containing a lanthanum fluoride electrode is given by the following equation:

$$E_{ise} = E^0 - \frac{RT}{F}\ln a_{F^-} \qquad 2.28$$

where E_{ise} is the potential of the electrode, E^0 is a constant and a_{F^-} is the activity of the fluoride ions. Commercial LaF_3 electrode can be used in the temperature range 273 K to 353 K. The response of the fluoride electrode is linear from 10 to 10^{-6} M.

Membranes prepared from single crystals or pressed disks of AgCl and Ag_2S forms the ion selective membrane for chloride ion [134]. Chloride ion diffuses into vacancies in the crystal lattice and changes the membrane conductivity. The response of the chloride ion selective electrode is linear from 10 to 5×10^{-5} M.

***Procedure*:** Melt samples were collected for the chemical analyses during the course of the electrowinning experiments and preserved under argon. These solidified melt samples were then analyzed for the Cl^- and F^- content by using appropriate ion selective electrodes. The ion selective electrode measurements were carried out using Orion 920 A+ procured from M/s. Thermo Electron Corporation, Ohio, USA. The calibration of ion selective electrodes selective for F^- and Cl^- was carried out using the standard solution (10 and 100 ppm) of NaF and KCl respectively. The ionic strength of the sample was adjusted by adding 400 µL of 5 M sodium nitrate solution to 20 mL of the test solution. Subsequently, the concentration of F^-/Cl^- was measured directly from the activity of the respective anion. These measurements had an uncertainty of about 5% of the reported value.

CHAPTER III

3.0 Results and discussion

Performance of the Ag/AgCl reference electrode (developed in this study) is presented. Electrochemistry of the deposition of boron from KCl-KF-MBF_4 (M = K and Na) melts is described. Determination of the concentration of oxide ion in KCl-KF melts by electrochemical method is given in detail. A plausible scheme of reaction(s) that governs the electrodeposition of boron from melts is presented.

3.1 Development and electrochemistry of a novel Ag/AgCl reference electrode for application in mixed chloride-fluoride melts

3.1.1 The Ag/AgCl electrode

The Ag/AgCl electrode is most suitable to be used as a reference electrode in molten salt systems owing to the desirable physical and chemical properties of AgCl [94]. It is not affected by oxide ion contamination, thanks to the instability of silver oxide at the operating temperature of most of the molten salt systems [94]. Aten *et al.* [135], demonstrated that the Ag/AgCl electrode was practically non-polarizable. In their investigations on molten silver chloride these authors deposited Ag both cathodically and anodically (polarization voltage: 0.5 V and current density: 1 A dm^{-2}). If any other metal ion contaminates the molten AgCl, it would only have a minor influence on the potential of the reference electrode. Due to the nobility of silver any other metal ion that contaminates the molten AgCl would get oxidized (Eqn. 3.1). The consequent minor reduction in the concentration of AgCl would not seriously perturb the equilibrium potential especially when an excess of AgCl is present.

$$M^{n+} + xAg^{+} = xAg + M^{(n+x)+} \quad 3.1$$

On the contrary, contamination of the melt by Ag^{+} ions would alter the measured values of the potentials at the working electrode. Hence, it is often recommended [136] that the Ag/AgCl electrode should be so designed as to permit, if inevitable, only the contamination of AgCl by the less noble metal ion and not vice-versa and further that it should contain large amounts of AgCl so that the traces of metal ions contaminating it would practically not affect its equilibrium potential.

3.1.2 Polarization test

The chronopotentiometric polarization test [130] at 1073 K showed that when a current of 1, 2, 3, 4 and 5 mA was passed, the initial value (2 mV) of the potential was re-established within 5 s (for 1 mA) and 10 s (for 2, 3, 4 and 5 mA) after the flow of current was stopped (Fig. 3.1). Similar tests for cathodic polarization were also carried out at 1073 K. In these experiments the potential of the electrode resumed to its equilibrium value after 5 s (-1 mA) or 9 s (-2, -3,-4 and -5 mA) (Fig. 3.1). Plots depicting the cathodic polarization at 1098 K show that the initial potential was re-established within 5 s (for i = 1 and 2 mA) and 10 s (for i = 3, 4 and 5 mA) after the flow of current was stopped (Fig. 3.2).

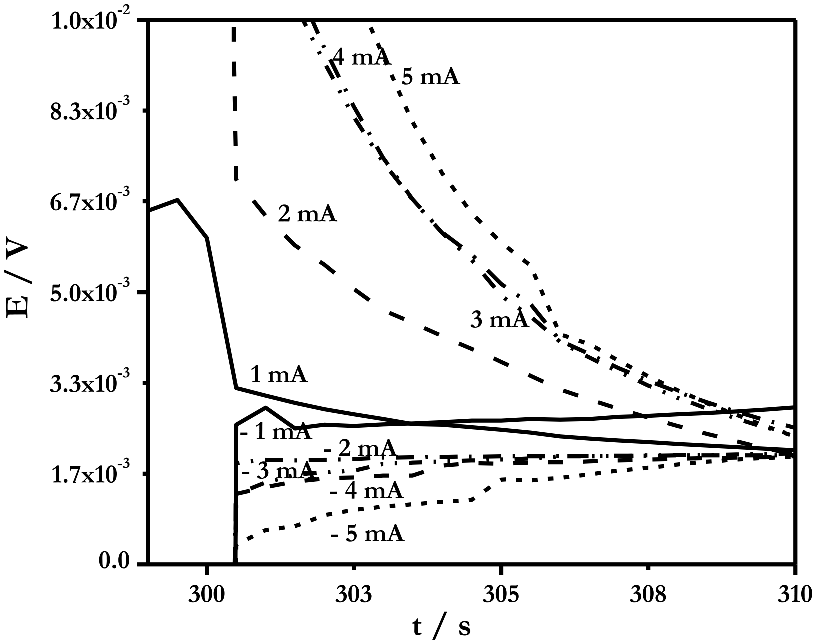

Fig. 3.1 Chronopotentiometric polarization plot for the Ag/AgCl reference electrode at 1073 K.

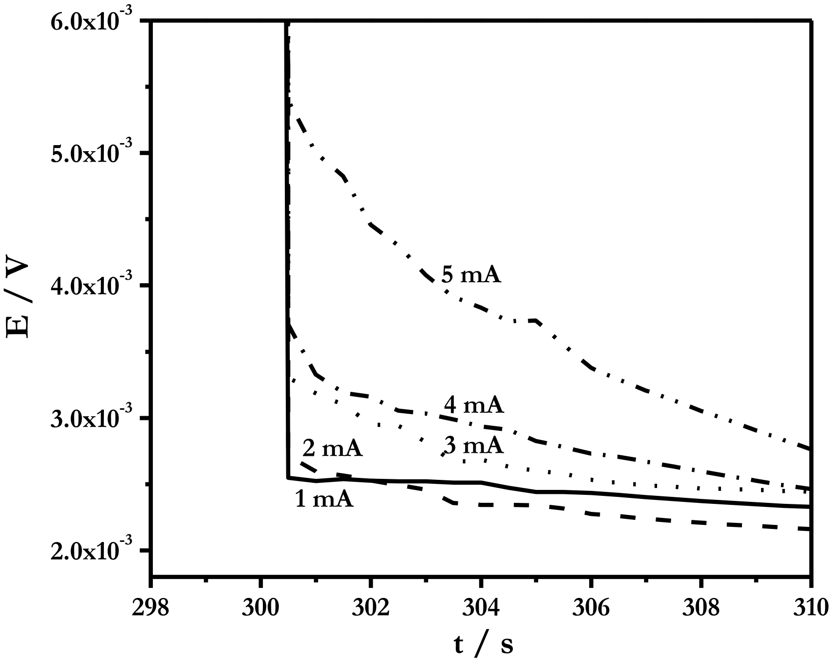

Fig. 3.2 Chronopotentiometric polarization plot for the Ag/AgCl reference electrode at 1098 K.

Cathodic polarization plots at 1123 K indicates that by passing –1 mA current the equilibrium potential was established within 60 s and when -2, -3 , -4 or -5 mA current was passed it took 250 s to establish the equilibrium potential (Fig. 3.3). Coriou *et al.* [94] performed a similar polarization test for their Ag/AgCl reference electrode at 1123 K in NaCl melt by passing a current of 1 mA for 300 s. The initial potential was reported to be re-established within 60 s. The Ag/AgCl reference electrode employed in this study was not polarized even at a current of 5 mA and in a more corrosive mixed chloride-fluoride melt.

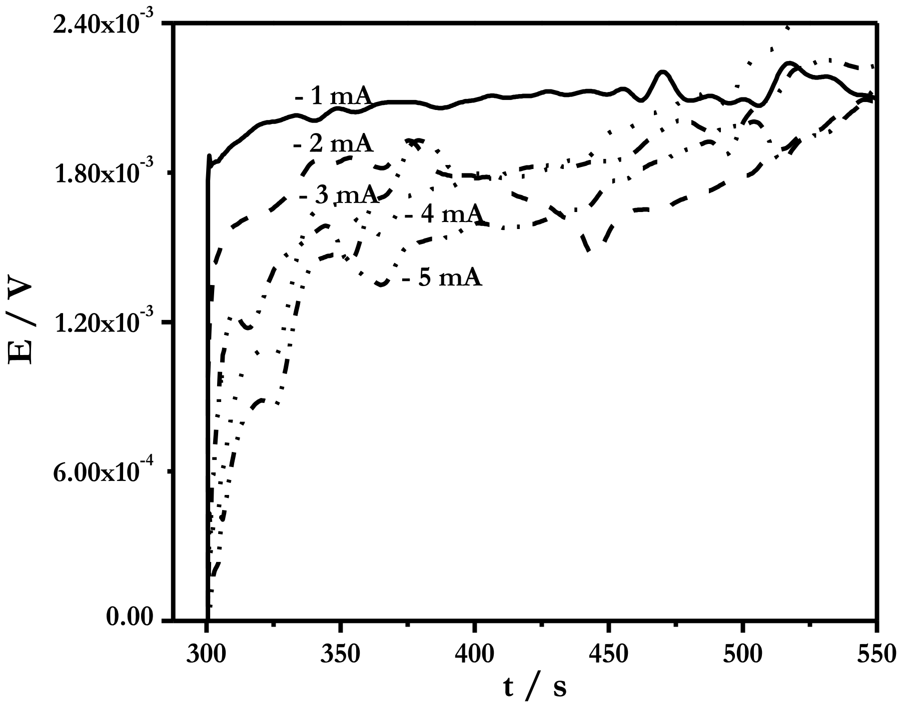

Fig. 3.3 Chronopotentiometric polarization plot for the Ag/AgCl reference electrode at 1123 K.

3.1.3 Reproducibility and reversibility

When reproducibility tests were carried out in the temperature range 1073 to 1123 K it was found that the potential difference between the two similar electrodes stabilized within 900 s to a value of about 2 mV. This small potential difference is probably due to some asymmetry in the construction of the two electrodes. Coriou *et al.* [94] observed a potential difference of 2 mV in a similar test between two Ag/AgCl reference electrodes in NaCl melt at 1123 K. The reversibility of the present reference electrode is comparable to that of Coriou *et al.* [94] while its reproducibility is better than the reference electrode reported by Gao *et al.* [137]. These authors developed an Ag/AgCl reference electrode for $CaCl_2$ based molten salts and the potential difference between two such electrodes in the melt was between 8 and 15 mV. In view of the above it is concluded that our reference electrode is suitable for use with mixed chloride-fluoride melts in the temperature range 1073 to 1123 K.

The plots obtained after carrying out micropolarization tests at 1073, 1098 and 1123 K showed a linear behaviour in the potential range ±5 mV (Fig. 3.4). The linear behaviour of the potential with current density, as reported in reference [130], indicated the reversibility of the reference electrode in the temperature range 1073 to 1123 K. However these plots showed a hysteresis only during anodic polarization. A difference in the polarization current density to the tune of 0.7 and 0.4 μAcm^{-2} was observed at 1073 and 1173 K respectively between the forward and reverse scans in the anodic region. From the plots pertaining to the micropolarization test it can be inferred that the reference electrode has a high exchange current density which is ensured by a fast electrode kinetics in the cathodic region in the temperature range 1073 to 1123 K.

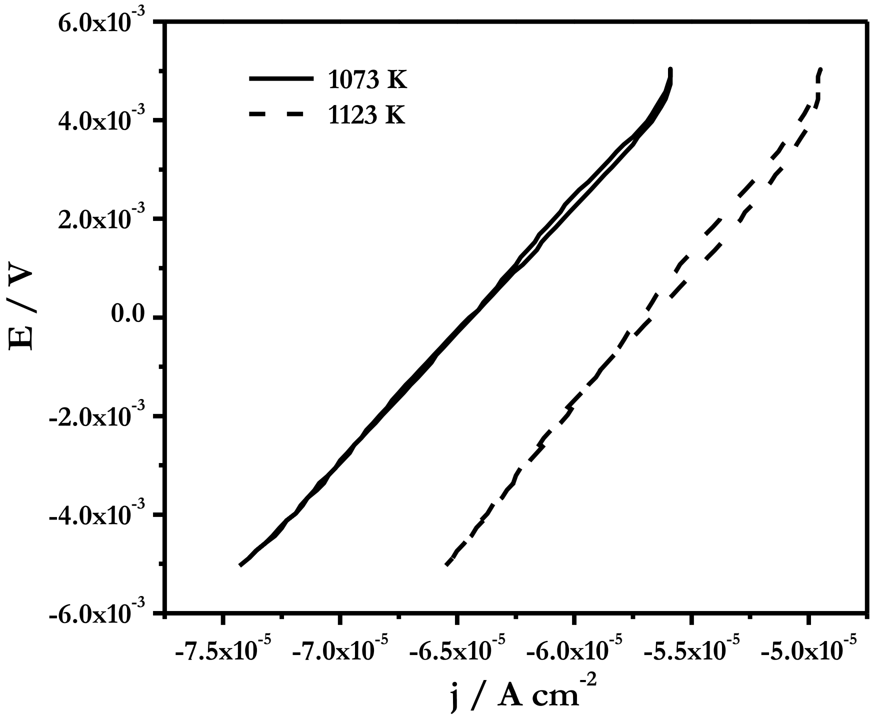

Fig. 3.4 Micropolarization plots for the Ag/AgCl reference electrode in KCl-KF melt at different temperatures.

3.1.4 Stability

The cyclic voltammetric scans carried out at 1073 K showed a variation of ±2 mV between the 2nd and 12th hour of measurement (Fig. 3.5). The variation in the span of the electrochemical window was within the typical experimental error usually encountered in cyclic voltammetry [137]. Cyclic voltammetric scans recorded after 12 h of equilibriation at 1123 K showed a similar shift in the potential (Fig. 3.6). No visible damage to the graphite tube as well as the graphite porous plug was noticed even after a continuous service for 12 h.

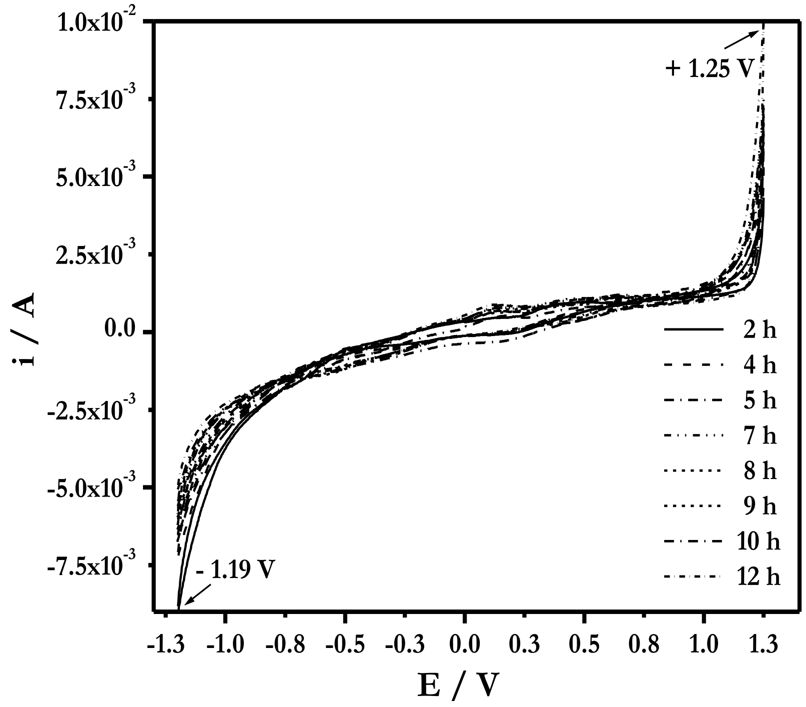

Fig. 3.5 Cyclic voltammetry of KCl-KF melt on Pt vs. Ag/AgCl at 1073 K and 0.25 Vs^{-1} scan rate.

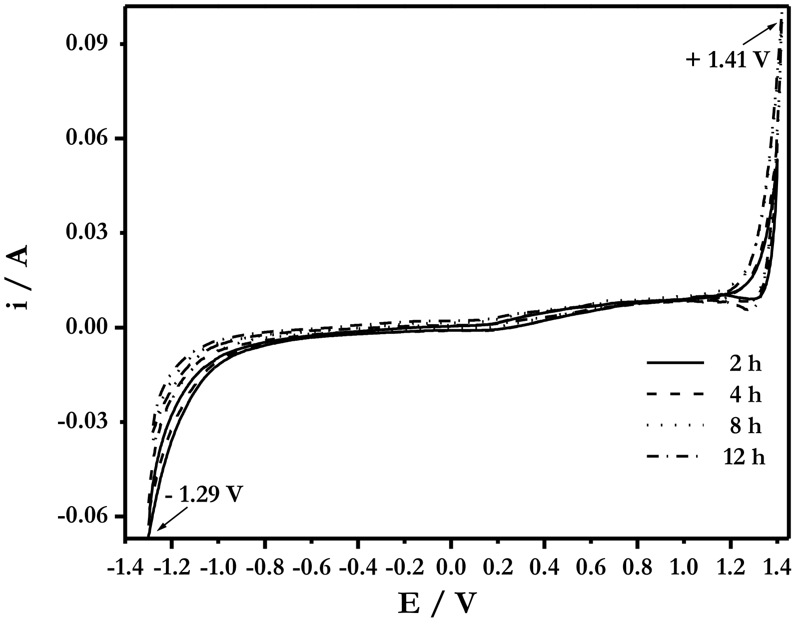

Fig. 3.6 Cyclic voltammetry of KCl-KF melt on Pt vs. Ag/AgCl at 1123 K and 0.25 Vs^{-1} scan rate.

3.1.5 Half cell potentials of Fe/Fe^{2+} and Ni /Ni^{2+} couples

The temperature dependence of the half cell potentials of the Fe/Fe^{2+} and Ni/Ni^{2+} couples with respect to the Ag/AgCl electrode in molten KF and KCl mixture in the temperature range 1073 to 1123 K, is depicted in Figs. 3.7 and 3.8 respectively. These data are being reported for the first time. Half cell potentials reported for these couples in other halide melt systems [130] are also presented in Table 3.1. These half cell potentials varied linearly with the temperature of the melt (Figs. 3.7 - 3.8). For the Fe/Fe^{2+} and Ni/Ni^{2+} couples in KCl-KF melt the linear regression analysis of emf vs. T plot (Figs. 3.7 - 3.8) yields the Eqns. 3.2 and 3.3 respectively.

$$E_{(Fe^{2+}/Fe)}\,(V) = [-1.8097 + 0.0015\,T] \pm 0.002\text{ V} \tag{3.2}$$

$$E_{(Ni^{2+}/Ni)}\,(V) = [-0.9816 + 8.0641 \times 10^{-4}\,T] \pm 0.002\text{ V} \tag{3.3}$$

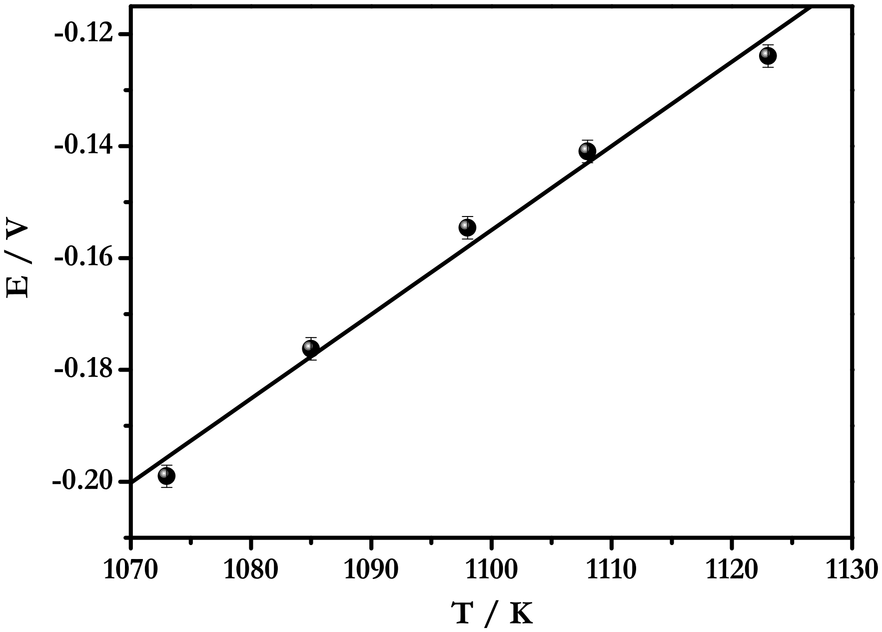

Fig. 3.7 Half cell potential of Fe/Fe^{2+} couple in KCl (81.54 mol%) – KF (18.45 mol%) melt vs. Ag/AgCl reference electrode.

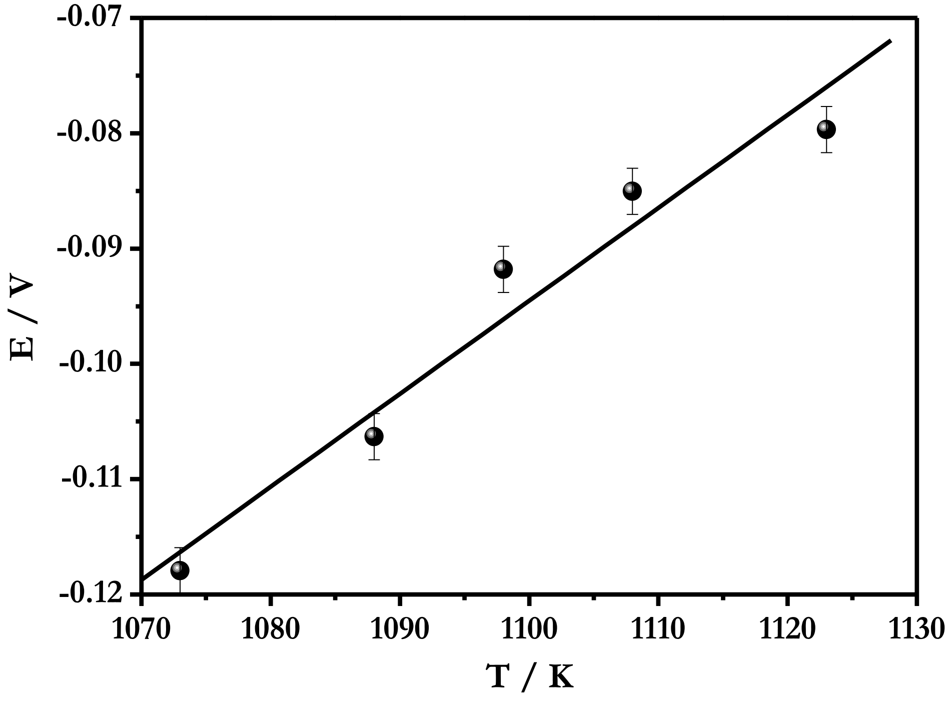

Fig. 3.8 Half cell potential of Ni/Ni^{2+} couple in KCl (81.54 mol%) – KF (18.45 mol%) melt vs. Ag/AgCl reference electrode.

Table 3.1 Half cell potential of Fe/Fe^{2+} and Ni/Ni^{2+} couples with respect to Ag/AgCl electrode in halide melts.

Melt	Temperature (K)	Fe/Fe2+ (V)	Ni/Ni2+ (V)	Reference
LiCl-KCl (Eutectic composition)	723	- 0.534	- 0.068	[130]
NaCl-KCl (Equimolar composition)	723	- 0.560	-	[130]

The Gibbs energy of formation [128, 129] of Fe^{2+} and Ni^{2+} can be calculated by utilizing the emf values (obtained from Eqns. 3.2 and 3.3) and plugging those values in Eqn. 2.18. Using these emf data, partial entropy $\left(\Delta\overline{S}\right)$ and partial enthalpy $\left(\Delta\overline{H}\right)$ [128, 129] of these systems can be determined by utilizing Eqns. 2.21 and 2.22. The calculated thermodynamic properties are presented in Table 3.2. These values are reported in this study for the first time.

Table 3.2 Thermodynamic quantities for Fe/Fe^{2+} and Ni/Ni^{2+} couples in KCl-KF melt at different temperatures.

Half cell	**Temperature (T)**	$\Delta\overline{G}$ **(kJ mol^{-1})**	$\Delta\overline{S}$ **(kJ mol^{-1} K^{-1})**	$\Delta\overline{H}$ **(kJ mol^{-1})**
Fe/Fe^{2+}	1073	38.64	0.29	349.27
Fe/Fe^{2+}	1098	31.40	0.29	349.27
Fe/Fe^{2+}	1123	24.16	0.29	349.27
Ni/Ni^{2+}	1073	22.45	0.16	189.45
Ni/Ni^{2+}	1098	18.57	0.16	189.45
Ni/Ni^{2+}	1123	14.69	0.16	189.45

3.2 Electrochemistry of deposition of boron from KCl-KF-KBF_4 melts: Voltammetric studies on platinum electrode

Electrochemical reduction of boron containing species in KCl-KF melt and the kinetic parameters of the electroreduction process have been evaluated. Transient electrochemical techniques like cyclic voltammetry, chronoamperometry and convolution voltammetry have been used in this study.

3.2.1 Cyclic voltammetry

The cyclic voltammograms (CV) of the melts KCl (81.54 mol%)-KF (18.45 mol%)-KBF_4 (1.6×10^{-4}, 4.1×10^{-4} and 7.73×10^{-4} mol cm^{-3}) were recorded over the temperature range 1073 – 1123 K. Repeated measurement of CVs at any particular scan rate did not show any appreciable shift in peak potential and the peak current. Moreover the open circuit potential (OCP) values did not change after each CV scan. Hence it is surmised that the amount of boron electrodeposited on the electrode during the cathodic cycle of the CV is minimal and does not affect the nature of the working electrode surface for each scan. Typical CVs of the melt (KBF_4 concentration: 1.6×10^{-4} mol cm^{-3}) at various scan rates (0.05 – 1.0 V s^{-1}) are shown in Fig. 3.9.

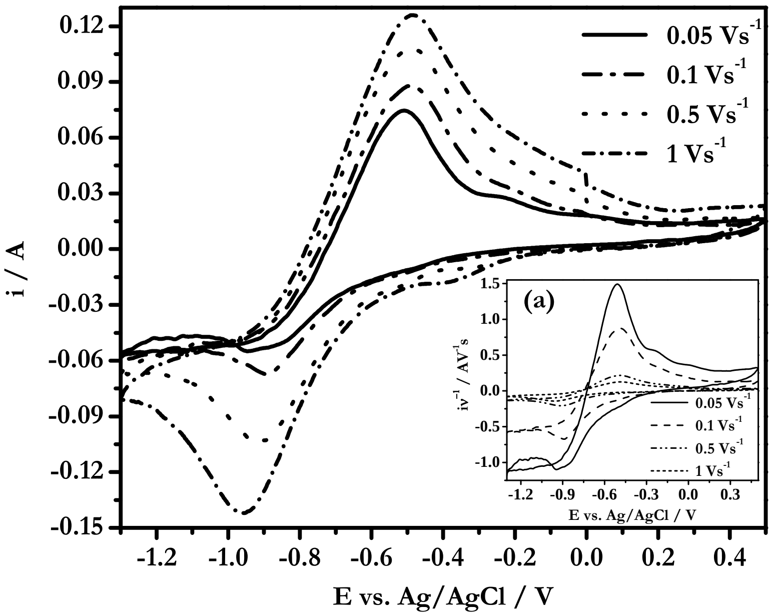

Fig. 3.9 Cyclic voltammetric scans of KCl-KF-KBF_4 (1.6×10^{-4} mol cm^{-3}) melt on a Pt electrode with varying scan rates at 1073 K. The inset [Fig. 3.9(a)] shows the normalized peak current with scan rate.

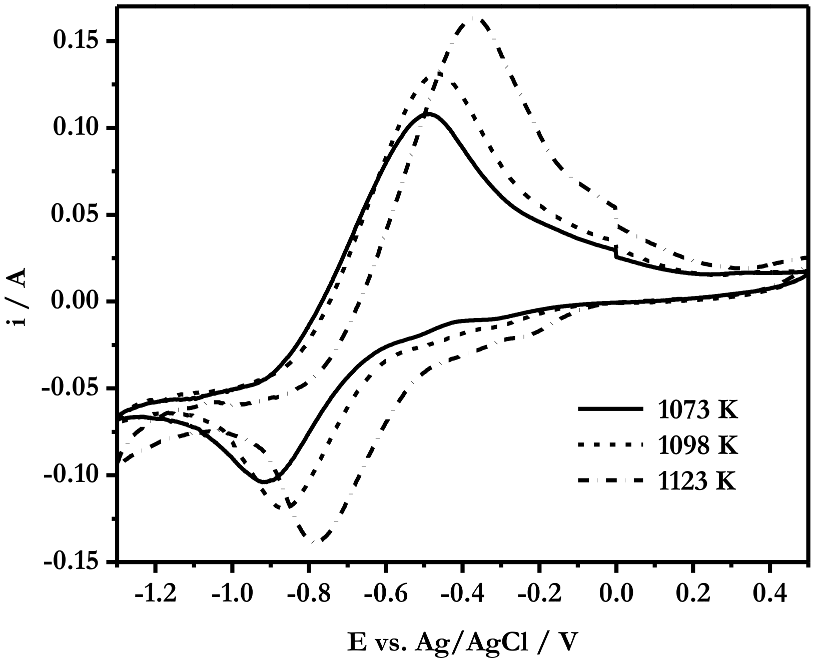

Fig. 3.10 Cyclic voltammetric scans of KCl-KF-KBF_4 (1.6×10^{-4} mol cm^{-3}) melt on a Pt electrode at different temperatures (scan rate: 0.5 Vs^{-1}).

It is seen that the cathodic peak shifts to a more negative potential and anodic peak shifts to a more positive potential with increasing scan rates. In addition the peak current increases with increase in scan rate. With the increase in scan rate the flux of the electroactive species arriving at the electrode by diffusion increases, as a result of which the peak current also increases, since the peak current is directly proportional to the square root of the scan rate. Fig. 3.10 shows the CVs of the melt with 1.6x10^{-4} mol cm^{-3} concentration of KBF_4 at 1073, 1098 and 1123 K. The cathodic (E_P^C) and anodic (E_P^A) peak potentials of the electroactive species as well as the average of cathodic and anodic peak potential, $(E_P^C + E_P^A)/2$, of this melt at different temperatures are given in Table 3.3. It is observed that the cathodic and anodic peak potentials are shifted to less negative values (Fig. 3.10) and the average values increase with increase in temperature (Table 3.3). In general the magnitude of $\mathbf{(}E_{P/2}^C - E_P^C\mathbf{)}$, ($E_{P/2}^C$ is cathodic half-peak potential), is larger than the value required for the reversible process with the formation of an insoluble substance ($\frac{0.071}{n}$ V at 1073 K where, n is the number of electrons transferred for the reduction process) [96, 118] indicating that the reduction of boron species on a platinum electrode from KCl-KF-KBF_4 melt is not reversible. Similar behaviour was observed by Polyakova *et al.* [96] for LiF-NaF-KF melt containing KBF_4.

It has also been observed that the cathodic peak for the reduction of the electroactive species shifts to a more cathodic potential with increase in the KBF_4 content (1.6×10^{-4} to 7.73×10^{-4} mol cm^{-3}) in the melt (Fig. 3.11). It is also seen from the CVs that there is a significant shift in the cathodic and anodic peak potentials suggesting that the electrode process is not completely reversible. A similar behaviour in the shift of anodic and cathodic peak potentials at different temperatures and compositions of KBF_4 is observed. The shift in the peak potential in the cathodic region (Fig. 3.11) is due to increase in the basicity of the melt as per the following exchange reaction [67].

$$BF_4^- + Cl^- \rightleftharpoons BF_3Cl^- + F^- \tag{3.4}$$

Table 3.3 Electrokinetic parameters calculated for the electroactive species in KCl-KF-KBF_4 (1.6×10^{-4} mol cm^{-3}) melt employing Pt electrode.

Temperature (T/K)	**Scan rate (v/V s^{-1})**	**Cathodic peak potential (E_P^C/V)**	**Anodic peak potential (E_P^A/V)**	$\frac{E_P^A + E_P^C}{2}$ **(V)**	$E_{P/2}^C - E_P^C$ **(V)**	**α From Eqn. 2.2**	**α From Eqn. 2.3**
1073	0.05	-0.890	-0.497	-0.693	0.143	0.40	
	0.1	-0.892	-0.507	-0.699	0.136	0.42	
	0.5	-0.917	-0.488	-0.702	0.146	0.39	
	1	-0.958	-0.487	-0.722	0.166	0.34	0.25
1098	0.05	-0.784	-0.473	-0.628	0.086	0.68	
	0.1	-0.821	-0.492	-0.656	0.102	0.57	
	0.5	-0.867	-0.465	-0.666	0.136	0.43	
	1	-0.918	-0.445	-0.681	0.157	0.37	0.28
1123	0.05	-0.717	-0.382	-0.549	0.109	0.54	
	0.1	-0.722	-0.415	-0.568	0.121	0.49	
	0.5	-0.784	-0.370	-0.577	0.147	0.40	
	1	-0.832	-0.359	-0.595	0.138	0.35	0.26

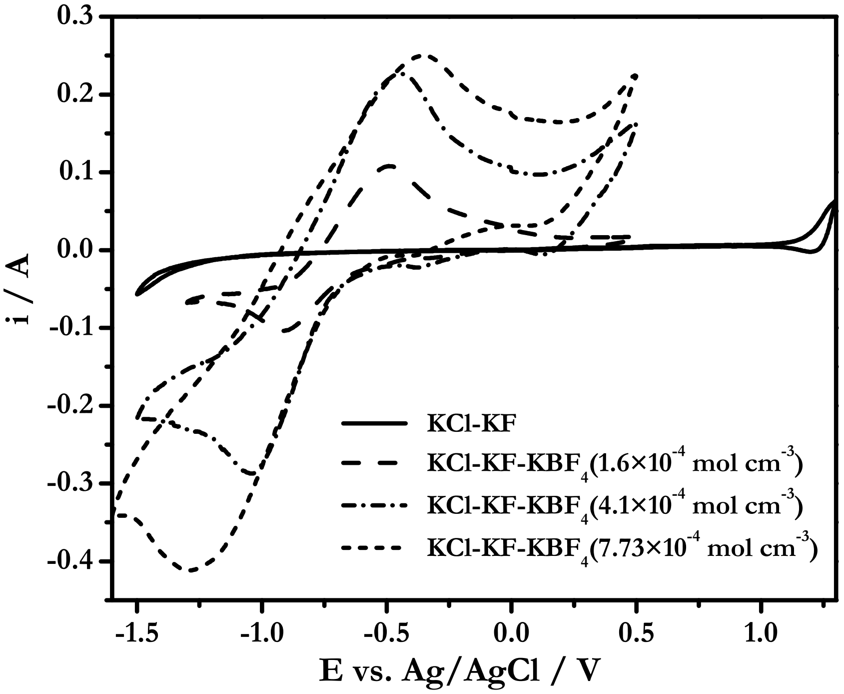

Fig. 3.11 Cyclic voltammetric scans of KCl-KF-KBF_4 melt with varying KBF_4 concentration on a Pt electrode at 0.5 Vs^{-1} scan rate and at 1073 K.

Fig. 3.12 shows the plot of $i_P^C / \nu^{1/2}$ vs. $\nu^{1/2}$ where, i_P^C is the cathodic peak current and ν is the scan rate. Fig. 3.12(a) shows a similar plot for the melt with different concentrations of KBF_4 at 1123 K. It is observed from these plots for the melt KCl-KF-KBF_4 (1.6×10^{-4} to 7.73×10^{-4} mol cm^{-3}) at 1073 – 1123 K that the $i_P^C / \nu^{1/2}$ values remained almost constant at the polarization rates in the interval of 0.05 to 2 V s^{-1}. This suggests that the process of electrodeposition of boron on Pt electrode is not complicated by chemical reactions as suggested by Tsiklauri *et al.* [94, 95] and also the product is not adsorbed at the electrode surface. A similar behaviour was reported by Kuznetsov [67] for NaCl-KCl-KBF_4 system.

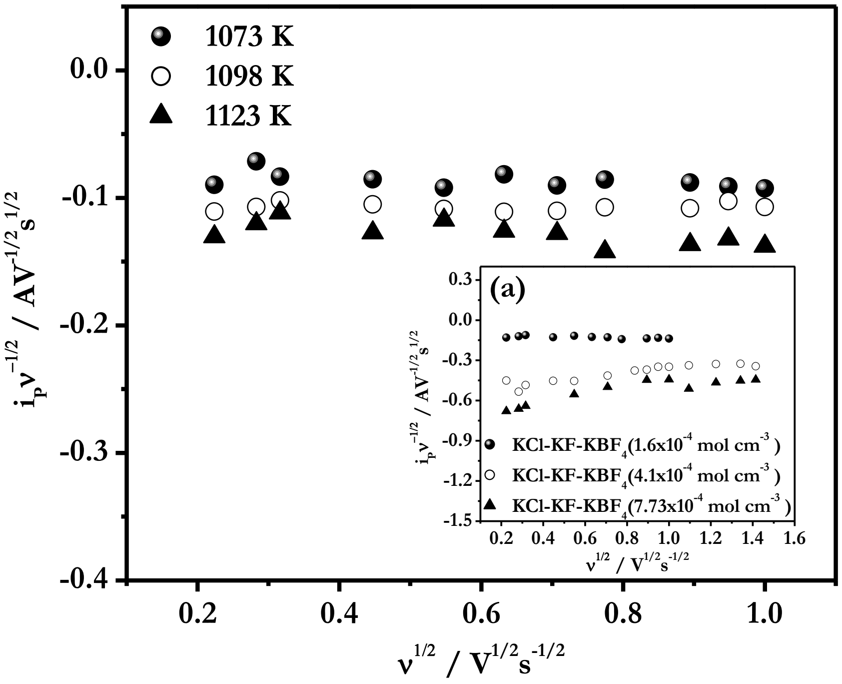

Fig. 3.12 Plot of $i_P^C / \nu^{1/2}$ vs. $\nu^{1/2}$ for the melt KCl-KF-KBF$_4$ (1.6×10^{-4} mol cm^{-3}) at 1073 to 1123 K. The inset shows the linear dependence of $i_P^C / \nu^{1/2}$ vs. $\nu^{1/2}$ for 1.6×10^{-4} to 7.73×10^{-4} mol cm^{-3} KBF$_4$-KCl-KF melt at 1123 K.

The variation of E_P^C with logarithm of scan rate, $\log \nu$, at different temperatures and concentration of KBF$_4$ in the melt are shown in Figs. 3.13 to 3.15. As seen from these figures, there is no change in the cathodic peak potential for the scan rates up to about 0.1 V s^{-1}. For the scan rates beyond 0.1 V s^{-1}, the peak potential changes linearly with $\log \nu$. These observations indicate that the reduction of electroactive boron species on platinum electrode could be quasi-reversible over the scan rate range of 0.05 to 0.1 V s^{-1} and irreversible beyond about 0.1 Vs^{-1}.

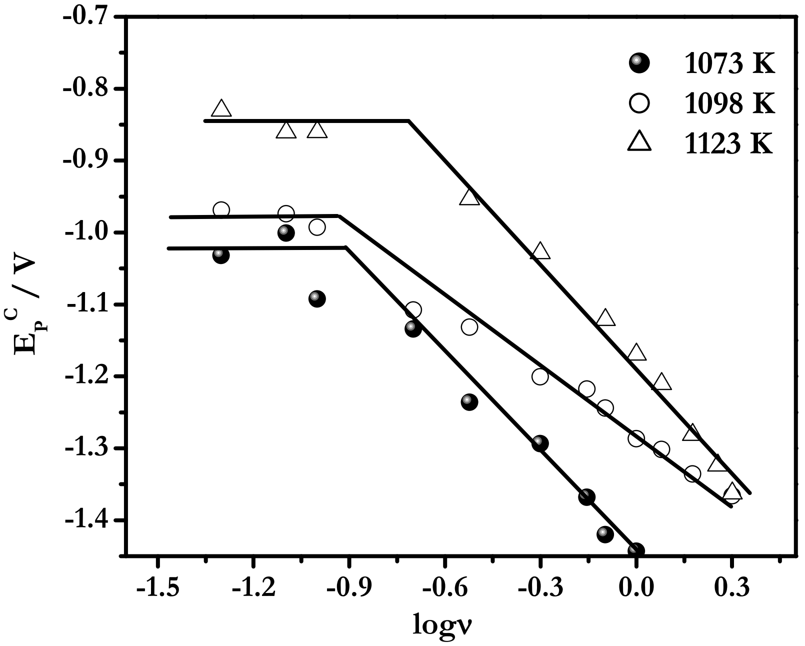

Fig. 3.13 Cathodic peak potential versus logarithm of scan rate measured at different temperatures on a Pt electrode in KCl-KF-KBF$_4$ (1.6×10^{-4} mol cm^{-3}) melt.

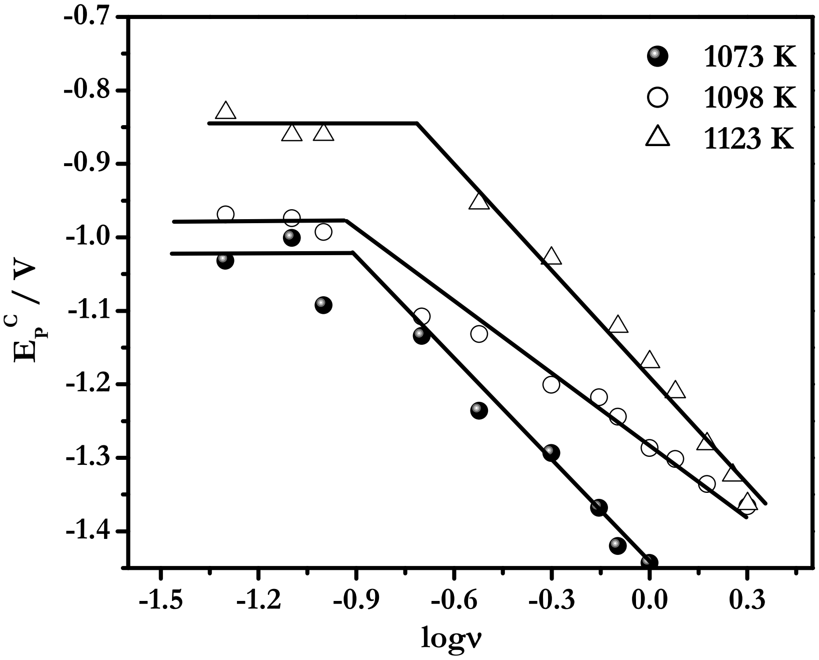

Fig. 3.14 Cathodic peak potential versus logarithm of scan rate measured at different temperatures on a Pt electrode in KCl-KF-KBF$_4$ (4.1×10^{-4} mol cm^{-3}) melt.

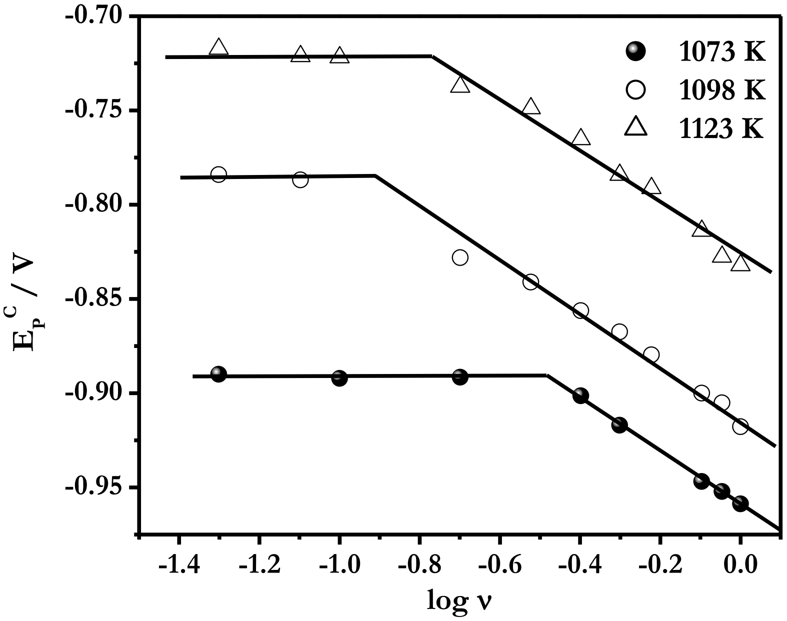

Fig. 3.15 Cathodic peak potential versus logarithm of scan rate measured at different temperatures on a Pt electrode in KCl-KF-KBF$_4$ (7.73×10^{-4} mol cm^{-3}) melt.

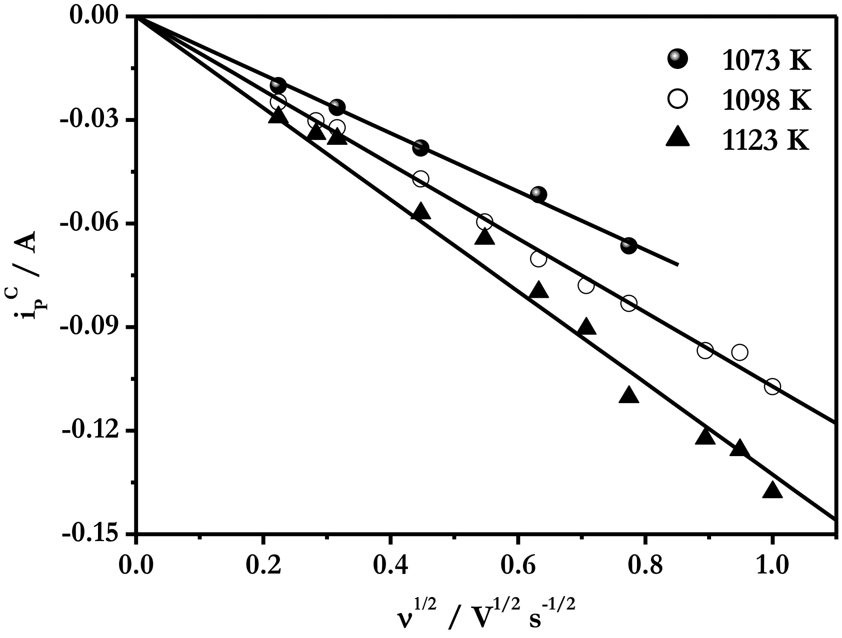

Fig. 3.16 Cathodic peak current versus square root of scan rate at different temperatures on a Pt electrode in KCl-KF-KBF$_4$ (1.6×10^{-4} mol cm^{-3}) melt.

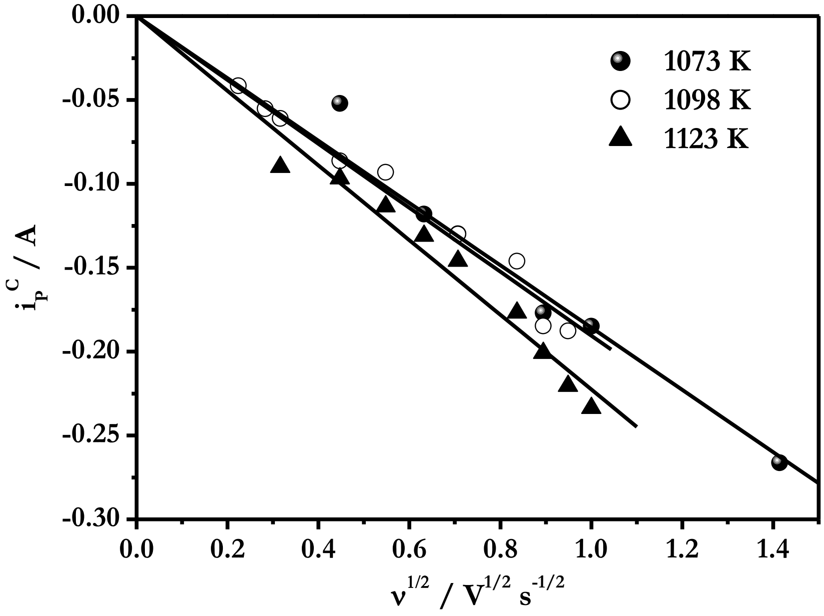

Fig. 3.17 Cathodic peak current versus square root of scan rate at different temperatures on a Pt electrode in KCl-KF-KBF_4 (4.1×10^{-4} mol cm^{-3}) melt.

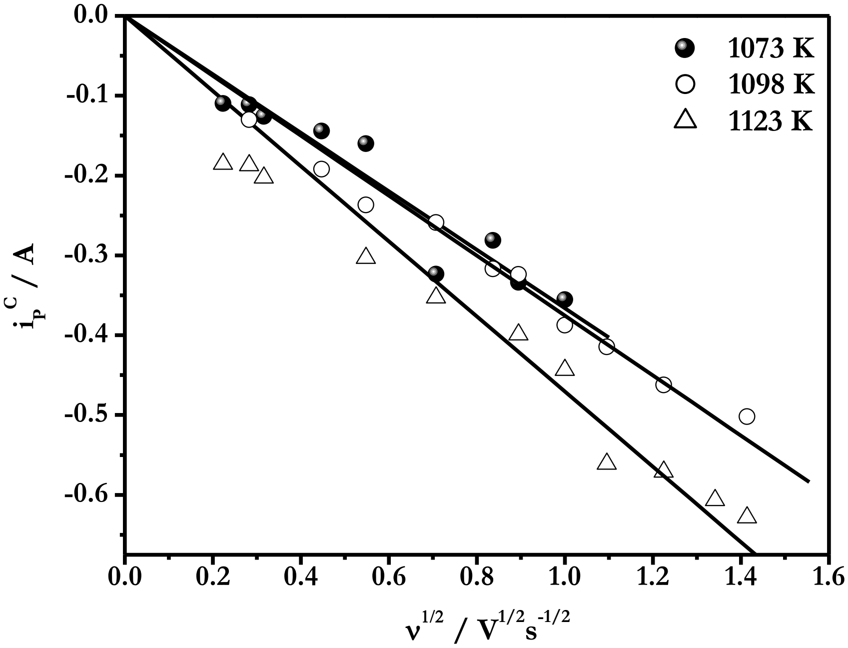

Fig. 3.18 Cathodic peak current versus square root of scan rate at different temperatures on a Pt electrode in KCl-KF-KBF_4 (7.73×10^{-4} mol cm^{-3}) melt.

Figs. 3.16 – 3.18 show the variation of the cathodic peak current, i_P^C, with the square root of scan rate, $\nu^{1/2}$, at different temperatures for the melt containing various concentrations of KBF_4. The linear relationship between i_P^C and $\nu^{1/2}$, as observed from these figures indicate that the electrode process is diffusion controlled.

3.2.2 Calculation of transfer coefficient

The transfer coefficients calculated from Eqn. 2.2 and 2.3 for the KCl-KF melt containing 1.6x10^{-4} mol cm^{-3} of KBF_4 are given in Table 3.3. At 1073, 1098 and 1123 K the transfer coefficients vary from 0.4 – 0.34, 0.68 – 0.37 and 0.54 – 0.35 respectively when the scan rates vary from 0.05 to 1 V s^{-1}, according to Eqn. 2.2. By using Eqn. 2.3 it is found that the transfer coefficients vary from 0.25 – 0.28 over the temperature range 1073 – 1123 K. The typical transfer coefficient values signify that the process is irreversible.

3.2.3 Logarithmic analysis of convolution voltammetry

A typical semiintegral convolution voltammogram of KCl-KF-KBF_4 (1.6x10^{-4} mol cm^{-3}) melt is presented in Fig. 3.19. Fig. 3.19(a) shows the plot of

$$\ln\left\{\frac{m^*(\infty)-m(t)\left[1+\exp\left\{\frac{RT}{nF}\left(E-E_{1/2}\right)\right\}\right]}{i(t)}\right\} \text{vs. } E(t)$$

. The values of n and α obtained by considering the reversible, quasireversible and irreversible conditions for the different concentrations of KBF_4 in KCl-KF melt at 0.1 and 1 V s^{-1} scan rates are given in Table 3.4.

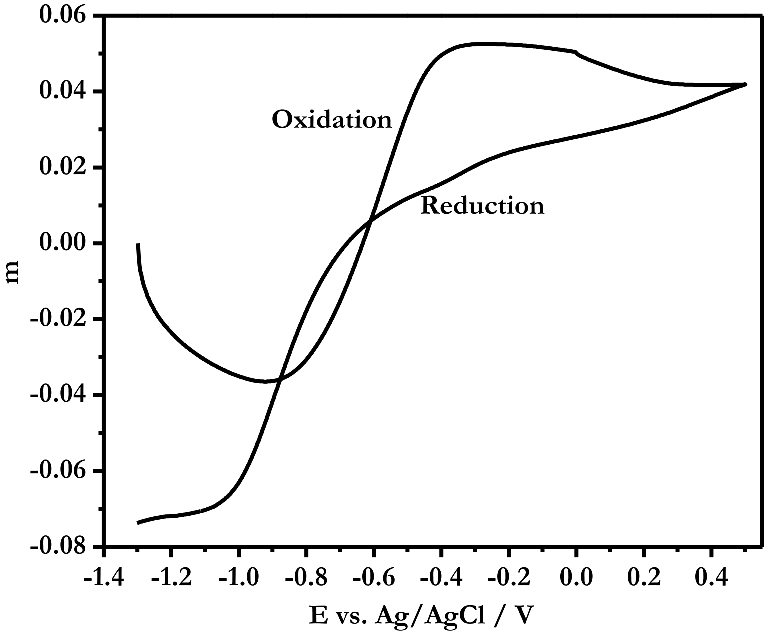

Fig. 3.19 Convoluted voltammogram of KCl-KF-KBF_4 (1.6×10^{-4} mol cm^{-3}) melt at 1073 K and 0.1 V s^{-1} scan rate.

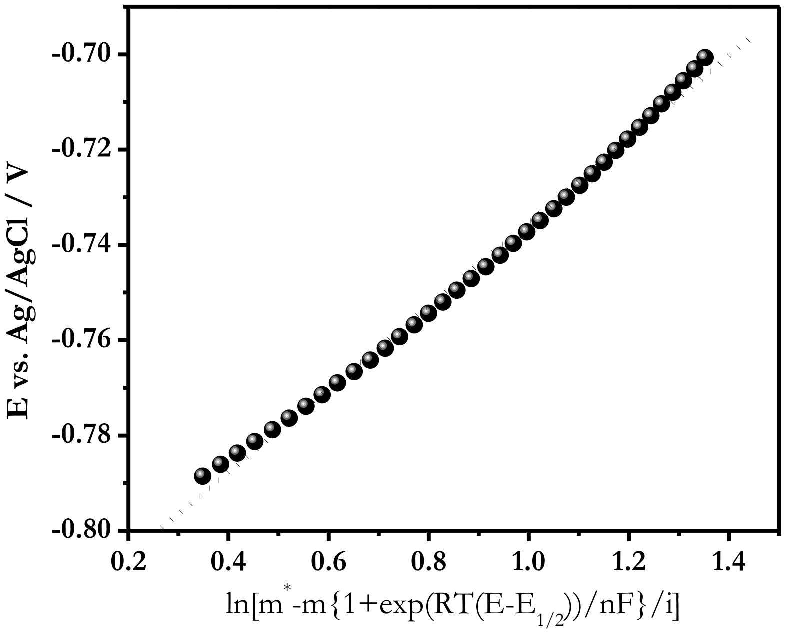

Fig. 3.19(a) Linear region of the logarithmic analysis of the convoluted curve for the reduction of boron species as per quasireversible hypothesis.

Table 3.4 Logarithmic analysis of the convoluted voltammograms of KBF_4 in KCl-KF melt.

Concentration of KBF_4 in KCl-KF melt (C_o^*/ mol cm^{-3})	**Temperature (T/K)**	**Scan rate (v/V s^{-1})**	**Reversible hypothesis**	**Quasi-reversible hypothesis (n = 3)**		**Irreversible hypothesis (n = 3)**	
			n	$n\alpha$	α	$n\alpha$	α
1.6×10^{-4}	1073	0.1	0.35	1.06	0.35	0.42	0.14
		1.0	0.02	1.02	0.33	0.74	0.15
	1098	0.1	0.35	1.27	0.42	0.42	0.14
		1.0	0.63	1.52	0.51	1.11	0.37
	1123	0.1	0.20	0.83	0.28	0.32	0.11
		1.0	0.66	1.43	0.48	0.95	0.32
4.1×10^{-4}	1073	0.1	0.25	1.05	0.35	0.42	0.14
		1.0	0.50	0.90	0.30	0.72	0.24
	1098	0.1	0.21	1.11	0.37	0.28	0.10
		1.0	0.27	0.80	0.27	0.67	0.22
	1123	0.1	0.45	1.39	0.46	0.36	0.12
		1.0	0.42	0.85	0.28	0.54	0.18
7.73×10^{-4}	1073	0.1	0.27	0.83	0.28	0.39	0.13
		1.0	0.34	0.70	0.23	0.60	0.20
	1098	0.1	0.28	0.97	0.32	0.45	0.15
		1.0	0.35	0.81	0.27	0.48	0.16
	1123	0.1	0.33	1.04	0.35	0.36	0.12
		1.0	0.34	0.58	0.19	0.48	0.16

The results (Table 3.4) show that the values of n (electrons involved in the reduction of electroactive boron species) obtained by considering reversible process is not reasonable as the process of reduction of boron species should involve three electrons. The α value obtained by considering quasireversible process is valid for the scan rate of 0.1 V s^{-1}. Irreversibility of the process is established by the typical α values obtained for the convoluted CVs at a scan rate of 1 V s^{-1}. The values of transfer coefficient obtained from Eqn. 2.3 and those using the quasireversible hypothesis are in good agreement suggesting that the process of reduction of boron species is quasireversible over the scan rate range of 0.05 to 0.1 V s^{-1}. Thus convolution voltammetry establishes that the process of reduction of boron species is a quasireversible and irreversible at the scan rates of 0.1 V s^{-1} and 1 V s^{-1} respectively.

3.2.4 Diffusion coefficients

A relationship between the cathodic peak current (i_P^C) and square root of the scan rate for an insoluble deposit in irreversible/quasireversible system is given by the expression 2.4 [122]. From the slope of the straight lines obtained by plotting i_P^C against $\nu^{1/2}$, the diffusion coefficients (D_O) of B(III) were determined and their values are given in Table 3.5. It is observed that the diffusion coefficients increase with increase in temperature. Makyta *et al.* [95] have reported the diffusion coefficient for boron complexes in the LiF-KF melt containing KBF_4 to be 4.4×10^{-5} cm^2 s^{-1} at 973 K. Zarutskii [138] has reported the diffusion coefficient of BF_4^- in NaCl-KCl-KF melt at 973 K to be $1.4 - 3.2\times10^{-5}$ cm^2 s^{-1}. Tsiklauri *et al.* [139] have reported the diffusion coefficient value as $0.7 - 5.11\times10^{-6}$ cm^2 s^{-1} following a change in the KBF_4 concentration from 1×10^{-5} to

1×10^{-4} mol cm^{-3} within the polarization rate of 0.5 to 2 V s^{-1}. Kuznetsov [67] has reported the values of diffusion coefficient varying from 2.65 to 4.22×10^{-5} cm^{2} s^{-1} in NaCl-KCl-KBF$_4$ melts and 2.12 to 3.24×10^{-5} cm^{2} s^{-1} in NaCl-KCl-NaF (5 wt%)-KBF$_4$ melts over the temperature range 973 to 1073 K. The difference in the values of the diffusion coefficients in different melt systems at different temperatures may be due to the varying physicochemical properties (viscosity and conductivity) of each system.

Table 3.5 Diffusion coefficient of the electroactive species in KCl-KF melt containing different concentration of KBF$_4$ at different temperatures.

KBF$_4$ concentration (C_o^*/mol cm^{-3})	**Temperature (*T*/K)**	**Diffusion coefficient ($D_O\times10^5$/cm^2 s^{-1})**		**Electron transfer rate constant ($k_s\times10^3$ /cm s^{-1})**
		Delahay Eqn.	**Chronoamperometry**	
1.60×10^{-4}	1073	2.5 ± 0.4	1.2 ± 0.3	3.9
	1098	3.7 ± 0.7	1.3 ± 0.1	3.4
	1123	5.1 ± 0.9	1.7 ± 0.4	4.8
4.10×10^{-4}	1073	2.4 ± 0.7	1.3 ± 0.2	5.8
	1098	2.6 ± 0.5	1.9 ± 0.6	9.3
	1123	2.9 ± 0.6	2.5 ± 0.7	11.9
7.73×10^{-4}	1073	3.4 ± 0.9	1.2 ± 0.5	8.3
	1098	4.2 ± 0.7	1.6 ± 0.4	8.7
	1123	6.0 ± 0.9	2.3 ± 0.2	10.2

The diffusion coefficient of the electroactive species can also be measured by chronoamperometry using Cottrell equation (Eqn. 2.15) [118]. Typical chronoamperograms of KCl-KF-KBF_4 (4.1×10^{-4} mol cm^{-3}) melt employing Pt electrode are shown in Fig. 3.20. A linear variation of i with $t^{-1/2}$ is observed as shown in Fig. 3.20(a) which indicates that the reduction of boron containing electroactive species in molten KCl-KF-KBF_4 system is diffusion controlled. The diffusion coefficient values thus obtained are shown in Table 3.5. As seen from Table 3.5, there is a reasonable agreement in the values of D_O calculated from cyclic voltammetry using Eqn. 2.4 and chronoamperometry using Eqn. 2.15.

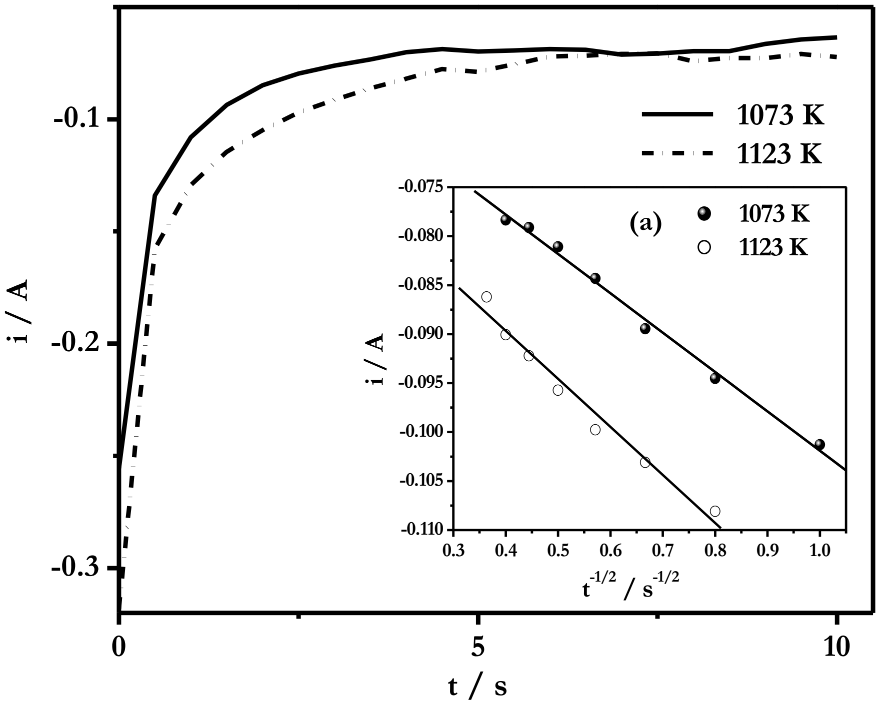

Fig. 3.20 Chronoamperograms of KCl-KF-KBF_4 (4.1×10^{-4} mol cm^{-3}) melt on a Pt electrode (0.2 cm^2 area) carried out at -1.0 V potential scan. The inset [Fig. 3.20(a)] shows the plot of i vs. $t^{-1/2}$.

3.2.5 Electron transfer rate constant

Klingler and Kochi [123] have derived an expression (Eqn. 2.5) for obtaining the electron transfer rate constant (k_s) by assuming that the electron-transfer reaction is irreversible.

By using the above equation the electron transfer rate constants for the irreversible electrode process at different KBF_4 concentrations in KCl-KF melt and over the temperature range 1073 to 1123 K have been calculated. The k_s values obtained by substituting the αn_α values obtained from Eqn. 2.2 at 1 V s^{-1} scan rate and D_O derived from Eqn. 2.15 are presented in Table 3.5. These values indicate sluggish electron transfer kinetics due to the fact that the oxidized boron (fluoro-chloro complex of boron) and the reduced boron (elemental boron) are structurally dissimilar and the activation barrier for the redox process is large.

3.2.6 Electrodeposition

Boron was electrodeposited on a planar platinum electrode (10 mm (W) x 15 mm (L)) from a KCl (81.54 mol%)-KF (18.45 mol%) melt containing 4.1×10^{-4} mol cm^{-3} KBF_4. The electrolysis was carried out at constant current of -0.2 A for 2 h. During the deposition process the cell resistance varied from 55 to 87×10^3 Ω cm^2 and the cell voltage changed from an initial value of 0.068 to 1.35 V. The open circuit potential varied from -0.172 to -1.13 V. During the progress of electrodeposition on platinum electrode the electrode surface area changes due to boron deposition. A black deposit (Fig. 3.21) was found on the electrode surface. It was found that the electrode side facing the counter electrode had less deposit compared to the side facing the reference electrode. The X-ray diffraction analysis of the electrodeposit shows it to be amorphous in nature. This black mass was found to be boron by chemical analysis. The scanning electron micrograph of the deposit is shown in Fig. 3.22. The micrograph shows that the deposition of boron on platinum electrode is uniform with minimum porosity. Energy-dispersive X-ray analysis (Fig. 3.22) shows the presence of F^-, Cl^- and K^+ as impurities. This is due to the adherence of the melt on the surface of the deposit.

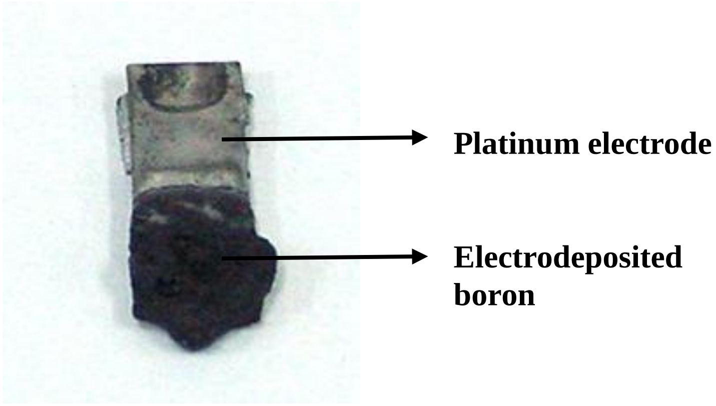

Fig. 3.21. Boron electrodeposited on a planar Pt electrode by carrying out constant current (-0.2 A) electrolysis for 2h at 1073 K.

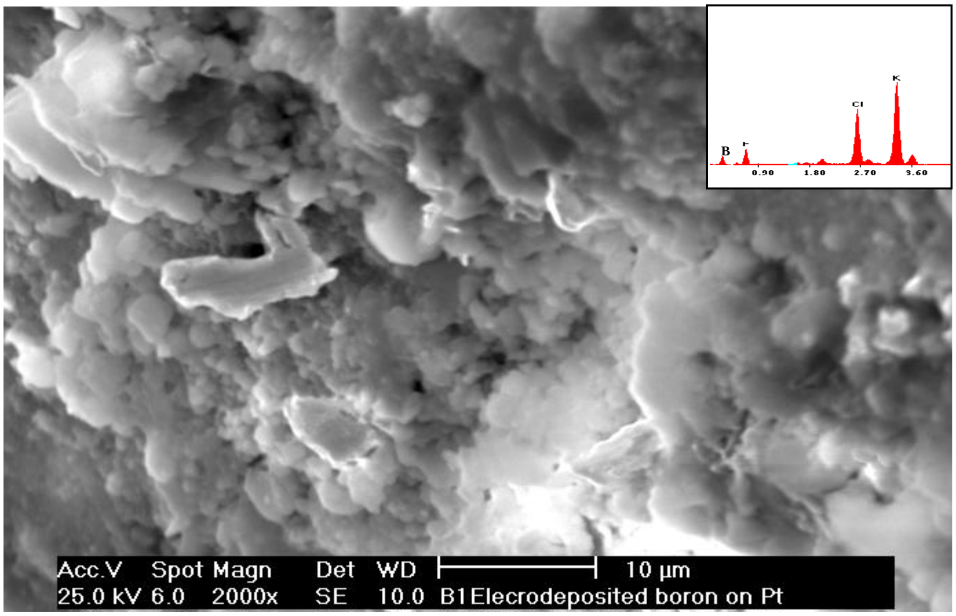

Fig. 3.22 Scanning electron micrograph of electrodeposited boron on a Pt electrode.

3.2.7 Boron nucleation potential

Crossover was not observed for the voltammetric scans measured at low scan rates (Fig. 3.9). Moreover, crossover of the cathodic and anodic current in voltammograms was observed after the cathodic peak by switching the potential scans to a more cathodic region for KCl-KF-KBF_4 (4.1×10^{-4} mol cm^{-3}) melt at a scan rate of 0.1 Vs^{-1} (Fig. 3.23). This crossover is attributed to the nucleation phenomenon asssociated with potassium deposition. Therefore the type of nucleation for boron deposition could not be ascertained in the present study.

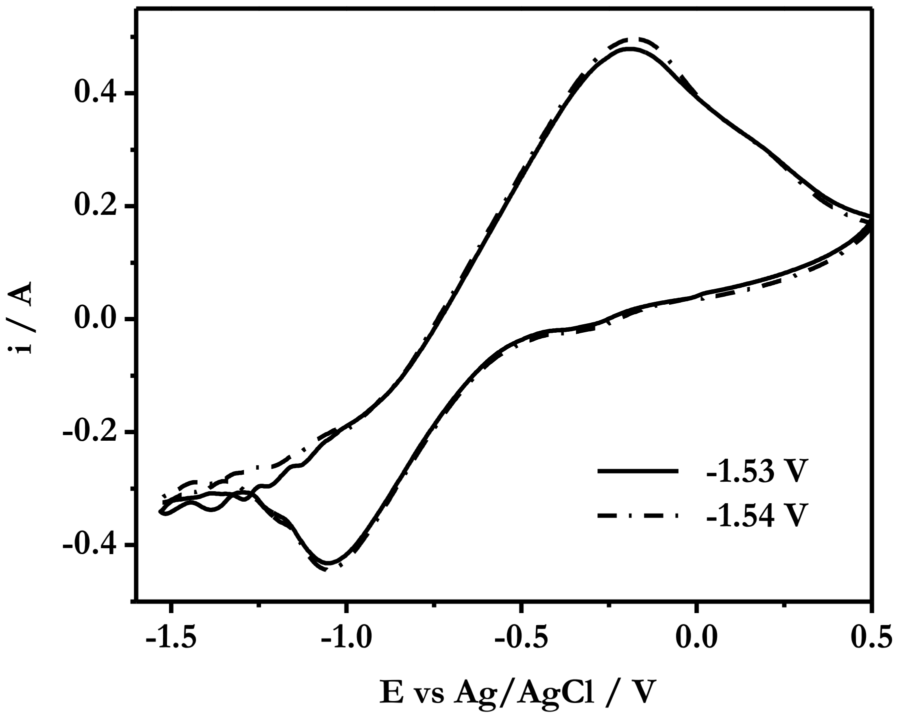

Fig. 3.23 Crossover of the voltammograms in the cathodic region attributed to potassium nucleation on Pt electrode at 0.1 V s^{-1} scan rate in KCl-KF-KBF_4 (4.1×10^{-4} mol cm^{-3}) at different cathodic switching potentials at 1073 K.

The nucleation potentials for boron on a platinum electrode with respect to Ag/AgCl reference electrode were obtained by linear extrapolation of the left edge of the anodic peak and right edge of the cathodic peak of CV to zero current at a particular scan rate [96, 140]. The potentials thus obtained for the cathodic and anodic peak are the anodic nucleation potential and cathodic nucleation potential respectively. The cathodic and anodic nucleation overpotentials were calculated as the difference between the boron equilibrium potential and nucleation potentials as reported by Polyakova *et al.* [96]. In the present study the boron equilibrium potentials were measured from the open circuit potentials of the electrodeposited boron on platinum electrode in KCl-KF-KBF_4 (4.1×10^{-4} mol cm^{-3}) melt over the temperature range 1073 to 1123 K. The boron nucleation potentials and nucleation overpotentials are presented in Table 3.6.

Table 3.6 Nucleation potential, equilibrium potential and nucleation overpotential calculated for B(III)/B redox couple in KCl-KF-KBF_4 (4.1×10^{-4} mol cm^{-3}) melt at different temperatures.

Temperature (K)	Anodic nucleation potential (V)	Cathodic nucleation potential (V)	Equilibrium potential (V)	Anodic nucleation overpotential (V)	Cathodic nucleation overpotential (V)
1073	-0.751	-0.678	-0.546	-0.205	-0.132
1098	-0.735	-0.558	-0.231	-0.504	-0.327
1123	-0.733	-0.549	-0.146	-0.588	-0.404

It is observed that both the potentials decrease with increase in temperature for a fixed boron concentration in the melt. Increase in concentration of KBF_4 in the melt may shift the boron nucleation potential to a more negative value due to increase in the basicity of the melt as per the exchange reaction (3.4) mentioned earlier in Section 3.2.1. Another reason could be the surface resistance of the boron film which would increase with increase in KBF_4 content in the melt (Table 3.7).

3.2.8 Apparent surface resistance

Polyakova *et al.* [96] have reported that the broadening of the cathodic peak in CV occurred due to the ohmic control of deposition of boron. These authors have presented linear plots of peak current and peak potentials against the square root of scan rate and concluded that a surface boron film formed on the electrode rendered the process to be controlled by ohmic resistance.

The "apparent surface resistance" (R_{app}) of the electrolyte in the pores of the boron film covering the electrode can be obtained from the reciprocal of the slope of peak current density (j_P) vs. peak potential (E_P) plots as reported by Polyakova *et al.* [96]. The plot for cathodic peak current density vs. cathodic peak potential for KCl-KF-KBF_4 (1.6×10^{-4} mol cm^{-3}) shows a linear behaviour (Fig. 3.24). The values of R_{app} calculated for varying KBF_4 concentrations in KCl-KF melt at different temperatures are presented in Table 3.7. It is observed (Table 3.7) that the R_{app} values decrease with increase in temperature and increase with increase in KBF_4 content in the melt. Polyakova *et al.* [96] reported a higher value of R_{app} (3.3 Ω cm^2 at 973 K) in LiF-NaF-KF-KBF_4 (15.9×10^{-2} mol%) melt. The typical resistance values obtained (Table 3.7) in our present study is very small and it is surmised that the effect of resistance on CVs is negligible and it does not quite affect the determination of alpha values from the cyclic voltammetric scans and convolution voltammetry.

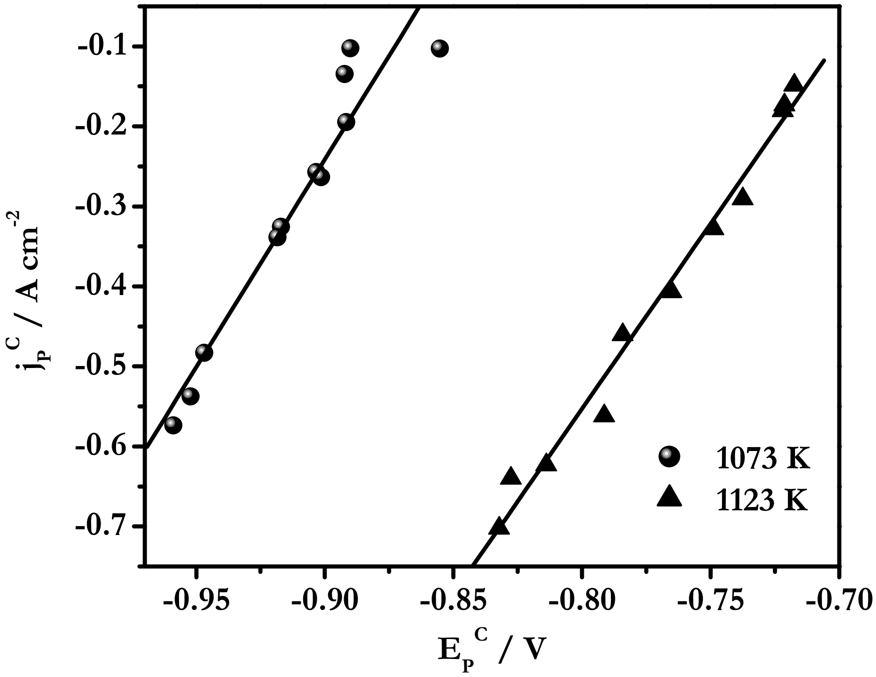

Fig. 3.24 Cathodic peak current density versus cathodic peak potential for boron deposition on Pt electrode in KCl-KF-KBF_4 (1.6×10^{-4} mol cm^{-3}) melt at different temperatures.

Table 3.7 Apparent surface resistance of the electrolyte on the platinum electrode for various KBF_4 concentrations in KCl-KF melts at different temperatures.

KBF_4 concentration in KCl-KF melt (mol cm^{-3})	**Temperature (K)**	**R_{app}(reciprocal slope of (j_P^C vs. E_P^C plot) (Ω cm^2)**
1.6×10^{-4}	1073	0.18 ± 0.02
	1123	0.21 ± 0.01
4.1×10^{-4}	1073	0.18 ± 0.01
	1123	0.27 ± 0.01
7.73×10^{-4}	1073	0.28 ± 0.04
	1123	0.22 ± 0.01

3.3 Electrochemistry of deposition of boron from KCl-KF-NaBF$_4$ melt

Electrochemical reduction of boron containing electroactive species in KCl-KF-NaBF$_4$ melt and the kinetic parameters of the electroreduction process were evaluated. A systematic study on boron deposition from alkali metal fluoroborates in KCl-KF melt is reported.

3.3.1 Cyclic voltammetry

The CV of the melt KCl (81.54 mol%) - KF (18.45 mol%) - NaBF$_4$ (1.67×10^{-4} mol cm^{-3}) (designated as melt A) was recorded over the temperature range 1073 – 1123 K. Typical CVs of this melt at various scan rates (0.05 – 1.5 V s^{-1}) are shown in Fig. 3.25. It is seen that the cathodic peak shifts to a more negative potential and the anodic peak shifts to a more positive potential with increasing scan rates. In addition the peak current increases with increase in scan rate. Fig. 3.26 shows the CVs of the melt A at 1073, 1098 and 1123 K. The cathodic (E_P^C) and anodic (E_P^A) peak potentials of the electroactive species as well as the average of cathodic and anodic peak potential, $(E_P^C + E_P^A)/2$, of this melt at different temperatures are given in Table 3.8. It is observed that the cathodic and anodic peak potentials are shifted to less negative values (Fig. 3.26) and the average values increase with increase in temperature (Table 3.8). It is also observed that the magnitude of ($E_{P/2}^C - E_P^C$), is larger than the value required for the reversible process with the formation of an insoluble substance ($\frac{0.071}{n}$ V at 1073 K where, n is the number of electrons transferred for the reduction process) [96, 118] indicating that the reduction of boron species on a platinum electrode from KCl-KF-NaBF$_4$ melt is not reversible.

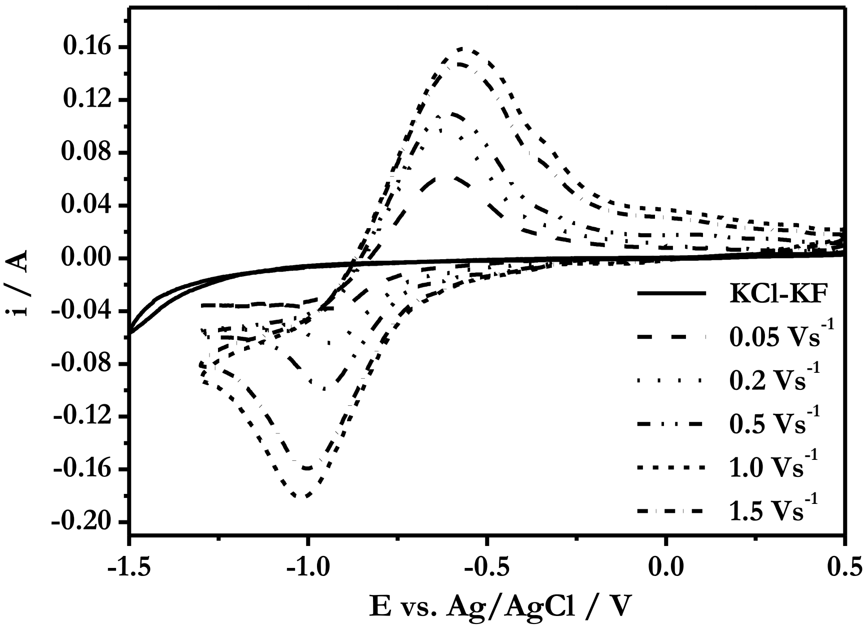

Fig. 3.25 Cyclic voltammetric scans of the melt A on Pt electrode with varying scan rates at 1073 K.

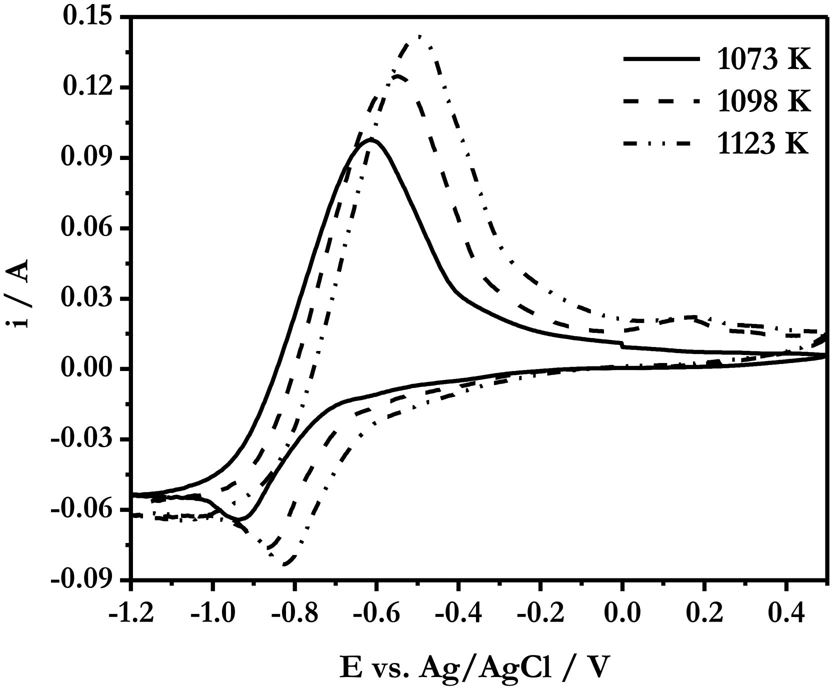

Fig. 3.26 Cyclic voltammetric scans of the melt A on Pt electrode at different temperatures (scan rate: 0.2 V s^{-1}).

Table 3.8 Electrokinetic parameters calculated for the electroactive species in the melt A employing platinum electrode.

Temperature (T/K)	**Scan rate (v/V s^{-1})**	**Cathodic peak potential (E_P^C / V)**	**Anodic peak potential (E_P^A /V)**	$E_{1/2}$ **(V)**	$E_{P/2}^C - E_P^C$ **(V)**	**α from Eqn. 2.2**	**α from Eqn. 2.3**
1073	0.1	-0.927	-0.614	-0.770	0.094	0.60	
	0.5	-0.955	-0.608	-0.781	0.118	0.48	
	1.0	-0.975	-0.590	-0.782	0.133	0.43	
	2.0	-1.018	-0.565	-0.791	0.160	0.36	0.34
1098	0.1	-0.854	-0.549	-0.701	0.083	0.69	
	0.5	-0.894	-0.554	-0.724	0.106	0.54	
	1.0	-0.925	-0.542	-0.733	0.125	0.46	
	2.0	-0.971	-0.517	-0.744	0.152	0.37	0.34
1123	0.1	-0.786	-0.493	-0.639	0.089	0.64	
	0.5	-0.802	-0.432	-0.617	0.109	0.52	
	1.0	-0.833	-0.426	-0.629	0.125	0.46	
	2.0	-0.879	-0.394	-0.636	0.149	0.38	0.31

The reduction potential of boron from boron containing electroactive species in the melt A was found to be more negative compared to that of the melt KCl (81.54 mol%) - KF (18.45 mol%) - KBF_4 (1.6×10^{-4} mol cm^{-3}) (designated as melt B) (Fig. 3.27).

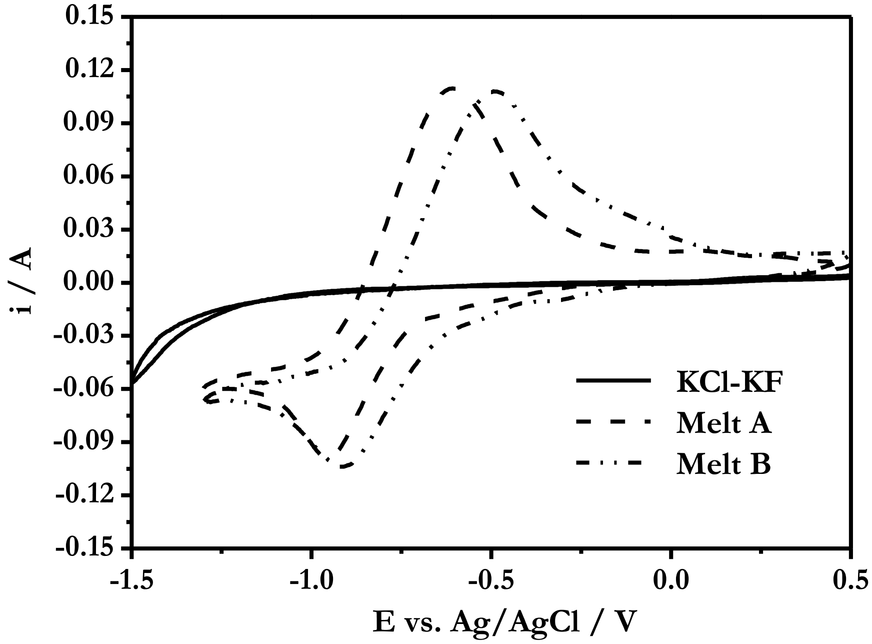

Fig. 3.27 Cyclic voltammetric scans of the melts A and B on Pt electrode at 1073 K and 0.5 V s^{-1} scan rate.

Fig. 3.28 shows the plot of $i_p^C / v^{1/2}$ vs. $v^{1/2}$. It is observed from these plots that for the melt A at 1073 K, the $i_p^C / v^{1/2}$ values remain almost constant in the polarization rate range of 0.05 to 2 V s^{-1}. This suggests that the process of electrodeposition of boron on Pt electrode is not complicated by chemical reactions as suggested by Tsiklauri *et al.* [97, 98]. In addition the electrodeposit is not adsorbed at the electrode surface. A similar behaviour was observed for the melts NaCl-KCl-KBF_4 [67] and the melt B. Thus it can be inferred that the electrodeposition of boron from alkali metal fluoroborate containing KCl-KF melts is not complicated by chemical reactions.

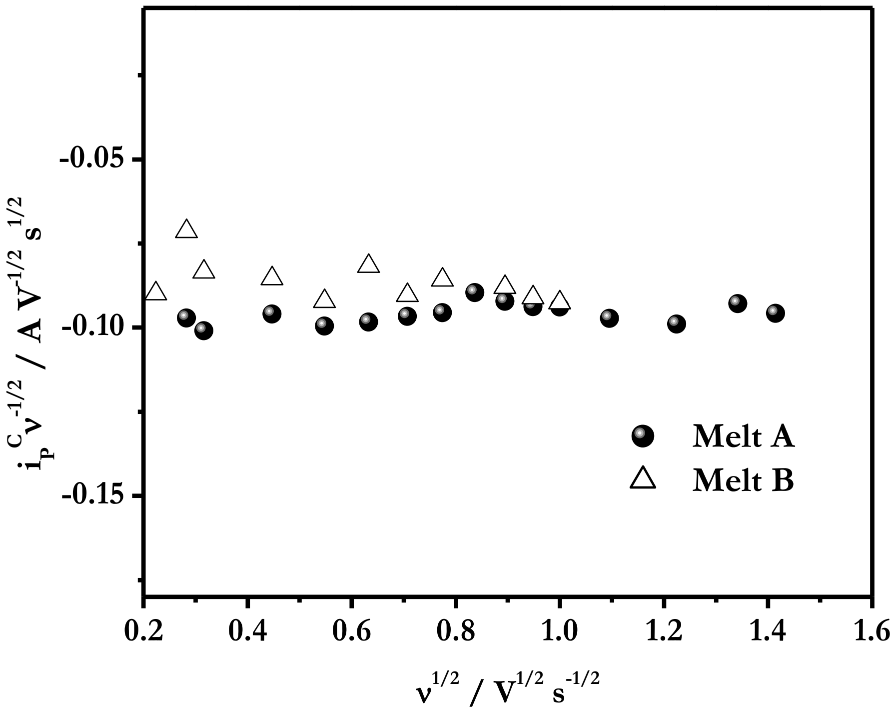

Fig. 3.28 Plot of $i_P^C / \nu^{1/2}$ vs. $\nu^{1/2}$ for the melts A and B at 1073 K.

The variation of E_P^C with logarithm of scan rate, $\log \nu$, at different temperatures for the melt A is shown in Fig. 3.29. As seen from the figure, the cathodic peak potential varies linearly with $\log \nu$. These observations indicate that the reduction of electroactive boron species on platinum electrode is quasi-reversible at low scan rates ($\nu < 0.1$ V s^{-1}) and irreversible at higher scan rates ($\nu > 0.1$ V s^{-1}).

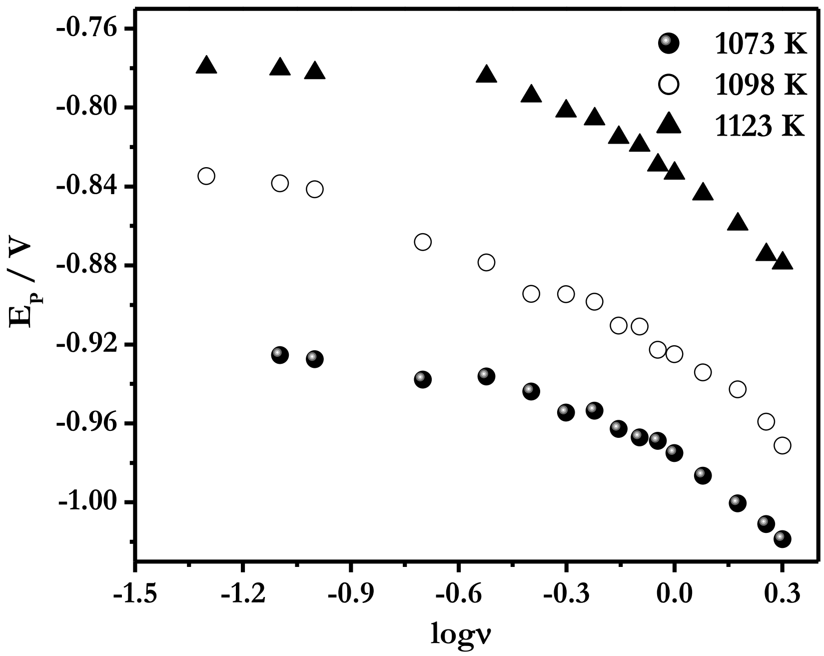

Fig. 3.29 Cathodic peak potential versus logarithm of scan rate measured at different temperatures on a Pt electrode in the melt A.

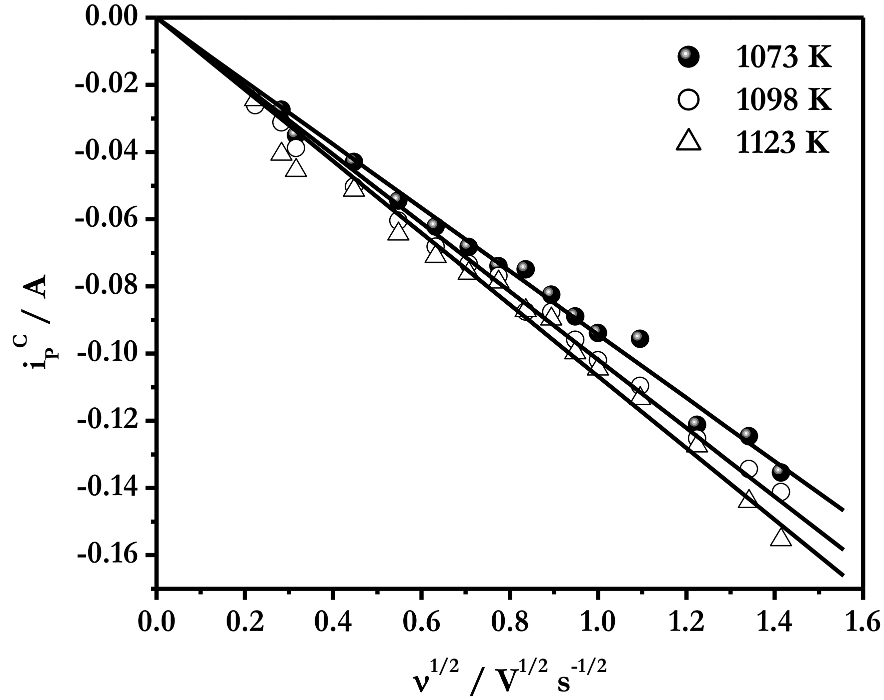

Fig. 3.30 Cathodic peak current versus square root of scan rate at different temperatures on a Pt electrode in the melt A.

The variation of the cathodic peak current, i_P^C, with the square root of scan rate, $\nu^{1/2}$, at different temperatures for the melt A is shown in Fig. 3.30. The linear relationship between i_P^C and $\nu^{1/2}$, as observed from these figures indicate that the process is diffusion controlled.

3.3.2 Calculation of transfer coefficient

The transfer coefficients calculated from Eqns. 2.2 and 2.3 for the melt A is given in Table 3.8. For the melt A at 1073, 1098 and 1123 K the transfer coefficients were found to vary from 0.60 – 0.36, 0.37 – 0.69 and 0.64 – 0.38 respectively. By using Eqn. 2.3 the transfer coefficients for the melt A was found to vary from 0.34 – 0.31. The typical transfer coefficient values signify that the process is irreversible. Similar inference has also been drawn for the melt B as mentioned in Section 3.2.2.

3.3.3 Diffusion coefficients

The diffusion coefficient of the electroactive species can be measured by chronoamperometry using Cottrell equation (Eqn. 2.15) [118]. Typical chronoamperograms of the melt A employing Pt electrode are shown in Fig. 3.31. A linear variation of i with $t^{-1/2}$ is observed as shown in Fig. 3.31(a).

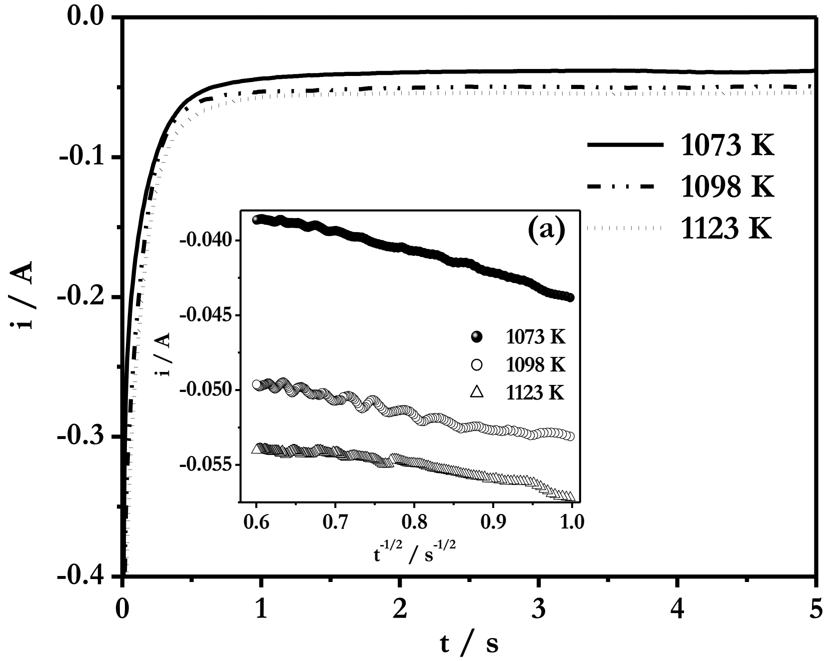

Fig. 3.31 Chronoamperograms of the melt A on a Pt electrode (0.23 cm^2 area) carried out at -0.85 V potential scan. The inset [Fig. 3.31(a)] shows the plot of i vs. $t^{-1/2}$.

This indicates that the reduction of boron containing electroactive species in the melt A is diffusion controlled. The diffusion coefficient of the electroactive species in the melt A was found to be 6.4×10^{-6} cm^2 s^{-1} at 1073 K (Table 3.9). Typical diffusion coefficient values for different alkali metal fluoroborate containing melt systems at different temperatures are presented in Table 3.9. A comparative study of D_O values of the boron containing electroactive species from different alkali metal fluoroborates in KCl-KF melts shows that $D_O^{NaBF_4} < D_O^{KBF_4}$. According to Stokes-Einstein equation (Eqn. 3.5), the diffusion coefficient of a species is inversely proportional to its solvodynamic radius (r_s).

$$D_O = \frac{kT}{C\pi\eta r_s} \qquad 3.5$$

where, k is the Boltzmann constant, C is a constant and η is the absolute or bulk viscosity of the solvent. It is surmised that the solvodynamic radius (r_s) of the boron containing electroactive species varies as $r_s^{NaBF_4} > r_s^{KBF_4}$ in KCl-KF melt containing different alkali metal fluoroborates.

Table 3.9 Diffusion coefficient and electron transfer rate constant of the electroactive species in KCl-KF melts containing alkali metal fluoroborates at different temperatures.

Melt	**Temperature (K)**	**Diffusion coefficient ($D_O \times 10^6$ / cm^2 s^{-1})**	**Electron transfer rate constant ($k_s \times 10^3$ / cm s^{-1})**
A	1073	6.4	2.0
	1098	7.3	1.8
	1123	8.9	1.8
B	1073	12	3.9
	1098	13	3.4
	1123	17	4.8

3.3.4 Electron transfer rate constant

By using the expression derived by Klingler and Kochi [123] (Eqn. 2.5) the electron transfer rate constants for the irreversible electrode process for sodium fluoroborate in KCl-KF melt over the temperature range 1073 to 1123 K were calculated. The k_s values obtained by substituting the αn_{α} values derived from Eqn. 2.2 at 1 V s^{-1} scan rate and D_O from Eqn. 2.15 are presented in Table 3.9. These values indicate sluggish electron transfer kinetics due to the fact that the oxidized boron (fluoro-chloro complex of boron) and the reduced boron (elemental boron) are structurally dissimilar and the activation barrier for the redox process is large.

3.3.5 Apparent surface resistance

The plots of cathodic peak current density vs. cathodic peak potential for the melt A show a linear behaviour (Fig. 3.32). The values of R_{app} calculated for different fluoroborates in KCl-KF melt at different temperatures are presented in Table 3.10. It is observed (Table 3.10) that the R_{app} values decrease with increase in temperature. Polyakova *et al.* [96] have reported a higher value of R_{app} (3.3 Ω cm^2 at 973 K) in the melt LiF-NaF-KF-KBF_4 (15.9×10^{-2} mol%). In Section 3.2.8 as discussed earlier for the melt B, the R_{app} (0.18 ± 0.02 Ω cm^2 at 1073 K) was found to be of similar magnitude. Thus R_{app} was found to be independent of the nature of alkali metal fluoroborate in KCl-KF melt. The typical resistance values obtained (Table 3.10) is very small and it is surmised that the effect of resistance on CVs is negligible and it does not quite affect the determination of α values from the cyclic voltammetric scans.

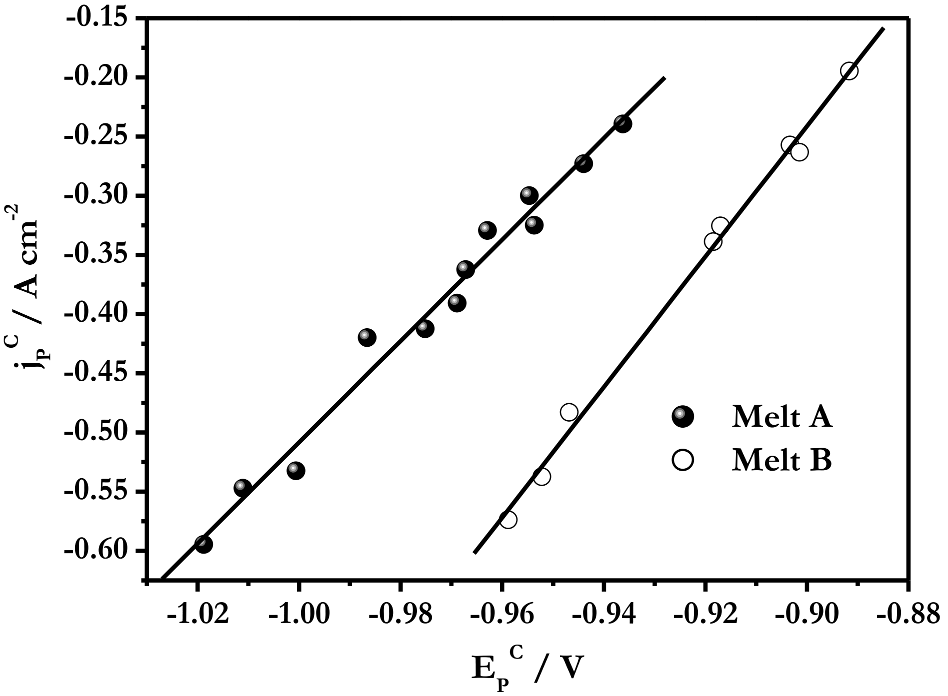

Fig. 3.32 Cathodic peak current density versus cathodic peak potential for boron deposition on Pt electrode in the melts A and B at 1073 K.

Table 3.10 Apparent surface resistance of the electrolyte on the platinum electrode for the melts A and B at different temperatures.

Melt	**Temperature (K)**	R_{app} **(Ω cm^2)**
A	1073	0.21 ± 0.01
	1123	0.24 ± 0.01
B	1073	0.18 ± 0.02
	1123	0.21± 0.01

3.4 Determination of oxide ion in KCl-KF melts by voltammetry

In this study LSV was employed for the determination of oxide ion content in KCl-KF melt at 1073 K since information on the electrochemical behaviour as well as methodology for the determination of oxide ion in mixed chloride-fluoride melts are not available in the literature. The LSV methodology was employed for titrating O^{2-} ions using the electrochemical oxidation peak of oxide ions and subsequent formation of gaseous CO_2 on a glassy carbon electrode.

3.4.1 Solubility of Na_2O in the melt

Melting point of Na_2O is 1405 K. Na_2O_2 decomposes to Na_2O at 873 K under vacuum [101]. Prior to the experiments, Na_2O containing 20 wt% Na_2O_2 was heated under vacuum at 873 K for 12 h to yield > 99.6% pure Na_2O. Based on similar studies reported for LiCl-KCl-KF [141] and LiF-NaF-KF melts [101], Na_2O was considered to be fully dissociated in KCl-KF melt. Thus one mole of Na_2O on dissolution liberates one mole of oxide ion in the melt.

In the present study the aqueous solution of the quenched KCl-KF-Na_2O (7.8×10^{-5} mol cm^{-3}) melt was found to be turbid with appearance of an insoluble residue. The solution was neutral (pH was found to be 7). This observation led to the conclusion that the solution was devoid of free oxide content. The insoluble residue may be due to the formation of oxo-chloro-fluoro complexes. It is surmised that the dissolution of Na_2O in KCl-KF melt is accompanied by a bridge involving cation-oxide-cation linkage frame work within the melt system as depicted below.

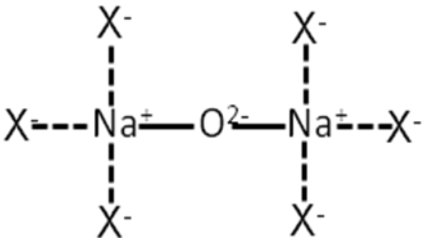

where X = Cl^-, F^-

Solvation of this crosslinking by chloride and fluoride ions results in relative stabilization of the dissolved oxide. Formation of similar bridge oxygen compounds has been earlier reported by Barbin *et al.* for NaCl-KCl-Li_2O melts [111].

3.4.2 Determination of oxide ion content in the melt

LSV at different scan rates for the KCl-KF melt at 1073 K showed the presence of two anodic peaks (Fig. 3.33) which might be due to adsorption followed by charge transfer of oxide ion (present in the melt due to residual oxide ions) on the glassy carbon electrode. A linear relationship was observed between the anodic current density (sum of adsorption peak current density and charge transfer peak current density) measured at different scan rates (0.1, 0.25 and 0.5 V s^{-1}) and the concentration of oxide ion in the melt (Fig. 3.34).

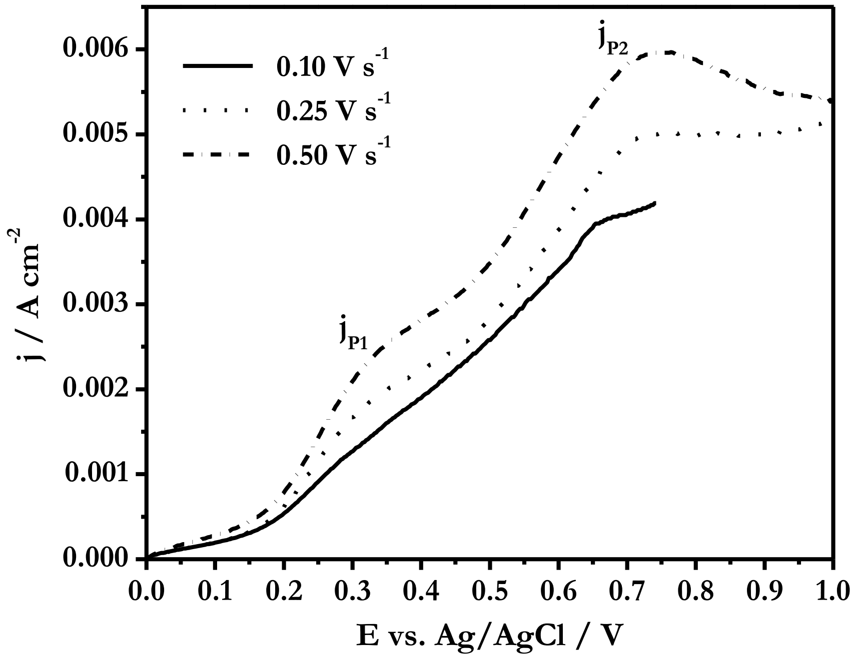

Fig. 3.33 Linear sweep voltammetric scans for KCl (81.54 mol%)-KF (18.45 mol%) melt at different scan rates on a glassy carbon electrode at 1073 K.

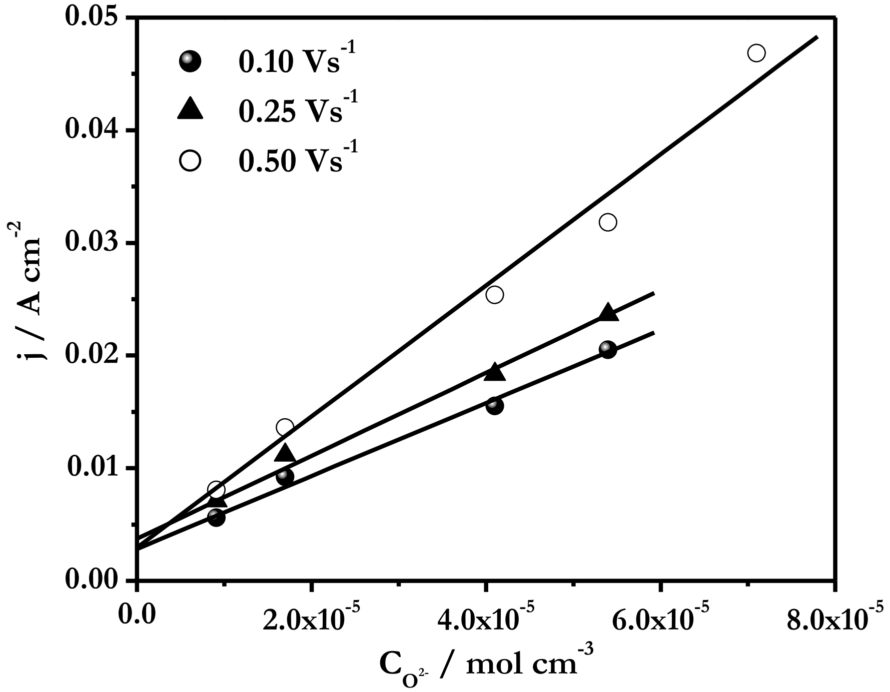

Fig. 3.34 Variation of anodic current density with oxide concentrations in KCl (81.54 mol%)-KF (18.45 mol%) melt at different scan rates on a glassy carbon electrode at 1073 K.

From the intercepts of these plots (Fig. 3.34 and also given in Table 3.11) the average residual (blank) oxide ion content in the KCl-KF melt was obtained and presented in Table 3.11. The anodic current density for the blank KCl-KF melt obtained from LSV and that obtained from the intercepts of plots of variation of anodic current density with oxide ion concentration in KCl-KF melt (Fig. 3.34) were found to be very close (Table 3.11).

Table 3.11 Comparison of the anodic current density values obtained from Fig. 3.34 and LSV measurements of KCl (81.54 mol%)-KF (18.45 mol%) melt at different scan rates at 1073 K.

Scan rate ($V\ s^{-1}$)	**Current density obtained from Fig. 3.34 intercept ($A\ cm^{-2}$)**	**Current density obtained from LSV ($A\ cm^{-2}$)**
0.10	$2.8\times10^{-3} \pm 7\times10^{-4}$	2.9×10^{-3}
0.25	$3.7\times10^{-3} \pm 8\times10^{-4}$	3.5×10^{-3}
0.50	$2.9\times10^{-3} \pm 1.8\times10^{-3}$	3.9×10^{-3}
	Mean: $3.1\times10^{-3} \pm 4.9\times10^{-4}$	Mean: $3.5\times10^{-3} \pm 5.4\times10^{-4}$

In order to remove the contribution from the initial oxide ion content in the melt (blank value) the average current density value obtained for the KCl-KF melt at different scan rates were subtracted from the anodic current density values obtained after oxide ion addition (Fig. 3.35). The linear regression of the anodic current density for different oxide ion content in KCl-KF melt at 0.25 and 0.5 V s^{-1} scan rates are represented as Eqns. 3.6 and 3.7 respectively.

$$j_P = (374.49 \pm 12.21) C_{O^{2-}} \qquad 3.6$$

$$j_P = (572.43 \pm 20.39) C_{O^{2-}} \qquad 3.7$$

where $C_{O^{2-}}$ is the concentration of oxide ion in mol cm^{-3}.

The blank oxide ion concentration in the KCl-KF melt was the average value of oxide ion concentration obtained from Eqns. 3.6 and 3.7. The average value was found to be $7.6\times10^{-6} \pm 2.2\times10^{-6}$ mol cm^{-3}. The corresponding anodic peak current density was found to be 3.5 ± 0.5 mA cm^{-2} (Table 3.11). Unknown concentration of oxide ion present in the KCl-KF melt can be obtained by measuring the anodic current density by LSV at appropriate scan rates and incorporating the values either in Eqn. 3.6 or in Eqn. 3.7.

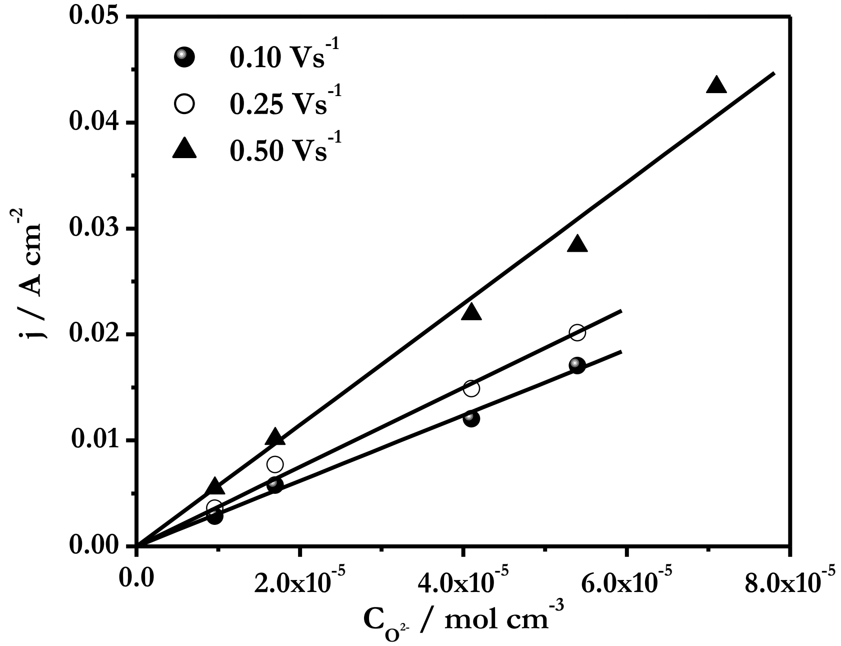

Fig. 3.35 Variation of anodic current density with oxide concentrations after subtracting the current density values obtained due to residual oxide content in KCl (81.54 mol%)-KF (18.45 mol%) melt (blank) at different scan rates on a glassy carbon electrode at 1073 K.

The peak current density values obtained in this study is relatively higher than those for the melts obtained through recrystallization or zone melting. However the salt purification method employed in this study is identical to the one being followed in industries for the large scale production of elemental boron by electrowinning process [82, 83]. The electrodeposited boron obtained from these melts was found to be suitable for the control rod applications in nuclear reactors [82, 83]. It is surmised that the residual oxide content in the melt might have some beneficial effect on the electrodeposition process. Similar effect of oxide ion during electrodeposition process has been reported in the literature [68, 101 - 102]. Hence the melt preparation (without direct recrystallization or zone melting of the salts) adopted was effective for the purpose of boron electrodeposition.

3.4.3 Linear sweep voltammetry (LSV) of oxide ion in KCl-KF melt

LSV was used to investigate the process of oxidation of O^{2-} ions in KCl-KF melt. The LSV of KCl-KF melt (Figs. 3.33 and 3.36) showed a prewave (j_{P1}) and a postwave (j_{P2}) in the anodic scan. Small additions of sodium oxide into the melt led to the growth of both the prewave and the postwave (Fig. 3.36). At higher concentrations of Na_2O the prewave was found to merge with the postwave. This behaviour allows us to associate the post wave peak to the discharge of the oxide ions.

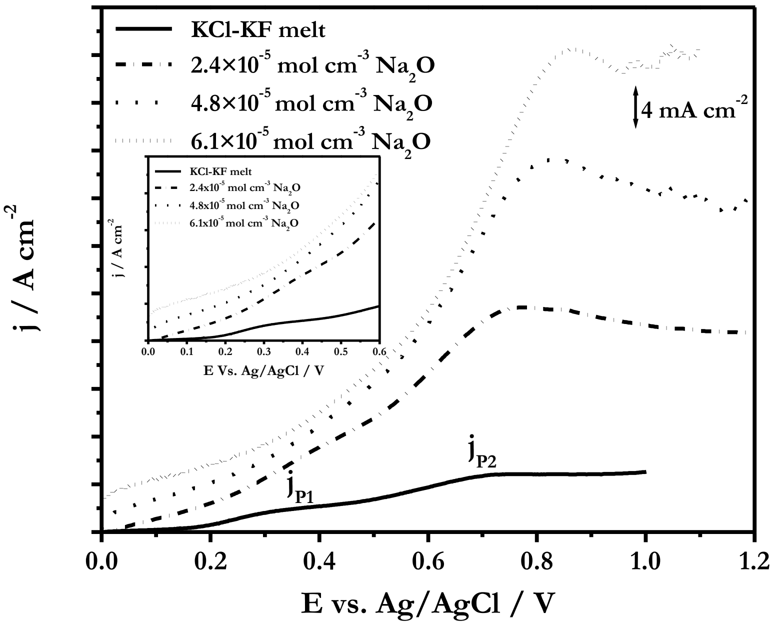

Fig. 3.36 Linear sweep voltammograms for KCl (81.54 mol%)-KF (18.45 mol%) and KCl-KF-Na_2O melts on a glassy carbon electrode at 0.25 V s^{-1} scan rate at 1073 K.

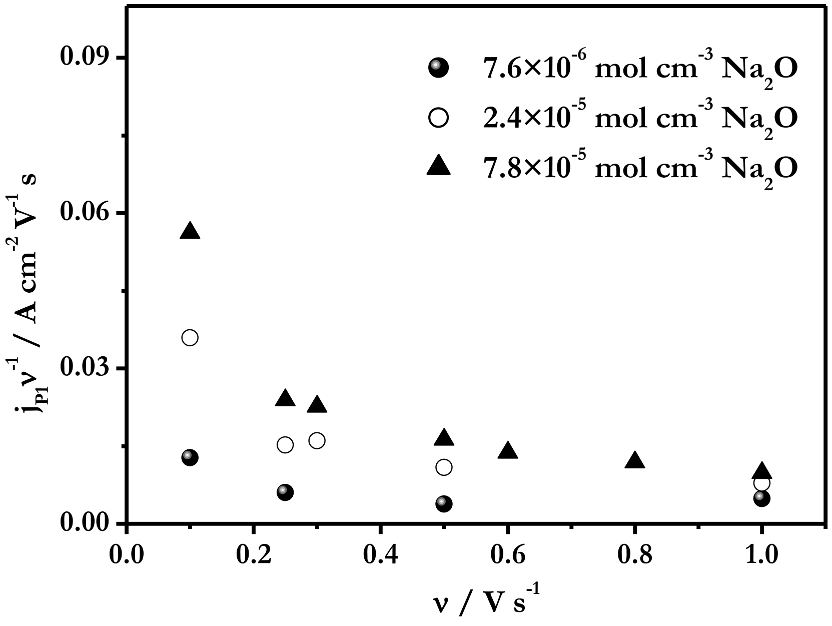

Fig. 3.37 Linear dependence of $i_{P1}\nu^{-1}$ vs. ν at 1073 K and different concentration of Na_2O in KCl-KF melts.

Constancy of $j_{p1}\nu^{-1}$ vs. ν (at scan rates > 0.1 Vs^{-1}) as presented in Fig. 3.37 is typical of adsorption peaks as reported earlier in the literature [111]. Linear behaviour of $j_{p2}\nu^{-1/2}$ vs. $\nu^{1/2}$ (Fig. 3.38) indicated that the electrode process associated with the second peak was charge transfer controlled [111]. The dependence of the second peak (postwave) current density, j_{p2} on the square root of scan rate ($\nu^{1/2}$) was found to be linear (Fig. 3.39). This indicates that the process associated with the second peak is charge transfer controlled. The peak potential (E_{P2}) shifted to the anodic region with an increase in the scan rate. The dependence of E_{P2} on $\log\nu$ (Fig. 3.40) was found to be linear at 1073 K. This indicates that the process is irreversible. Thus the postwave is due to charge transfer of O^{2-} at the electrode.

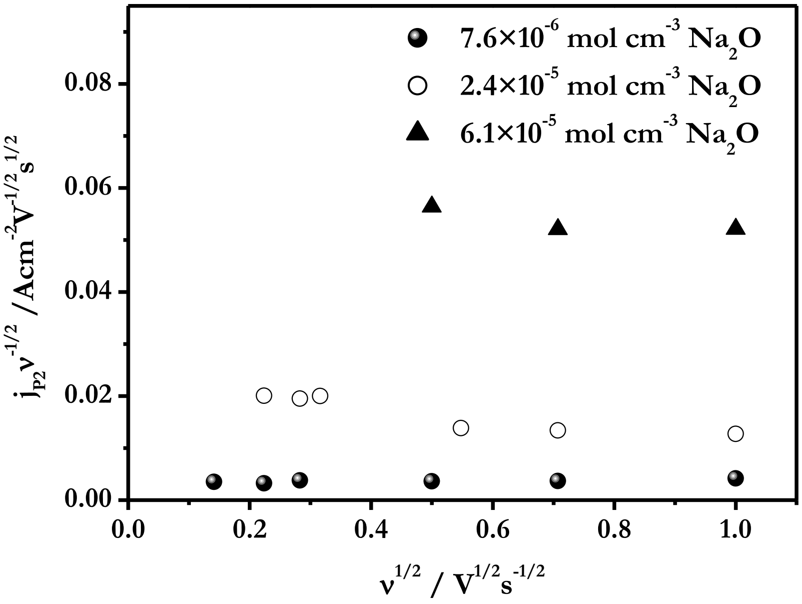

Fig. 3.38 Linear dependence of $i_{P2}\nu^{-1/2}$ vs. $\nu^{1/2}$ at 1073 K and at different concentration of Na_2O in KCl-KF melts.

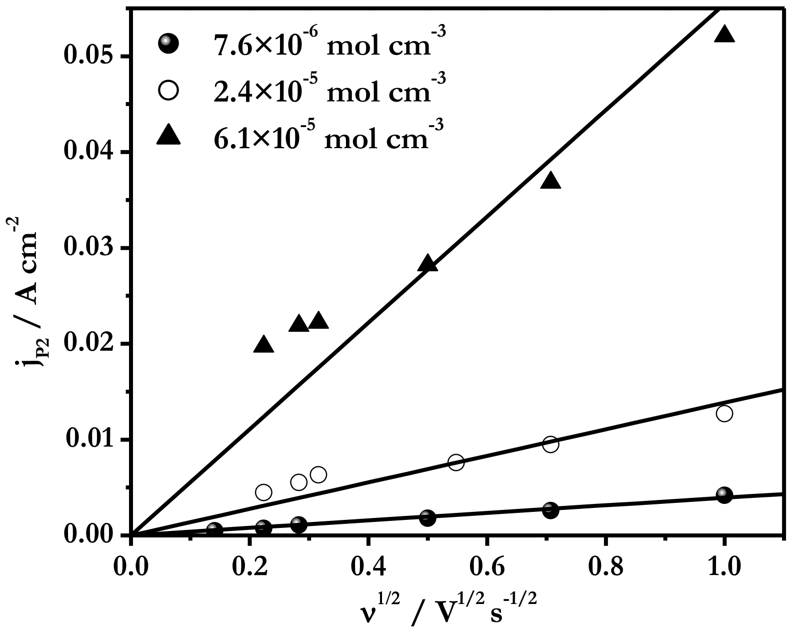

Fig. 3.39 A plot of peak current density (desorption peak) with square root of the scan rate for KCl-KF melt containing varying amounts of oxide ion at 1073 K.

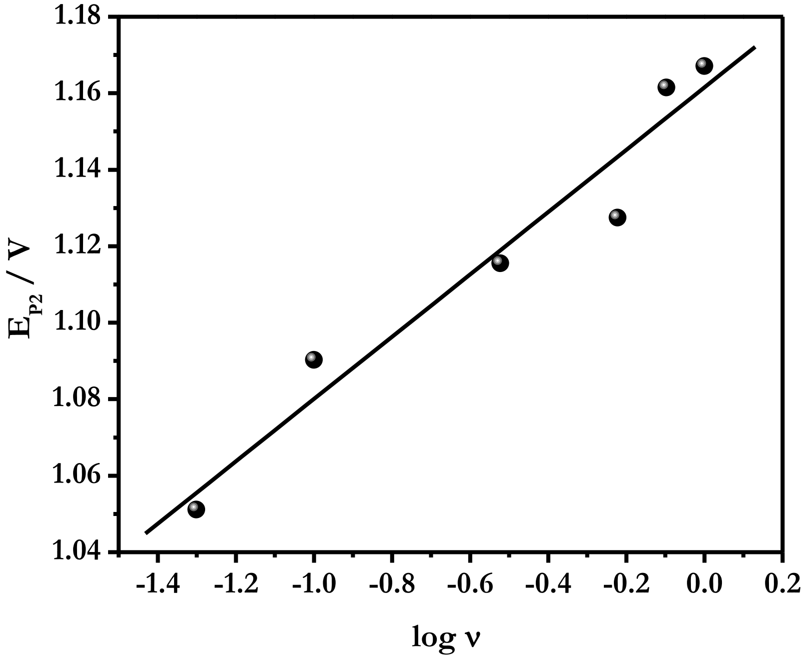

Fig. 3.40 A plot of oxide ion desorption peak potential with logarithm of the scan rate for KCl-KF-Na_2O (7.8×10^{-5} mol cm^{-3}) melt on a glassy carbon electrode at 1073

From the above observations it can be inferred that the anodic process is a two-step process (Eqns. 3.8 and 3.9) which was also observed by Polyakova *et al.* for CsCl-KCl-NaCl eutectic melts [109] on a glassy carbon working electrode. Similar observations were also reported by Nekrasov *et al.* [110] for the oxochloride melts.

$$O^{2-} + xC - 2e \rightarrow C_xO_{(ads)} \qquad 3.8$$

$$O^{2-} + C_xO_{(ads)} - 2e \rightarrow CO_2(g) + (x-1)C \qquad 3.9$$

Similar to our observation Polyakova *et al.* [109] also have reported that the peak currents for the adsorption and diffusion processes were not comparable in magnitude. They have suggested that the reaction represented by Eqn. 3.10 occurred along with the reaction represented by Eqn. 3.9 which gave rise to the peak (j_{p2}).

$$O^{2-} + \frac{1}{2}C - 2e \rightarrow \frac{1}{2}CO_2(g) \qquad 3.10$$

The total current of both these stages obtained from the foot of the first wave to the top of the second wave was found to be proportional to the oxide ion concentration in the melt (Figs. 3.33 and 3.34).

According to Eqn. 3.10, the oxide ion diffusing from the melt to the glassy carbon electrode surface reacts to evolve CO_2. The oxide ion may react with evolved CO_2 to form CO_3^{2-} as per Eqn.3.11.

$$CO_2(g) + O^{2-} \rightarrow CO_3^{2-} \qquad 3.11$$

However the formation of carbonate occurs only at high positive potentials. Moreover the glassy carbon electrode employed in the present study was not polarized to high positive potentials. Since it is surmised that there is no formation of carbonate ion, the electrochemical reactions represented by Eqns. 3.9 and 3.10 are valid.

3.5 Description of the melt stoichiometry in the electrodeposition of boron from KCl-KF-KBF$_4$ melts

This work attempts to describe a plausible scheme of reaction(s) that governs the electrodeposition of boron from melts containing KCl, KF and KBF_4 (at 1073 K). Probable electrochemical reactions taking place on the electrodes during the course of electrodeposition of boron from $KCl-KF-KBF_4$ melt at 1073 K is depicted in Table 3.12.

Table 3.12 Probable electrochemical reactions taking place on the electrodes.

Electrochemical reactions	**Cathode**	**Anode**
a.	$BF_4^- + 3e \rightarrow B + 4F^-$	$3F^- \rightarrow \frac{3}{2}F_2 + 3e$
b.	$BF_3Cl^- + 3e \rightarrow B + 3F^- + Cl^-$	$3F^- \rightarrow \frac{3}{2}F_2 + 3e$ $3Cl^- \rightarrow \frac{3}{2}Cl_2 + 3e$
c.	$BF_2Cl_2^- + 3e \rightarrow B + 2F^- + 2Cl^-$	$3F^- \rightarrow \frac{3}{2}F_2 + 3e$ $3Cl^- \rightarrow \frac{3}{2}Cl_2 + 3e$
d.	$BFCl_3^- + 3e \rightarrow B + F^- + 3Cl^-$	$3F^- \rightarrow \frac{3}{2}F_2 + 3e$ $3Cl^- \rightarrow \frac{3}{2}Cl_2 + 3e$
e.	$BCl_4^- + 3e \rightarrow B + 4Cl^-$	$3Cl^- \rightarrow \frac{3}{2}Cl_2 + 3e$

Four stoichiometric equations, Eqn. 1.8, 3.12 to 3.14, as depicted were formulated based on the formation of different boron containing mixed chloride-fluoride species [114, 116] in the melt.

$$0.5KCl + KBF_4 \rightarrow B + 1.5KF + 0.25Cl_2 + 1.25F_2 \tag{1.8}$$

$$KBF_4 + 1.25KCl \rightarrow B + 0.625Cl_2 + 2.25KF + 0.875F_2 \tag{3.12}$$

$$KBF_4 + 2.3KCl \rightarrow B + 1.15Cl_2 + 3.3KF + 0.35F_2 \tag{3.13}$$

$$KBF_4 + 3KCl \rightarrow B + 1.5Cl_2 + 4KF \tag{3.14}$$

Eqn. 1.8 considers that only BF_4^- is present in the melt and Cl_2 and F_2 are evolved during the electrowinning process.

Eqn. 3.12 was arrived at by considering the existence of BF_3Cl^- and BF_4^- species with Cl_2 evolution, by using the following procedure. The equation pertaining to the reduction of KBF_3Cl could be represented as,

$$KBF_3Cl + KCl \rightarrow B + Cl_2 + 2KF + 0.5F_2 \tag{3.15}$$

Addition of Eqns. 1.8 and 3.15 yields Eqn. 3.16,

$$KBF_4 + KBF_3Cl + 1.5KCl \rightarrow 2B + 1.25Cl_2 + 3.5KF + 1.75F_2 \tag{3.16}$$

In order to express this reaction in terms of the initial constituents of the melt the stoichiometric equivalence given by Eqn. 3.17 was incorporated into Eqn. 3.16.

$$KBF_4 + KCl \rightarrow KBF_3Cl + KF \tag{3.17}$$

The resultant expression is represented by Eqn. 3.12.

Similarly by considering the presence of BF_4^-, BF_3Cl^-, $BF_2Cl_2^-$, $BFCl_3^-$ and BCl_4^- species along with the evolution of Cl_2 and F_2, Eqn. 3.13 was obtained.

The reduction of the moieties KBF_3Cl, KBF_2Cl_2, $KBFCl_3$ and $KBCl_4$ are represented by Eqns. 3.15, 3.18, 3.19 and 3.20 respectively.

$$KBF_2Cl_2 + KCl \rightarrow B + 1.5Cl_2 + 2KF \tag{3.18}$$

$$KBFCl_3 \rightarrow B + 1.5Cl_2 + KF \tag{3.19}$$

$$KBCl_4 \rightarrow B + 1.5Cl_2 + KCl \tag{3.20}$$

Addition of the decomposition reactions represented by Eqns. 3.15, 3.18, 3.19 and 3.20 results in Eqn. 3.21.

$$KBF_4 + KBF_3Cl + KBF_2Cl_2 + KBFCl_3 + KBCl_4 + 1.5KCl \rightarrow 5B + 5.75Cl_2 + 6.5KF + 1.75F_2 \tag{3.21}$$

The formation reactions of KBF_2Cl_2, $KBFCl_3$ and $KBCl_4$ are represented by Eqns. 3.22, 3.23 and 3.24.

$$KBF_4 + 2KCl \rightarrow KBF_2Cl_2 + 2KF \tag{3.22}$$

$$KBF_4 + 3KCl \rightarrow KBFCl_3 + 3KF \tag{3.23}$$

$$KBF_4 + 4KCl \rightarrow KBCl_4 + 4KF \tag{3.24}$$

Combination of these formation reactions along with the formation reaction of KBF_3Cl represented by Eqn. 3.17 yields an expression for the overall reaction (Eqn. 3.25).

$$4KBF_4 + 10KCl \rightarrow KBF_3Cl + KBF_2Cl_2 + KBFCl_3 + KBCl_4 + 10KF \tag{3.25}$$

When the species $BF_2Cl_2^-$, $BFCl_3^-$ and BCl_4^- are reduced with the attendant evolution of Cl_2, the reaction could be represented by Eqn. 3.26.

$$KBF_2Cl_2 + KBFCl_3 + KBCl_4 \rightarrow 3B + 4.5Cl_2 + 3KF \tag{3.26}$$

It is evident by comparison that Eqn. 3.26 was derived by adding Eqns. 3.18, 3.19 and 3.20.

By comparing reactions viz. 3.21 and 3.25 the formation of boron from KBF_4 and

KCl with the attendant evolution of Cl_2 and F_2 could be represented by Eqn. 3.13.

The formation reactions represented by Eqns. 3.22, 3.23 and 3.24 were combined to yield the overall reaction (Eqn. 3.27).

$$3KBF_4 + 9KCl \rightarrow KBF_2Cl_2 + KBFCl_3 + KBCl_4 + 9KF \qquad 3.27$$

By combining Eqns. 3.26 and 3.27 the formation of boron from KBF_4 and KCl with the attendant evolution of Cl_2 alone could be obtained (Eqn. 3.14).

Time dependant concentration profiles of the constituent ions in the melt were computed with the help of Eqns. 1.8, 3.12 to 3.14, and by assuming a linear rate (9 g h^{-1}) of B electrodeposition from the melt. All these reactions represent depletion of one mole of boron but the amount of KCl consumed increases progressively from 0.5 moles in Eqn. 1.8 to 3 moles in Eqn. 3.14. In addition, the KF generated in these reactions increases from 1.5 moles in Eqn. 1.8 to 4 moles in Eqn. 3.14.

The chloride and fluoride concentrations were derived by considering the presence of Cl^-, F^- and BF_4^- alone in the salt samples. This would be appropriate and easy for comparison, if in the aqueous solutions these would be the only species present. This premise was validated by comparing the values of the concentrations of Cl^- and F^- in the aqueous solutions prepared from the fresh melt at the start of electrolysis with those obtained with the help of the above assumption (Table 3.13). For a 12 kg salt mixture an ideal value of 3946.72 g of Cl^-, 463.73 g of F^- and 8.51 for **R** (where **R** = n_{Cl^-} / n_{F^-}; n_{Cl^-} and n_{F^-} are the amount of chloride ions in g and fluoride ions in g in the aqueous solutions made from the salt samples withdrawn from the melt) should have been obtained. Considering that the estimations had an uncertainty of about 5% and that a variation of about 1% in handling and transferring of the salts is inevitable, these values were considered to be in good agreement with the above assumption. The major uncertainty in the experimental estimation could be due to hydrolysis of the BF_4^- ion which is unlikely to take place in these solutions for the latter contain a large excess of Cl^- and F^- that provide a very high ionic strength. Further, if at all this hydrolysis reaction still prevails, the uncertainty arising from the same could be minimized by carrying out the estimation quickly after the dissolution, thanks to the slow kinetics of this reaction [142].

The experimental data presented in this work pertains to about one hundred and twelve electrodepositions (Table 3.14) carried out under controlled conditions. Even though qualitatively the presence of chlorine and fluorine could be ascertained in the gas emanating from the electrowinning cell, quantitative measurements were not successful. Since these experiments were carried out at a production scale the experimental system was not amenable for carrying out experiments aimed at the electrochemical speciation of the melt. In addition, quantitative estimation of the ionic species in the melt has not been reported even in the earlier electrochemical investigations in the literature [112, 114 - 116]. Even though efforts are underway in our laboratory to estimate these with a test system, these are out of the scope of the present study. Miller [68] had reported that the chlorine to fluorine ratio in their experiments was around 5. However, it should be noted that this author reiterates that he was not certain about the actual reaction involved in the electrowinning. Ref. [68] does not provide the details of the estimation of the gases. The concentration of the ionic species in the melt has also not been reported. Moreover, it is not clear if a constant ratio of fluorine to chlorine was maintained in the gases evolved during electrowinning throughout the production trials. In other words evolution of the concentration profile with time during the course of the electrowinning is being reported for the first time only in this study. In view of the above, it is rather difficult to make a meaningful comparison of the data cited by Miller [68] and those obtained in the present work.

In the absence of the possible key parameters, (viz., composition of the gas phase and the actual composition of the melt in terms of the complex ions) that could be used to follow the course of the reactions during the electrowinning of boron, it is appropriate to use the ratio (**R**), as an indicator for understanding the scheme of reactions occurring in the melt. The intermediate formed in the melt would have a bearing on the value of **R** and this value would be different for the four reaction schemes represented by the Eqns. 1.8, 3.12 to 3.14, and were designated as **R_1, R_2, R_3** and **R_4** respectively.

These values were computed by using the following simple relations.

$$W_{Cl_2} = \left(\frac{N_{Cl_2}}{N_B} \right) \times M_B \times t \times M_{Cl_2} \qquad 3.28$$

$$W_{F_2} = \left(\frac{N_{F_2}}{N_B} \right) \times M_B \times t \times M_{F_2} \qquad 3.29$$

$$W_B = 9 \;\; g \;\; h^{-1} \qquad 3.30$$

where $\left(\frac{N_{Cl_2}}{N_B} \right)$ and $\left(\frac{N_{F_2}}{N_B} \right)$ refer to the number of moles of chlorine and fluorine produced in an hour, per mole of boron deposited, t is the duration of the deposition and M_{Cl_2} and M_{F_2} are the molecular weights of Cl_2 and F_2 respectively. W_{Cl_2} and W_{F_2} refer to the weights of chlorine and fluorine escaping from the melt after time t. W_B refers to the weight of

B deposited per hour. The corresponding change in the concentration of Cl^- and F^- in the melt has been computed with the help of the following relations.

$$W_{KCl} = W_{s,KCl} - \left[\left(\frac{W_{Cl_2}}{2M_{Cl_2}} \right) \times M_{KCl} \right] \times t \qquad 3.31$$

$$W_{KF} = W_{s,KF} - \left[\left(\frac{W_{F_2}}{2M_{F_2}} \right) \times M_{KF} \right] \times t \qquad 3.32$$

$$W_{KBF_4} = W_{s,KBF_4} - \left[\left(\frac{W_B}{M_B} \right) \times M_{KBF_4} \right] \times t \qquad 3.33$$

$$\frac{W_{Cl^-}}{W_{F^-}} = \frac{n_{cl^-}}{n_{F^-}} \left(By \;\; definition \right) = R = \left(\frac{W_{KCl}}{W_{KF}} \right) \left(\frac{M_{F_2}}{M_{Cl_2}} \right) \qquad 3.34$$

where, $W_{s,KCl}$, $W_{s,KF}$ and W_{s,KBF_4} are the initial weight of KCl, KF and KBF_4 respectively in the melt. With the help of the chemical assay of the salt samples withdrawn at periodic intervals, a time dependent evolution of these ratios has been obtained. These along with the ratios cited above are depicted in Figs. 3.41 to 3.45. The uncertainties in the values of the experimentally estimated concentrations of the fluoride and chloride ions are much smaller compared to the separation between the concentration profiles pertaining to the Eqns. 1.8, 3.12 to 3.14. Hence, this scheme of equations and computations could be compared with the experimental estimates and meaningful conclusions could be drawn from such an analysis.

The values of these ratios at certain stages in the electrolysis are listed in Table 3.13. From these values it is evident that the values of these ratios decrease in the following order $\mathbf{R_1} > \mathbf{R_2} > \mathbf{R_3} > \mathbf{R_4}$. This is as expected for these reactions require increasing amounts of chloride as given in the Eqns. 1.8, 3.12 to 3.14. In general, the trends observed in the actual experiments are in conformance with these four schemes.

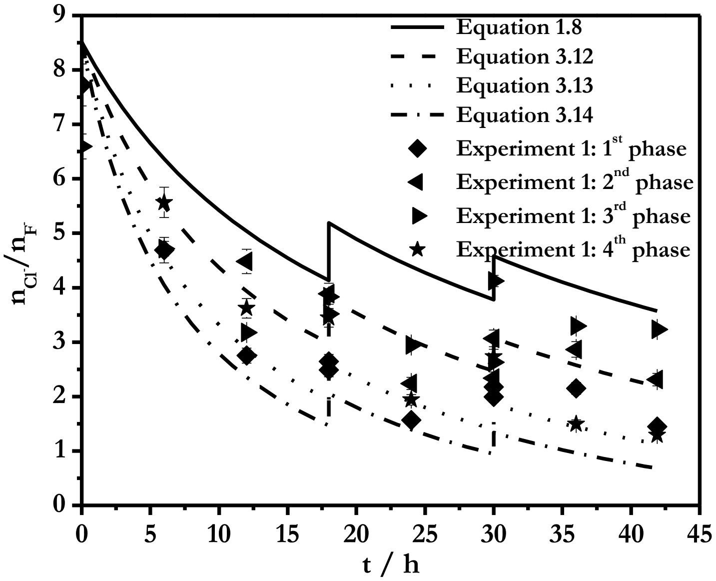

Fig. 3.41 Comparison of the variation of n_{Cl^-}/n_{F^-} ratio with the progress of boron electrodeposition based on the stoichiometric equations and data on the experiment 1.

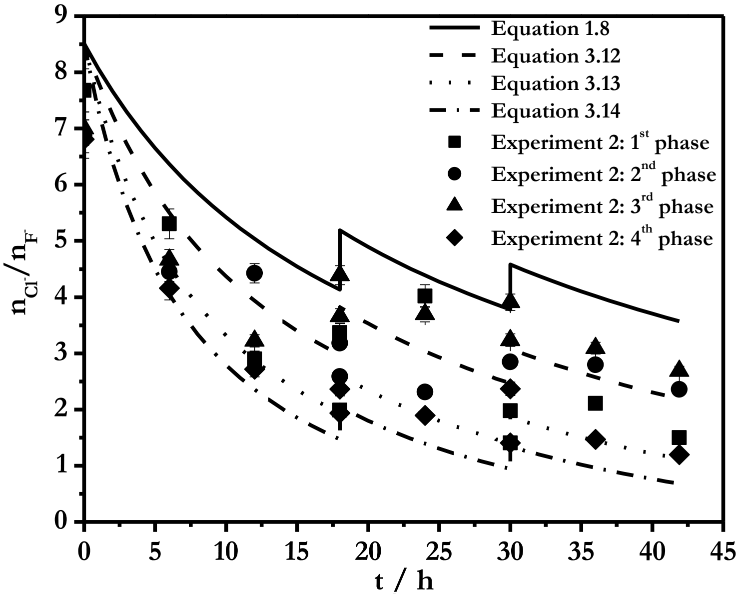

Fig. 3.42 Comparison of the variation of n_{Cl^-}/n_{F^-} ratio with the progress of boron electrodeposition based on the stoichiometric equations and data on the experiment 2.

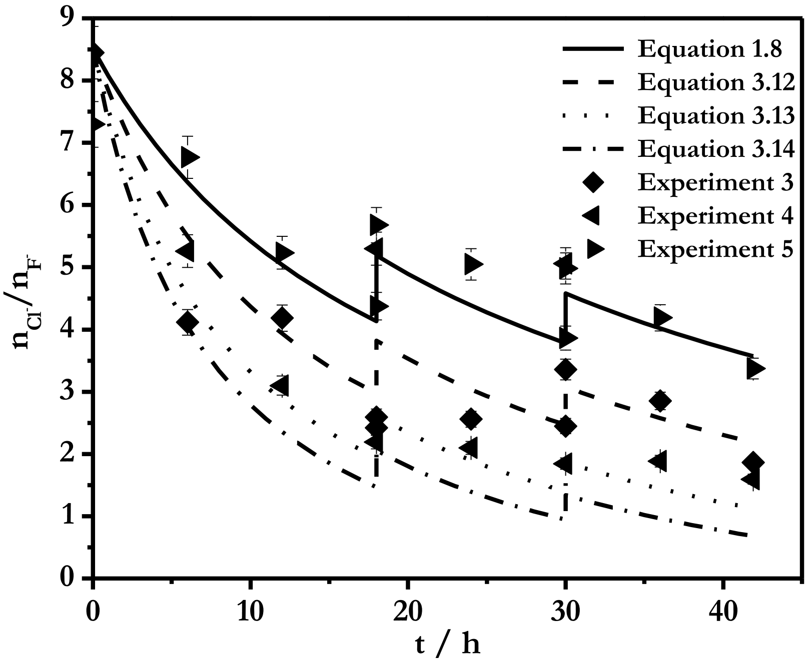

Fig. 3.43 Comparison of the variation of n_{Cl^-}/n_{F^-} ratio with the progress of boron electrodeposition based on the stoichiometric equations and data on the experiments 3, 4 and 5.

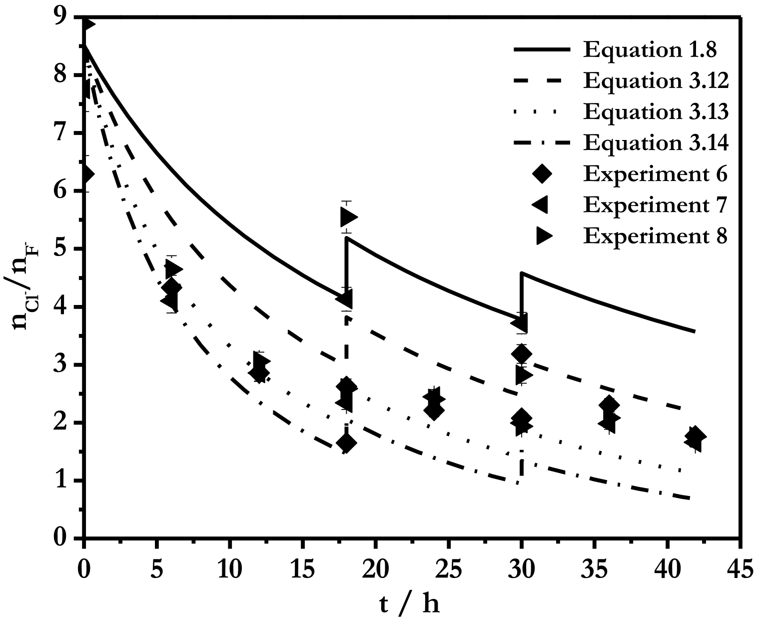

Fig. 3.44 Comparison of the variation of n_{Cl^-}/n_{F^-} ratio with the progress of boron electrodeposition based on the stoichiometric equations and data on the experiments 6, 7 and 8.

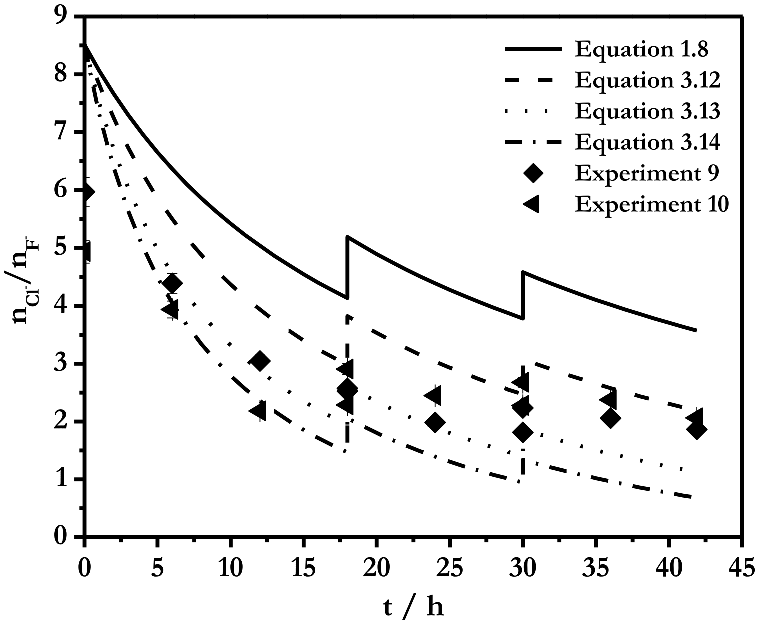

Fig. 3.45 Comparison of the variation of n_{Cl^-}/n_{F^-} ratio with the progress of boron electrodeposition based on the stoichiometric equations and data on the experiments 9 and 10.

Further these observations have clearly established that the evolution of fluorine always takes place. From the data obtained in this study the Eqns. 3.12 and 3.13 appear to be most probable. KBF_4 derived from two different sources were used in the present study. The fluoroborate used in all the experiments, excepting expt. 5 were obtained from boric acid, while the sample used in the latter was boron derived by reacting $BF_3 : O(C_2H_5)_2$ with an aqueous solution of KF . It is interesting to note that the results obtained in the experiment 5 is rather different compared to the others. This is the only process wherein throughout the electrolysis trials (depositions 1 to 7) an **R** value close to that predicted by Eqn. 1.8 was observed (as also reported by Miller [68] and Nair *et al.* [71]). The reason for this behaviour is not clear. Further investigations are indeed necessary in order to discern the factors responsible for this behaviour. Such a mechanism would be the most preferred for the production for it would mean the liberation of a least corroding gaseous effluent.

Table 3.13 Comparison of the **R** values computed and experimentally obtained.

Sl. No.	**Process**	**R = n_{Cl^-} / n_{F^-} computed**				**R = n_{Cl^-} / n_{F^-} actual in experiments 1 to 10**									
						1 (1st phase)	**2 (1st phase)**	**3**	**4**	**5**	**6**	**7**	**8**	**9**	**10**
1.	Start	8.51				7.7	7.7	8.4	8.3	7.3	6.3	7.8	8.5	5.9	4.9
		R_1	**R_2**	**R_3**	**R_4**										
2.	End of E1	6.36	5.5	4.55	4.05	4.7	5.3	4.1	5.3	6.7	4.3	4.1	4.6	4.4	3.9
3.	End of E2	5.04	3.93	2.87	2.36	2.8	2.9	4.1	3.1	5.2	2.9	2.8	3.1	3.1	2.2
4.	End of E3	4.13	2.97	1.94	1.47	2.6	1.9	2.6	2.2	4.3	1.6	2.3	2.6	2.5	2.3
5.	Make up 1	5.18	3.82	2.61	2.05	2.5	3.4	2.4	5.3	5.7	2.6	4.1	5.5	2.6	2.9
6.	End of E4	4.38	3.04	1.89	1.39	1.6	4.0	2.6	2.1	5.0	2.2	2.4	2.4	1.9	2.5
7.	End of E5	3.78	2.46	1.4	0.94	2.0	1.4	2.4	1.8	3.8	2.0	1.9	1.9	1.8	2.2
8.	Make up 2	4.57	3.08	1.86	1.34	2.2	1.9	3.4	5.1	4.9	3.2	3.7	2.8	2.6	2.7
9.	End of E6	4.02	2.57	1.44	0.96	2.1	2.1	2.8	1.9	4.2	2.3	1.9	2.1	2.1	2.4
10.	End of E7	3.57	2.19	1.12	0.67	1.4	1.5	1.8	1.6	3.3	1.8	1.6	1.7	1.8	2.1

*E1 to E7 denotes the seven electrodeposition trial runs carried out.

Table 3.14 The experimental conditions and results during boron electrowinning.

Expt. No.	**Experimental condition**	**Electrolysis at 1073 K**		**Electrolysis time (h)**	n_{Cl^-} / n_{F^-} **ratio obtained from melt analysis**
		Voltage (V)	**Current (A)**		
Expt. 1:	Fresh charge			0	7.7
1st phase	1st deposition	4.2	75	6	4.7
	2nd deposition	4.3	75	12	2.8
	3rd deposition	4.5	75	18	2.6
	1st make-up charge			18	2.5
	1st deposition	4.5	66	24	1.6
	2nd deposition	4.4	75		2.0
	2nd make-up charge			30	2.2
	1st deposition	4.4	75	36	2.1
	2nd deposition	4.5	75	42	1.4
Expt. 1:	Fresh charge			0	
2nd phase	1st deposition	4.0	70	6	
	2nd deposition	4.2	75	12	4.5
	3rd deposition	4.3	70	18	3.9
	1st make-up charge			18	
	1st deposition	4.5	75	24	2.2
	2nd deposition	4.5	67	30	2.3
	2nd make-up charge			30	3.1
	1st deposition	4.2	75	36	2.8
	2nd deposition	4.3	75	42	2.3
Expt. 1:	Fresh charge			0	6.6
3rd phase	1st deposition	4.2	75	6	4.7
	2nd deposition	4.1	75	12	3.2
	3rd deposition	4.3	76	18	3.8
	1st make-up charge			18	3.5
	1st deposition	4.1	75	24	2.9
	2nd deposition	4.1	75	30	2.6
	2nd make-up charge			30	4.1
	1st deposition	4.0	75	36	3.3
	2nd deposition	4.1	75	42	3.2
Expt. 1:	Fresh charge			0	
4th phase	1st deposition	4.1	75	6	5.6
	2nd deposition	4.1	75	12	3.6

	3rd deposition	4.4	75	18	2.6
	1st make-up charge			18	3.4
	1st deposition	4.2	75	24	1.9
	2nd deposition	4.4	75	30	
	2nd make-up charge			30	2.7
	1st deposition	4.2	75	36	1.5
	2nd deposition	4.3	75	42	1.3
Expt. 2:	Fresh charge			0	7.7
1st phase	1st deposition	4.2	75	6	5.3
	2nd deposition	4.2	75	12	2.9
	3rd deposition	4.3	75	18	1.9
	1st make-up charge			18	3.4
	1st deposition	4.3	75	24	4.0
	2nd deposition	4.3	75	30	1.4
	2nd make-up charge			30	1.9
	1st deposition	4.3	75	36	2.1
	2nd deposition	4.5	73	42	1.5
Expt. 2:	Fresh charge			0	6.8
2nd phase	1st deposition	4.2	75	6	4.5
	2nd deposition	4.3	75	12	4.4
	3rd deposition	4.4	75	18	2.6
	1st make-up charge			18	3.2
	1st deposition	4.4	75	24	2.3
	2nd deposition	4.5	58	30	
	2nd make-up charge			30	2.8
	1st deposition	4.3	75	36	2.7
	2nd deposition	4.5	53	42	2.3
Expt. 2:	Fresh charge			0	7.0
3rd phase	1st deposition	4.3	75	6	4.6
	2nd deposition	4.3	75	12	3.2
	3rd deposition	4.5	74	18	3.7
	1st make-up charge			18	4.4
	1st deposition	4.3	75	24	3.7
	2nd deposition	4.4	78	30	3.2
	2nd make-up charge			30	3.9
	1st deposition	4.4	75	36	3.1
	2nd deposition	4.5	75	42	2.7
Expt. 2:	Fresh charge			0	6.8
4th phase	1st deposition	4.5	73	6	4.2
	2nd deposition	4.5	75	12	2.7
	3rd deposition	4.5	61	18	1.9

	1st make-up charge			18	2.4
	1st deposition	4.5	67	24	1.9
	2nd deposition	4.5	56	30	1.4
	2nd make-up charge			30	2.4
	1st deposition	4.5	75	36	1.5
	2nd deposition	4.5	59	42	1.2
Expt. 3	Fresh charge			0	8.4
	1st deposition	4.4	75	6	4.1
	2nd deposition	4.5	74	12	4.1
	3rd deposition	4.1	53	18	2.6
	1st make-up charge			18	2.4
	1st deposition	4.5	42	24	2.6
	2nd deposition	4.5	42	30	2.4
	2nd make-up charge			30	3.4
	1st deposition	4.5	67	36	2.8
	2nd deposition	4.5	72	42	1.8
Expt. 4	Fresh charge			0	8.3
	1st deposition	4.0	75	6	5.3
	2nd deposition	4.1	75	12	3.1
	3rd deposition	4.5	70	18	2.2
	1st make-up charge	4.3	75	18	5.3
	1st deposition	4.5	59	24	2.1
	2nd deposition			30	1.8
	2nd make-up charge			30	5.1
	1st deposition	4.5	72	36	1.9
	2nd deposition	4.2	59	42	1.6
Expt. 5	Fresh charge			0	7.3
	1st deposition	4.1	31	6	6.7
	2nd deposition	4.3	24	12	5.2
	3rd deposition	4.3	22	18	4.3
	1st make-up charge			18	5.7
	1st deposition	4.2	26	24	5.0
	2nd deposition	4.3	28	30	3.8
	2nd make-up charge			30	4.9
	1st deposition	4.5	26	36	4.2
	2nd deposition	4.3	62	42	3.3
Expt. 6	Fresh charge			0	6.3
	1st deposition	4.2	75	6	4.3
	2nd deposition	4.5	70	12	2.9
	3rd deposition	4.5	72	18	1.6
	1st make-up charge			18	2.6

	1st deposition	4.5	25	24	2.2
	2nd deposition	4.5	31	30	2.0
	2nd make-up charge			30	3.2
	1st deposition	4.5	49	36	2.3
	2nd deposition	4.5	47	42	1.8
Expt. 7	Fresh charge			0	7.8
	1st deposition	4.5	69	6	4.1
	2nd deposition	4.5	67	12	2.8
	3rd deposition	4.5	47	18	2.3
	1st make-up charge			18	4.1
	1st deposition	4.5	57	24	2.4
	2nd deposition	4.5	47	30	1.9
	2nd make-up charge			30	3.7
	1st deposition	4.5	53	36	1.9
	2nd deposition	4.5	48	42	1.6
Expt. 8	Fresh charge			0	8.5
	1st deposition	4.5	60	6	4.6
	2nd deposition	4.5	58	12	3.1
	3rd deposition	4.5	44	18	2.6
	1st make-up charge			18	5.5
	1st deposition	4.5	54	24	2.4
	2nd deposition	4.5	51	30	1.9
	2nd make-up charge			30	2.8
	1st deposition	4.5	55	36	2.1
	2nd deposition	4.5	49	42	1.7
Expt. 9	Fresh charge			0	5.9
	1st deposition	4.5	75	6	4.4
	2nd deposition	4.5	70	12	3.1
	3rd deposition	4.5	68	18	2.5
	1st make-up charge			18	2.6
	1st deposition	4.5	70	24	1.9
	2nd deposition	4.5	65	30	1.8
	2nd make-up charge			30	2.6
	1st deposition	4.5	65	36	2.1
	2nd deposition	4.5	55	42	1.8
Expt. 10	Fresh charge			0	4.9
	1st deposition	4.5	75	6	3.9
	2nd deposition	4.5	69	12	2.2
	3rd deposition	4.5	61	18	2.3
	1st make-up charge			18	2.9
	1st deposition	4.5	52	24	2.5

2nd deposition	4.5	65	30	2.2
2nd make-up charge			30	2.7
1st deposition	4.5	67	36	2.4
2nd deposition	4.5	54	42	2.1

CHAPTER IV

4.0 Conclusions

An Ag/AgCl reference electrode designed and fabricated for studying the electrochemistry of chloride-fluoride melts was shown to be reversible with respect to the chloride ion. Its stability and non-polarizability were tested and it was found to be performing satisfactorily in the temperature range 1073 to 1123 K. By using this electrode the reduction potentials of Fe^{2+}/Fe and Ni^{2+}/Ni in the melt KF – KCl were measured for the first time in the temperature range 1073 – 1123 K.

The electrochemical reduction of $B(III) + 3e \rightarrow B$ in KCl (81.54 mol%)-KF (18.45 mol%)-KBF_4 (1.6×10^{-4} to 7.73×10^{-4} mol cm^{-3}) melt on a Pt electrode was studied by cyclic voltammetry over the temperature range 1073 to 1123 K. It is inferred that at a sweep rate of $\nu < 0.1$ Vs^{-1} the electroreduction is quasireversible and at $\nu > 0.1$ Vs^{-1}, both diffusion of electroactive species and electron transfer were found to play a role in the reduction process. It was also established that the reduction of B(III) to B occurred by a single-step three-electron process. The transfer coefficients were evaluated by various hypotheses of convolution voltammetry. The diffusion coefficients calculated for the reduction of B(III) to B using cyclic voltammetry and chronoamperometry were found to be comparable. Boron electrodeposited on Pt electrode at 1073 K was found to be amorphous in nature.

The electrochemical reduction of $B(III) + 3e \rightarrow B$ in KCl (81.54 mol%)-KF (18.45 mol%)- $NaBF_4$ (1.67×10^{-4} mol cm^{-3}) melt on a Pt electrode was studied by cyclic voltammetry over the temperature range 1073 to 1123 K. It is inferred that at a sweep rate of $\nu < 0.1$ Vs^{-1} the electroreduction is quasireversible and at $\nu > 0.1$ Vs^{-1}, both the diffusion of electroactive species and the electron transfer play a role in the reduction process. It is established that the reduction of B(III) to B occurs by a single-step three-electron process. Using chronoamperometry, the diffusion coefficients of the boron containing electroactive species (B(III)) were calculated for the sodium fluoroborate melt system and it was found that $D_O^{NaBF_4} < D_O^{KBF_4}$. The values of α and R_{app} were found to be independent of the nature of alkali metal fluoroborate in KCl-KF melt.

The electrochemical behaviour of oxide ions in KCl (81.54 mol%) – KF (18.45 mol%) melt was investigated by LSV using a glassy carbon electrode. It was observed that the oxidation of O^{2-} ions proceeded through a two-step process involving adsorption of the O^{2-} ions on the electrode surface followed by charge transfer. A linear relationship between the peak current density and the O^{2-} content in the melt was observed. An equation was derived for calculating the oxide ion content in the melt system. This methodology could be used to monitor the purity of the chloride-fluoride melt during the electrolytic process.

The progress of the electrowinning of boron from the melt $KCl - KF - KBF_4$ was investigated by assaying the aqueous solutions of the salt residues withdrawn from the melt at periodic intervals of time. For the first time such a systematic investigation on the electrowinning of boron is reported. Empirical reactions were formulated in order to arrive at the most probable reaction during the course of the electrolysis. It appears that the reaction scheme is possibly influenced by many factors including the melt composition. This study has established that further investigations on this system require quantitative speciation of the ionic moieties in the melt and the dependence of the ionic composition of the melt on the relative proportions of the initial constituents.

CHAPTER V

5.0 Scope of future studies

KCl-KF-KBF_4 is a potential electrolyte for electrodeposition of boron. The phase diagram of this ternary system has not been studied extensively. Using thermal analysis, the phase diagram could be studied. The temperatures of primary crystallization for different compositions of this ternary system could be established using thermal analysis. The dependence of the excess Gibbs energy of mixing on the melt composition could be calculated using the existing solution models. The ionic interaction parameters in the melt system could be established by this study.

It has been reported that a mixed chloride-fluoride melt is essential to minimize the loss of boron in the form of BF_3 gas during the electrowinning of boron from KBF_4 containing melts. More conclusions could be drawn if the gas phase is analyzed during melting process. TG-DTA analysis of the KCl-KF-KBF_4 condensed phase in conjunction with MS (Mass Spectrometry) analysis of the gas phase would give some information on the nature of the species in the head space of the melt.

Electronic, vibrational and ESR spectra are incapable of distinguishing stable complexes and short lived random aggregates from one another in the melt. Thus electronic and vibrational spectra for melts cannot serve as the crucial evidence in favour of the formation of complexes in a system. A stable complex ionic species is one which is capable of performing translational diffusion and possesses a lifetime of 10^{-8} s or longer. NMR spectroscopic method could recognize the long lived complexes and distinguish them from the instantaneous species whose lifetime lie in the picoseconds or subpicosecond range. A detailed study on the nature of the boron containing complexes existing in the melt could be possible through NMR spectroscopy.

Borides are a large class of compounds having very promising properties but relatively narrow applications in technology today. This is mostly due to the quite expensive routes to their production. Therefore the development of economic and environmental friendly technological routes for the production of refractory borides is one of the challenges of today’s materials scientists. Molten salts generally could be considered as a very promising medium for electrochemical synthesis of different compounds. Electrochemical synthesis has the following advantages, as compared with other possible techniques of production of refractory borides:

1. Smooth coatings even at surfaces of complicated geometry.
2. Single crystals, polycrystalline coatings and even ultra-disperse powder deposition depending on the parameters of the process.
3. Precisely controlled process parameters influence the composition of the deposit.
4. Relatively low temperature of synthesis (down to 873 K), cheap and simple technological background and the cheap raw materials required to make the process attractive from the economic point of view.

More detailed studies on the thermodynamic properties of the melts containing boron and different transition metals could assist in finding the appropriate melt for the electrochemical synthesis of refractory borides. The role of the hetero-nuclear complexes existing in the melts and their effect could be studied. The influence of the process parameters on the morphology, appearance and properties of the borides could be investigated.

References

1. Daniel N. Lapedes, *Encyclopedia of Energy*, McGraw-Hill (1976).
2. http://www.indiaenergyportal.org/overview.php
3. *South Asia Monitor*, Center of Strategic and International Studies, Washington D. C., No. 98, September 7 (2006).
4. Monthly report (Dec 2010) and annual report 2009-10, Central Electricity Authority, Ministry of Power.
5. http://www.cea.nic.in/sitemap.html
6. S. P. Sukhatme, *Current Science* 101(5), 624 (2011).
7. Report on Power scenario at a glance, Planning Wing, Central Electricity Authority, India, April (2010).
8. Department of Atomic Energy 2001, Nuclear Power for National Development: An Indian Perspective, Doc. No. PA-01, Gov. India, Bombay.
9. A. Gopalakrishnan, *Annu. Rev. Energy Environ*. 27, 369 (2002).
10. http://www.world-nuclear.org/info/inf01.html
11. http://www.world-nuclear.org/NuclearDatabase/rdResults.aspx?id=27569
12. C. K. Gupta, *Materials in Nuclear Energy Applications*, Vol. II, CRC Press, Inc., Boca Raton, Florida, USA (1989).
13. http://www.indiaenergyportal.org/subthemes_link.php?text=nuclear&themeid=12
14. http://www.barc.ernet.in/about/anu1.html
15. D. R. Olander, *Fundamental aspects of nuclear reactor fuel elements*, Springfield, Virginia (1985).
16. V. R. Babu, S. Govindarajan, S. C. Chetal, *Proc. Of Seminar on Inherent*

Engineered Safety Aspects of PFBR Design, IGCAR, Kalpakkam, India, April 30 (1996).

17. V. Rajan Babu, R. Veerasamy, Sudheer Patri, S. Ignatius Sundar Raj, S.C.S.P. Kumar Krovvidi, S.K. Dash, C. Meikandamurthy, K.K. Rajan, P. Puthiyavinayagam, P. Chellapandi, G. Vaidyanathan, S.C. Chetal, *Nuclear Engineering and Design* 240, 1728 (2010).
18. V. I. Matkovich, *Boron and Refractory Borides*, Springer-Verlag Berlin Heidelberg Newyork (1977).
19. http://www.mii.org/Minerals/photohafn.html
20. *Radiation Protection Procedures*, Safety Ser. International Atomic Energy Agency, No. 38, Vienna (1973).
21. D. D. Sood, *Nuclear Materials*, Indian Association of Nuclear Chemists and Allied Scientists, India, pp. 17-39 (1996).
22. W. G. Woods, *Environ Health Perspect.* 102, 5 (1994).
23. C. K. Narula, J. E. Allison, D. R. Bauer, H. S. Gandhi, *Chem. Mater.* 8, 984 (1996).
24. H. Nakano, T. Itabashi, H. Akahoshi, US Pat. 6,680,540 B2, Jan. 20 (2004).
25. S. Yamazaki, H. Ohtani, T. Fukunaga, US Pat. 6,031,249, Feb. 29 (2000).
26. S. C. Amendola, S. L. Sharp-Goldman, M. S. Janjua, M. S. Spencer, M. T. Kelly, P. J. Petillo, M. Binder, *Int. J. Hydrogen Energy* 25, 969 (2000).
27. R. Aiello, M. A. Matthews, D. L. Reger, J. E. Collins, *Int. J. Hydrogen Energy* 23, 1103 (1998).
28. T. Oku, M. Kuno, H. Kitahara, I. Narita, *Int. J. Inorg. Mater.* 3, 597 (2001).

29. M. G. Hu, R. A. Geanangel, W. W. Wendlandt, *Thermochim. Acta* 23, 249 (1978).

30. G. Wolf, J. Baumann, F. Baitalow, F. P. Hofmann, *Thermochim. Acta* 343, 19 (2000).

31. S. P. Rawal, *JOM* 53, 14 (2001).

32. O. D. Sherby, I. C. Huseby, R. Whalen, S. L. Robinson, US Pat. 3,955,933, May 11 (1976).

33. V. V. Efremkin, A. S. Mikulnskii, *Trans. Ural's Sci. Res. Inst. Chem.* Vol. V, 211, Moscow: Goschimizdat (1957).

34. V. V. Efremkin, *Trans. Ural's Sci. Res. Inst. Chem.* Vol. V, 152, Moscow: Goschimizdat (1957).

35. V. V. Efremkin, S. S. Sheveleva, *Trans. Ural's Sci. Res. Inst. Chem.* Vol. V, 232, Moscow: Goschimizdat (1957).

36. H. Moissan, *C.R. Acad. Sci.* (Paris) 114, 392 (1892).

37. L. Ya. Markovskii, M.P. Belov, *Zhur. Prik. Chim.* (J. Appl. Chem.) 37, 1658 (1964).

38. L. Ya. Markovskii, M.P. Belov, *Zhur. Prik. Chim.* (J. Appl. Chem.) 40, 727 (1967).

39. P. Pichat, D. Forest, *Bull. Soc. Chim.* 10, 3825 (1967).

40. T. F. Fedorov, F. I. Shamrai, L. A. Niselson, I. V. Petrusevich, *Zhur. Neorg. Chim.* (Inorg. Chem.) 5, 226 (1960).

41. L. A. Niselson, I. V. Petrusevich, F. I. Shamrai, G. V. Fedorov, *High Temperature Inorganic Compounds*, p.362, Kiev: Naukova Dumka (1965).

42. D. R. Stern, L. Lynds, *J. Electrochem. Soc.* 105 (11), 676 (1958).

43. J. Cueilleron, *Ann. Chim.* 19, 459 (1944).

44. L. V. McCarty, D. R. Carpenter, *J. Electrochem. Soc.* 107, 38 (1960).

45. E. Amberger, W. Dietze, *Z. Anorg. Allg. Chem.* 332, 131 (1964).

46. F. Meyer, R. Zappner, *Ber.* 54B, 550 (1921).

47. A. E. Arkel, *Metallwirtschaft* 13, 405 (1934).

48. L. Apker, E. Taft, J. Dickey, *Phys. Rev.* 74, 1462 (1948).

49. H. L. Johnston, H. N. Hersh, E. C. Kerr, *J. Am. Chem. Soc.* 73, 1112 (1951).

50. J. Lagrenaudie, *J. Chem. Phys.* 50, 629 (1953).

51. G. G. Devyatykh, *Preparation and Analysis of Super Pure Substances*, p. 15, Moskow: Nauka (1966).

52. I. Hinz, H. Wirth, *Boron* (Ed. G. K. Gaule), Vol. II, p. 9, New York: Plenum Press (1965).

53. C. K. Gupta, *Chemical Metallurgy Principles and Practice*, p.694, WILEY-VCH, (2003).

54. D. R. Sadoway, *Materials Science Forum* 73-75, 555 (1991).

55. H. H. Kahlenberg, *Trans. Am. Electrochem. Soc.* 47, 23 (1925).

56. L. Andrieux, *Ann. Chem. Phys.* 12, 432 (1929).

57. L. Andrieux, W. Deiss, *Bull. Soc. Chim.* 838 (1955).

58. H. S. Cooper., US Patent 2572248 (1951).

59. H. S. Cooper, US Patent 2572249 (1951).

60. S. Russel, F. A. Young, J. D. Kellner, US Patent 3843497 (1974).

61. Nelson F. Murphy, Richard S. Tinsley, US Patent 2848396 (1958).

62. A. Alvin Uchiyama, David Russel Stern, Q. H. McKenna, US Patent 2940911 (1960).

63. D. R. Stern, Q. H. McKenna, US Patent 2892762 (1959).

64. R. B. Ellis, US Patent 2810683 (1957).

65. N. F. Nies, E. W. Fajans, L. L. Thomas, US Patent 2832730 (1958).

66. H. C. Brookes, P. S. Gibson, G. J. Hills, N. Narayan, A. Wigley, *Trans. Inst. Met. Finish.* 54, 191 (1976).

67. S. A. Kuznetsov, *Russ. J.Electrochem.* 32 (7), 763 (1996).

68. G. T. Miller, *J. Electrochem. Soc.* 106 (9), 815 (1959).

69. V. I. Taranenko, I. V. Zarutskii, V. I. Shapoval, M. Makyta, K. Matiasovsky, *Electrochim. Acta* 37, 263 (1992).

70. J. D. Kellner, *J. Electrochem. Soc.* 120 (6), 713 (1973).

71. K. U. Nair, D. K. Bose, C. K. Gupta, *Mineral Processing and Extractive Metallurgy Review* 9, 283 (1992).

72. M. Makyta, K. Matiasovsky, P. Fellner, *Electrochim. Acta* 29, 1653 (1984).

73. K. Akashi, I. Egami, *Seisan-Kenkyu* 15, 427 (1963).

74. A. E. Newkirk, Elemental Boron in Roy M. Adams, Ed., Boron, *Metallo-Boron Compounds and Boranes*, pp. 301-371, Interscience Publishers, New York (1964).

75. S. Kenkyujo, Japanese Patent, 6243, April 4 (1966).

76. V. G. Selivanov, *Tr. Dnepropetr. Khim.-Tekhnol. Inst.* Pt. 1 (12), 171 (1959).

77. H. S. Cooper, U. S. Patent 2,984,605 May 16 (1961).

78. T. Yano, A. Komatsu, Japanese Patent, 12,503 August 31 (1962).

79. D. Z. Hobbs, T. T. Campbell, F. E. Block, U. S. Bur. Mines, Report Invest. No. 5893 (1961).

80. N. P. Nies, U. S. Patent, 2, 909, 471, October 20 (1959).

81. N. P. Nies, *J. Electrochem. Soc.* 107, 817 (1960).

82. Ashish Jain, S. Anthonysamy, K. Ananthasivan, R. Ranganathan, Vinit Mittal, S. V. Narasimhan, P. R. Vasudeva Rao, *Mater. Charact.* 59, 890 (2008).

83. Ashish Jain, Ph. D. Dissertation, Indian Institute of Science, Bangalore, India, February (2012).

84. Ashish Jain, C. Ghosh, T. R. Ravindran, S. Anthonysamy, R. Divakar, E. Mohandas, G. S. Gupta, *Bull. Mater. Sci.* 2012 (Article in press).

85. S. H. White, *Molten salt Techniques*, Vol. 1, p.19, Plenum Press, New York, (1983).

86. F. Lantelme, D. Inman, D. G. Lovering, *Molten Salt Techniques*, Vol. 2, p.137 Plenum Press, New York, (1984).

87. N. Q. Minh, L. Redey, *Molten Salt Techniques*, Vol. 3, p.105, Plenum Press, New York, (1987).

88. H. W. Jenkins, G. Mamantov, D. L. Manning, *J. Electroanal Chem.* 19, 385 (1968).

89. K. B. Kuskhov, V. V. Malyshev, A. A. Tischenko, V. I. Shapoval, *Por. Met*. 1, 8 (1993).

90. H. Wendt, K. Reuhl, V. Schwartz, *Electrochim. Acta* 37, 237 (1992).

91. A. F. Alabyshev, M. F. Lantratov, A.G. Morachevskiy, *Reference Electrodes for Molten Salts*, Metallurgiya, Moskow (1965).

92. V. N. Nekrasov, D. Sc. Dissertation, Institute of Electrochemistry, Ural Scientific Center, Sverdlovsk, Ukraine (1986).

93. L. P. Polyakova, E. G. Polyakov, A. I. Sorokin, P. T. Stangrit, *J. Appl. Electrochem.* 22, 628 (1992).

94. H. Coriou, J. Dirian, J. Hure, *J. Chim. Phys.* 52, 479 (1955).

95. M. Makyta, K. Matiasovsky, V. I. Taranenko, *Electrochim. Acta*, 34 (6), 861 (1989).

96. L. P. Polyakova, G. A. Bukatova , E. G. Polyakov, E. Christensen, J. H. Von Barner and N. J. Bjerrum, *J. Electrochem. Soc.* 143 (10), 3178 (1996).

97. O. G. Tsiklauri, V. I. Shapoval, A. Sh. Avaliani and N. V. Dvali, *Ionic Melts and Solid Electrolytes*, Kiev: Naukova Dumka, 1, 47 (1986).

98. O. G. Tsiklauri, A. Sh. Avaliani, I. A. Bairammashvili, *Soobshch. Acad. Nauk Gruz. SSR*, 134, 133 (1989).

99. L. I. Jun, L. I. Bing, *Rare Metals* 26 (1), 74 (2007).

100. V. Danek, I. Votava, K. Matiasovsky, *Chem Zvesti* 30, 377 (1976).

101. E. Christensen, X. Wang, J. H. von Barner, T. Ostvold, N. J. Bjerrum, *J. Electrochem. Soc.* 141, 1212 (1994).

102. A. Khalidi, P. Taxil, B. Lanfage, A.P. Lanmaze, *Mater. Sci. Forum* 421, 73 (1991).

103. S. H. White, *Molten Salts Techniques*, Vol. 1, (Edited by D. Lovering, R. Gale), Plenum Press, New York, 1983, pp. 50-51.

104. C. Wagner, *Naturwiss.* 31, 265 (1943).

105. J. D. Van Norman, R. A. Osteryoung, *Anal. Chem.* 32, 389 (1960).

106. G. Letisse, B. Tremillon, *J. Electroanal. Chem.* 17, 387 (1968).

107. B. Tremillon, A. Bermond, R. Molina, *J. Electroanal. Chem.* 74, 53 (1972).

108. F. Seon, Ph.D. Thesis, University Pierre et Marie Curie, Paris, France (1981).

109. L. Polyakova, Z. Kononova, E. Polyakov, *Portugaliae Electrochim. Acta* 13, 293 (1995).

110. V. N. Nekrasov, N. N. Barbin, L. E. Ivanovskiy, *Rasplavy* (Rus.) 6, 51 (1989).

111. N. M. Barbin, V. N. Nekrasov, *Electrochim. Acta* 44, 4479 (1999).

112. L. R. Bezarashvili, N. I. Buryak, S. V. Volkov, O. G. Tsiklauri, *Ukr. Khim. Zhur.* 54, 769 (1988).

113. V. V. Solovev, O. G. Tsiklauri, V. I. Shapoval, A. Yu. Abramov, *Ukr. Khim. Zh.* 62, 21 (1996).

114. V. I. Shapoval, I. V. Zarutskii, V. V. Malyshev, N. N. Uskova, *Russ. Chem. Rev.* 68, 925 (1999).

115. V. I. Shapoval, V. V. Solov'ev, V. V. Malyshev, *Russ. Chem. Rev.* 70, 161 (2001).

116. Vladimir Danek, *Physico-Chemical Analysis of Molten Electrolytes*, Ch. 2, Elsevier B. V., Amsterdam, The Netherlands (2006).

117. Bryant W. Rossiter, John F. Hamilton, *Physical Methods Of Chemistry, Vol. II, Electrochemical Methods*, John Wiley & Sons, Inc., U. S. (1986).

118. A. J. Bard, L. R. Faulkner, *Electrochemical Methods: Fundamentals and Applications*, Wiley, New York (1980).

119. R. G. Compton, C. E. Banks, *Understanding Voltammetry* p. 74, World Scientific Publishing Co. Pte. Ltd. (2009).

120. H. Matsuda, Y. Ayabe, *Z. Electrochem.* 59, 494 (1955).

121. V. A. Golovin, G. A. Dobrenkov, *Trans. Kazan. Khim.-Tekhnol. Inst.* 34, 202 (1965).

122. P. Delahay, *New Instrumental Methods in Electrochemistry: Theory, Instrumentation and Application to Analytical and Physical Chemistry*, Interscience, New York (1954).

123. R. J. Klingler, J. K. Kochi, *J. Phys. Chem.* 85, 1731 (1981).

124. M. Grenness, K. B. Oldham, *Anal. Chem.* 44, 1121 (1972).

125. M. Goto, K. B. Oldham, *Anal. Chem.* 45, 2043 (1973).

126. M. Goto, K. B. Oldham, *Anal. Chem.* 46, 1522 (1974).

127. M. Goto, K. B. Oldham, *Anal. Chem.* 48, 1671 (1976).

128. H. Ipser, A. Mikula, I. Katayama, *CALPHAD: Comput. Coupling Phase Diagrams Thermochem.* 34, 271 (2010).

129. Z. Moser, K. Fitzner, *Thermochim. Acta* 332, 1 (1999).

130. D. G. Lovering, R. J. Gale, *Molten Salt Techniques*, Vol. 3, Ch. 4, Plenum Press, New York (1987).

131. Robert Thomas, *Practical Guide to ICP-MS*, Marcel Dekker, Inc., New York, Basel (2004).

132. L. Reimer, *Scanning Electron Microscopy: Physics of image formation and microanalysis*, 2nd edition, Springer-Verlag, Berlin Heidelberg (1998).

133. C. Suryanarayana, M. Grant Norton, *X-Ray Diffraction: A Practical Approach*, Plenum Press, New York and London (1998).

134. J. Koryta, *Anal. Chim. Acta* 91, 1 (1977).

135. A. H. W. Aten, H. J. den Hertog, L. Westenberg, *Trans. Electrochem. Soc.* 47 265 (1925).

136. S. Senderoff, A. Brenner, *J. Electrochem. Soc.* 101, 31 (1954).

137. P. Gao, X. Jin, D. Wang, X. Hu, G. Z. Chen, *J. Electroanal. Chem.* 579, 321 (2005).

138. I. V. Zarutskii, Cand. Sci. (Chem.) Dissertation, Kiev: Inst. Of Gen. and Inorg. Chem., Acad. Sci. Ukr. SSR (1991).

139. O. G. Tsiklauri, G. A. Gelovani, *Rasplavy* 5, 35 (1989).

140. S. K. Preto, Z. Tomczuk, S. von Winbush, M. F. Roche, *J. Electrochem. Soc.* 130, 264 (1983).

141. B. Gillesberg, N. J. Bjerrum, J. H. von Barner, F. Lantelme, *J. Electrochem. Soc.* 144, 3435 (1997).

142. Maria C. B. Moraes, Jose G. A. Brito Nito, Claudimir L. do Lago, *J. Anal. At. Spectrom.* 16, 1259 (2001).

List of Publications

International Publications:

1. Electrochemistry of deposition of boron from KCl-KF-KBF_4 melts: Voltammetric studies on platinum electrode, Rahul Pal, S. Anthonysamy, V. Ganesan, *Journal of The Electrochemical Society*, 159, 6, F157 - F165 (2012).
2. Description of the melt stoichiometry in the electrodeposition of boron from KCl-KF-KBF_4 melts, Rahul Pal, K. Ananthasivan, S. Anthonysamy, V. Ganesan, *Electrochimica Acta*, 61, 165 – 172 (2012).
3. Development and electrochemistry of a novel Ag/AgCl reference electrode suitable for mixed chloride-fluoride melts, Rahul Pal, K. Ananthasivan, S. Anthonysamy, V. Ganesan, *Electrochimica Acta*, 56, 4276 – 4280 (2011).
4. Electrochemistry of deposition of boron from KCl-KF-$NaBF_4$ melt, Rahul Pal, S. Anthonysamy
   (Communicated)
5. Voltammetric determination of oxide ion in KCl-KF melts, Rahul Pal, S. Anthonysamy
   (Manuscript under preparation)

List of conference and symposia papers:

International conferences and symposia:

1. An Ag/AgCl reference electrode suitable for electrochemical studies in chloride-fluoride melts, Rahul Pal, K. Ananthasivan, S. Anthonysamy, V. Ganesan, ISAEST-9, Chennai, 2-4 December, 2010.

National conferences and symposia:

1. Determination of oxide ion impurity in KCl-KF melt by linear sweep voltammetry, Rahul Pal, S. Anthonysamy, NCE16, PSGR College, Coimbatore, 15-16 December 2011.
2. Determination of fluorooxoborate species in boron containing mixed chloride-fluoride melts using linear sweep voltammetric (LSV) technique, Rahul Pal, S. Anthonysamy, CRSM, IGCAR, Kalpakkam, 14-15 July, 2011.
3. Electrochemistry of boron deposition from KCl-KF-KBF$_4$ melt: Voltammetric studies on a platinum electrode, Rahul Pal, K. Ananthasivan, S. Anthonysamy, V. Ganesan, Indo-Italian Workshop on Frontiers of Fundamental and Industrial Electrochemistry: The Challenge of Science for a Better World, University of Delhi, Delhi, 30 - 31 August, 2010.
4. Optimisation of some of the process parameters for the production of elemental boron through electrowinning process, Rahul Pal, K. Ananthasivan, S. Anthonysamy, V. Ganesan, MR09, IIT Mumbai, 2-5 May, 2009.